


December 2013

Evaluation of Vdr-coactivator Inhibitors Using Biochemical and Cell-based Assays

Athena Marie Baranowski
University of Wisconsin-Milwaukee

Follow this and additional works at: <https://dc.uwm.edu/etd>

 Part of the [Biochemistry Commons](#), [Chemistry Commons](#), and the [Pharmacy and Pharmaceutical Sciences Commons](#)

Recommended Citation

Baranowski, Athena Marie, "Evaluation of Vdr-coactivator Inhibitors Using Biochemical and Cell-based Assays" (2013). *Theses and Dissertations*. 353.
<https://dc.uwm.edu/etd/353>

This Thesis is brought to you for free and open access by UWM Digital Commons. It has been accepted for inclusion in Theses and Dissertations by an authorized administrator of UWM Digital Commons. For more information, please contact open-access@uwm.edu.

EVALUATION OF VDR-COACTIVATOR INHIBITORS
USING BIOCHEMICAL AND CELL-BASED ASSAYS

by

Athena Baranowski

A Thesis Submitted in

Partial Fulfillment of the

Requirements of the Degree of

Master of Science

in Chemistry

at

The University of Wisconsin-Milwaukee

December 2013

ABSTRACT

EVALUATION OF VDR-COACTIVATOR INHIBITORS USING BIOCHEMICAL AND CELL-BASED ASSAYS

by

Athena Baranowski

The University of Wisconsin-Milwaukee, 2013
Under the Supervision of Dr. Alexander Arnold

The vitamin D receptor (VDR) is a ligand-dependent transcription factor, which belongs to the nuclear receptor superfamily. VDR-mediated gene regulation is governed by coregulators (coactivators and corepressors). VDR coregulator binding inhibitors (CBIs), which were discovered using high throughput screening (HTS), were evaluated using cell-based assays and biochemical assays to determine their ability to inhibit the interaction between VDR and steroid receptor coactivator-2 (SRC-2). Determining their ability to inhibit the VDR-SRC-2 interaction can lead to the development of novel and safer pharmaceutical treatments for VDR-related disorders, such as cancer, autoimmune diseases, and cardiovascular disease; therefore, the study of transcription, toxicity, and protein-protein interactions are critical to the development of pharmaceutical treatments.

The methods used to study CBIs include a cell-based transcription assay, which was based on the formation of β -lactamase in the *Hek 293T* cell line. The readout of this assay was fluorescence resonance energy transfer (FRET) of a cell-permeable substrate in the event of transcription inhibition, and a blue fluorescent signal in the event of

transcription activation. Active CBIs, such as compound WL052410G (31b), exhibit a reduced blue to green fluorescent ratio.

A luciferase-based viability assay, which detected ATP levels from metabolically active *Hek 293T* cells, was used to determine the toxicity of the CBIs, in hopes of detecting partial toxicity for pharmaceutical targets of VDR, such as compound WL052410G (31b).

Different co-immunoprecipitation pull-down assays were developed to precipitate and isolate target proteins, such as VDR, SRC-2, and SRC-2-3, using affinity-based tagging, in order to determine the ability of CBIs to disrupt the protein-protein interaction between VDR and SRC-2 coactivator. The VDR-SRC-2 interaction was visualized using a fluorescently tagged antibody, which was realized using a laser imager.

The most active compounds for all the assays performed belong to a series of 3-indolyl-methanamines and include a highly selective and active compound, WL052410G (31b).

TABLE OF CONTENTS

Chapter 1: Introduction	xvi
Chapter 2: Cell Culture and Gene BLAzer Assay	8
Chapter 2.1: <i>HEP G2</i> Cells and Culture Methods of <i>HEP G2</i> Cells	8
Chapter 2.2: Description of <i>Hek 293T</i> Cell Line	9
Chapter 2.3: Background and Description of the Gene BLAzer FRET Assay	11
Chapter 2.4: Gene BLAzer FRET Assay Methods	16
Chapter 2.5: Fluorescence Detection	18
Chapter 2.6: <i>Hek 293T</i> Cell Culture Methods.....	25
Chapter 2.7: Summary of the Results of the Gene BLAzer Assay	27
Chapter 2.8: Detailed Results and Figures of the Gene BLAzer Assay.....	29
Chapter 2.9: Discussion of the Results of the Gene BLAzer Assay	42
Chapter 3: Cell Titer-Glo Luciferase Assay	45
Chapter 3.1: Background and Description of the Cell Titer-Glo Luciferase Assay	45
Chapter 3.2: Luminescence	47
Chapter 3.3: Luminescence Detection	48
Chapter 3.4: The Cell Titer-Glo Luciferase Assay	49

Chapter 3.5: Summary of the Results of the Cell Titer-Glo Luciferase Assay	52
Chapter 3.6: Detailed Results and Figures of the Cell Titer-Glo Luciferase Assay.....	53
Chapter 3.7: Discussion of the Results of the Cell Titer-Glo Luminescence Assay.....	66
Chapter 4: VDR, SRC-2, and SRC-2-3 Protein Expression and Purification	69
Chapter 4.1: Protein Expression.....	69
Chapter 4.2: Protein Purification.....	72
Chapter 5: Co-Immunoprecipitation and Pull-Down Assay	77
Chapter 5.1: Pull-Down Assay using a Solid-Supported VDR and an <i>in situ</i> -Generated SRC-2-Biotin with the TNT Transcription and Translation System for the Identification of VDR-CBIs (Promega)	77
Chapter 5.1.1: Experimental Procedure for the above Pull-Down Assay	78
Chapter 5.1.1.1: Solid-Supported VDR	78
Chapter 5.1.1.2: <i>In situ</i> -Generated SRC-2	78
Chapter 5.1.1.3: Quantification of SRC-2-Biotin for the Pull-Down Assay	78
Chapter 5.2: Second Pull-Down Assay: Evaluating VDR-CBI, WL042210D (32a), Inhibition	82
Chapter 5.3: Third Pull-Down Assay using a Solid-Supported SRC-2 and VDR-LBD for the Identification of VDR-CBIs	85
Chapter 5.3.1: Experimental Procedure for the Third Pull-Down Assay.....	88

Chapter 5.3.2: Results of the Third Pull-Down Assay.....	90
Chapter 5.3.3: The Fourth Pull-Down Assay with CBIs WL052410G (31b) and CBT-1.....	91
Chapter 5.4: Co-Immunoprecipitation Pull-Down Assay using a Solid-Supported SRC-2 and VDR-LBD for the Identification of VDR-CBIs	94
Chapter 5.4.1: Experimental Procedure for the First Co-Immunoprecipitation Pull-Down Assay	97
Chapter 5.4.1.1: Antibodies used for the Co-IP Pull-Down Assay.....	98
Chapter 5.4.2: Results of the First Co-Immunoprecipitation Pull-Down Assay.....	99
Chapter 5.4.3: The Second Co-Immunoprecipitation Pull-Down Assay.....	100
Chapter 5.5: Co-Immunoprecipitation Pull-Down Assay using a Solid-Supported SRC-2 and VDR-LBD for the Identification of a Reversible VDR-CBI, Compound GW 0742	101
Chapter 5.6: Discussion of the Results of the Co-Immunoprecipitation Pull-Down Assays.....	105
Chapter 6: References	108
Appendix.....	113

LIST OF FIGURES

Figure 1: Chemical structure of 1, 25-(OH) ₂ D ₃ .	1
Figure 2: Vitamin D metabolism. Vitamin D, the precursor for calcitriol, or 1 α , 25-(OH) ₂ D ₃ , is synthesized from 7-dehydrocholesterol through photolysis occurring in the skin. The formation of 1, 25-(OH) ₂ D ₃ occurs in the liver and kidneys.	2
Figure 3: Ribbon structure of the VDR-LBD with the ligand, 1, 25-dihydroxyvitamin D ₃ , bound in the pocket. Helix 12 of the AF-2 and the DRIP interacting protein are also depicted. ⁶	3
Figure 4: Chimeric plasmid vector of VDR-LBD and <i>Gal4</i> -DBD.	10
Figure 5: β -lactamase and UAS chimeric plasmid vector.	10
Figure 6: Binding of the first chimeric plasmid vector to the UAS of the second chimeric plasmid vector.	11
Figure 7: Structure of the CCF4-AM FRET substrate.	12
Figure 8: Jablonski diagram. An electron is excited with an energy source, and light is emitted when the electron returns to the ground state. This diagram shows possible routes that an excited electron can take when returning to ground state. A rapid return to ground state results in fluorescence emission, and a slow return to ground state results in phosphorescence, after light crosses to the triplet state and undergoes internal conversion.	13
Figure 9: FRET diagram. The electron donor is excited to a singlet state and energy is transferred to an electron acceptor through resonance transfer by overlapping emission spectra.	14
Figure 10: In-cell FRET diagram. The substrate permeates through the cell membrane and is cleaved by esterases to form a highly fluorescent compound, CCF4. Cleavage by β -lactamase releases the fluorescent coumarin derivative.	15

Figure 11: Hepatocytometer depiction. Approximately 30 μ L of cell suspension was pipetted into this whole area. Cells were then counted in three separate red boxes and averaged. The volume of each of the red boxes was a 100 nL. Multiplication by 10,000 of the amount of cells counted gave the concentration of cells in cell per mL.	17
Figure 12: Entire fluorescent optical system, which consists of the light source, the fluorescent top and bottom optics, and the fluorescence detection unit..	19
Figure 13: Fluorescence optics used for top and bottom reading of fluorescence intensity measurement. The right-hand side is an enlargement of the bottom fluorescence measurement, which is similar to the top fluorescence measurement.	22
Figure 14: Z prime calculation. The Z prime value indicates the correlation of the experimental data. Z prime values from 0.50 to 1.0 indicate useful data sets.	24
Figure 15: Hygromycin (15A) and Zeocin (15B) antibiotic structures.	26
Figure 16: Inhibition of VDR-mediated transcription of compounds F1387-0020, F1387-0036, F1217-0092, F0910-7407, and F0743-0032.	29
Figure 17: Inhibition of VDR-mediated transcription of compounds F0842-0039, F1387-0021, F1387-0022, F1387-0034, and F1420-1568.	30
Figure 18: Inhibition of VDR-mediated transcription of compounds F1387-0028, F1298-0533, F1298-0551, F1298-0074, and F1298-0581.	32
Figure 19: Inhibition of VDR-mediated transcription of compounds F1298-0621, F1298-0587, and F1298-0522.	33
Figure 20: Inhibition of VDR-mediated transcription of compounds D093-0045, D093-0086, and F1298-0025.	34
Figure 21: Inhibition of VDR-mediated transcription of compounds WL052410D, WL052510D, WL052510F, and WL052510H.	35

Figure 22: Inhibition of VDR-mediated transcription of compounds WL052510K and WL052510M.	36
Figure 23: Inhibition of VDR-mediated transcription of compounds WL052410G, WL052410K, WL052410N, and WL060110G.	37
Figure 24: Inhibition of VDR-mediated transcription of compounds WL060110H, WL040710D, and WL042210G.	38
Figure 25: Inhibition of VDR-mediated transcription of compounds WL061410C, WL042210D, WL060310C, and WL061410K.	39
Figure 26: Inhibition of VDR-mediated transcription of compounds WL042210G, WL042210K, and WL060110G.	40
Figure 27: Structure of GW 0742.	41
Figure 28: Inhibition of VDR-mediated transcription of compound GW 0742.	41
Figure 29: Enzymatic reaction of luciferase.	46
Figure 30: The interaction between ATP and luciferin in the presence of luciferase, magnesium cations, and oxygen.	47
Figure 31: Luminometer detection system.	49
Figure 32: Z prime calculation. The Z prime value indicates the correlation of the experimental data. Z prime values from 0.50 to 1.0 indicate useful data sets.	51
Figure 33: Toxicity of compounds F1387-0020, F1387-0036, F1217-0092, F0910-7407, and F0743-0032.	53
Figure 34: Toxicity of compounds F0842-0039, F1387-0021, F1387-0022, F1387-0034, and F1420-1568.	55

Figure 35: Toxicity of compounds F1387-0028, F1298-0533, F1298-0551, F1298-0074, and F1298-0581.	56
Figure 36: Toxicity of compounds F1298-0621, F1298-0587, and F1298-0522.	57
Figure 37: Toxicity of compounds D093-0045, D093-0086, and F1298-0025.	58
Figure 38: Toxicity of compounds WL052410D, WL052510D, WL052510F, and WL052510H.	59
Figure 39: Toxicity of compounds WL052510M and WL052510K.	60
Figure 40: Toxicity of compounds WL052410G, WL052410K, WL052410N, and WL060110G.	61
Figure 41: Toxicity of compounds WL060110H, WL040710D, and WL042210G.	62
Figure 42: Toxicity of compounds WL061410C, WL042210D, WL060310C, and WL061410K.	63
Figure 43: Toxicity of compounds WL042210G, WL042210K, and WL060110G.	64
Figure 44: Structure of compound GW 0742.	65
Figure 45: Toxicity of compound GW 0742.	65
Figure 46: Maltose binding protein (MBP) attached to an amylose resin. MBP is a member of the maltose and maltodextrin system of <i>E. Coli</i> , which is responsible for the catabolism of maltodextrins. Maltose can be immobilized by cross-linking to a solid-support amylose resin. The purified MBP fusion protein can be dissociated and eluted by the addition of excess maltose (10 mM).	73
Figure 47: Glutathione S-transferase (GST) bead. Glutathione is a tripeptide (Glu-Cys-Gly) that is the specific substrate for GST. When reduced, glutathione is immobilized through its sulfhydryl group to a solid support, such as a cross-linked agarose bead.	

Glutathione can be used to capture GST-tagged proteins via the enzyme-substrate binding reaction. The purified GST-fusion protein can be dissociated and eluted from glutathione by addition of excess reduced glutathione (10 mM).73

Figure 48: Histidine (His) nickel-nitrilotriacetic acid (NTA) resin. A string of 6 to 9 histidine residues form an easily identifiable tag, which is fused to either the amino or carboxyl terminal. His-tagged proteins are easily purified and detected because the His-tag binds to nickel, which is an immobilized metal ion. A chelating group, such as NTA, which is attached to a solid support, in this case, agarose, helps to immobilize the nickel ion, which then attaches to the His-tag. Elution of the His-tagged protein is done with 250 mM imidazole solution. The imidazole replaces the nickel in the resin, which releases the protein.74

Figure 49: Scheme of the first pull-down assay.77

Figure 50: Western blot assembly.80

Figure 51: Colorimetric alkaline phosphatase assay.....81

Figure 52: Stained PVDF membrane.....82

Figure 53: Stained PVDF membrane of the 5 pull-down reactions using VDR-CBI, WL042210D (32a).85

Figure 54: Scheme of the third pull-down assay.86

Figure 55: SDS-PAGE gel of VDR-coactivator pull-down assay using compound WL042210D (32a).90

Figure 56: SDS-PAGE gel of VDR-coactivator pull-down assay using compounds WL052410G (31b) and CBT-1.93

Figure 57: Co-IP pull-down assay scheme.94

Figure 58: Basic structure of an antibody.....98

Figure 59: First co-IP VDR-coactivator pull-down assay using compound WL052410G (31b).....	99
Figure 60: Second co-IP VDR-coactivator pull-down assay using compound WL052410G (31b).....	100
Figure 61: Chemical structure of compound GW 0742.....	101
Figure 62: Inhibition of the VDR–SRC-2 interaction by compound GW 0742, analyzed by a co-IP pull-down assay.	104

LIST OF TABLES

Table 1: Comparison of the Z prime values of 384-well plates containing compound GW 0742, which were run with and without a bottom sticker and of 384-well plates that were not multi-plexed with the Gene BLAzer assay and that were multi-plexed with the Gene BLAzer assay.	51
Table 2A: Condition 1: High Concentration of CBI (200 μ M)	83
Table 2B: Condition 2: Medium Concentration of CBI (50 μ M)	83
Table 2C: Condition 3: Low Concentration of CBI (1 μ M)	83
Table 2D: Condition 4: VDR-SRC-2 Interaction (Negative Control; No CBI).....	83
Table 2E: Condition 5: No VDR Ligand (Positive Control; No CBI or VDR Ligand) ...	83
Table 3A: Condition 1: High Concentration of CBI (200 μ M)	87
Table 3B: Condition 2: Medium Concentration of CBI (50 μ M)	87
Table 3C: Condition 3: Low Concentration of CBI (1 μ M)	87
Table 3D: Condition 4: VDR-SRC-2 Interaction (Negative Control; No CBI)	87
Table 3E: Condition 5: No VDR Ligand (Positive Control; No CBI or VDR Ligand) ...	87
Table 4A: Condition 1: High Concentration of CBI (200 μ M)	92
Table 4B: Condition 2: Medium High Concentration of CBI (100 μ M)	92
Table 4C: Condition 3: Medium Low Concentration of CBI (50 μ M)	92
Table 4D: Condition 4: Low Concentration of CBI (1 μ M)	92

Table 4E: Condition 5: VDR-SRC-2 Interaction (Negative Control; No CBI).....	92
Table 5A: Condition 1: High Concentration of CBI (200 μ M)	95
Table 5B: Condition 2: Medium High Concentration of CBI (100 μ M)	95
Table 5C: Condition 3: Medium Low Concentration of CBI (50 μ M)	95
Table 5D: Condition 4: Low Concentration of CBI (1 μ M)	95
Table 5E: Condition 5: VDR-SRC-2 Interaction (Negative Control; No CBI).....	95
Table 5F: Condition 6: No VDR Ligand (Positive Control; No CBI or Ligand)	96
Table 5G: Condition 7: SRC-2 Beads Only (SRC-2 Protein Only)	96
Table 5H: Condition 8: VDR Protein Only	96
Table 6A: Condition 1: Concentration One of CBI (120 μ M).....	102
Table 6B: Condition 2: Concentration Two of CBI (80 μ M)	102
Table 6C: Condition 3: Concentration Three of CBI (50 μ M)	102
Table 6D: Condition 4: Concentration Four of CBI (20 μ M)	102
Table 6E: Condition 5: Concentration Five of CBI (10 μ M).....	103
Table 6F: Condition 6: Concentration Six of CBI (1 μ M)	103
Table 6G: Condition 7: Concentration Seven of CBI (0.1 μ M)	103

Table 6H: Condition 8: VDR-SRC-2 Interaction (Negative Control; No CBI).....	103
Table 6I: Condition 9: No VDR Ligand (Positive Control; No CBI or Ligand).....	103
Table 6J: Condition 10: SRC-2 Beads Only (SRC-2 Protein Only)	104
Table 6K: Condition 11: VDR Protein Only	104
Table 7: Summary of the compounds tested, with respect to their ability to inhibit VDR-mediated transcription using the Gene BLAzer assay, as well as their cytotoxicity, which was determined by the Cell Titer-Glo luminescence assay. All results are given in micromolar concentrations.....	113

ACKNOWLEDGEMENTS

Most importantly, I would like to dedicate this thesis to and to thank Dr. Alexander “Leggy” Arnold for his endless patience, encouragement, wisdom, and sense of humor. He has been a great mentor, and has always believed in me, even when I did not believe in myself. I could not have accomplished all of my dreams without his assistance, dedication, and inspiration. I will forever be in his debt.

I would also like to thank Dr. Nick Silvaggi and Dr. Joseph Aldstadt for serving on my master’s committee, for giving words of advice, or just for sharing a beer at “nach sitzen.”

Additionally, I would like to thank Dr. Nick Silvaggi and his research group, as well as Dr. David Frick and his research group, and Dr. Guilherme Indig and his research group for helping and letting me use the instrumentation in their labs.

I would also like to dedicate this thesis to and to thank Ms. Gloria Freschl for being my mentor in student education and for being an inspiration in my pursuit of a career in chemical education.

Similarly, I would like to dedicate this thesis to and to thank my parents, Al and Jenny Baranowski, for supporting me in all my dreams, for encouraging me when it was difficult to go on, and for making me believe that I could reach for the stars. It means more to me than anyone will ever know.

Likewise, I would like to dedicate this thesis to and to thank my fiancé, Jason Bink, for making me laugh when I need it the most, for believing in me when I did not believe in myself, and for being the best friend a girl could ever want.

Finally, I would like to thank anyone who helped me through graduate school, especially the wonderful people in my research group, whether they offered a smile, a laugh, a drink, or to teach me calculus. I am grateful to everyone who helped me through my degree.

Chapter 1: Introduction

The vitamin D receptor (VDR) is a ligand-activated transcription factor, which is one of the 48 nuclear receptors (NRs) discovered in the human genome, and mediates the transcription of the genes responsible for cell proliferation, cell differentiation, and calcium homeostasis.¹ VDR is a pharmaceutical target for the treatment of metabolic disorders, skin diseases, cancer, autoimmune diseases, and cardiovascular diseases. VDR has several functional domains, such as a DNA binding domain (VDR-DBD) and a ligand binding domain (VDR-LBD), which mediate ligand-dependent gene regulation.²

VDR binds DNA at the VDR-DBD and forms a heterodimer with the retinoid X receptor (RXR). RXR is a nuclear receptor for 9-*cis* retinoic acid and is essential for VDR-mediated transcription, because it is required to bind with VDR in order for the complex to bind to the vitamin D response element (VDRE), which is typically located in the promoter region of VDR-regulated genes.³

Vitamin D, the precursor for calcitriol, or 1, 25-dihydroxyvitamin D₃ (1 α , 25-(OH)₂D₃), as seen in Figure 1, can be obtained through foods or synthesized from 7-dehydrocholesterol through photolysis occurring in the skin. The formation of 1, 25-(OH)₂D₃ occurs in the liver and kidneys.

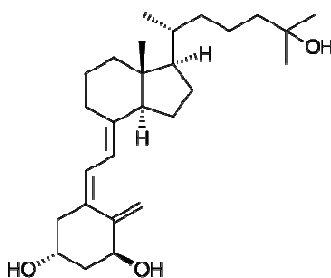


Figure 1: Chemical structure of 1, 25-(OH)₂D₃.

The vitamin D binding protein binds vitamin D₃ and transports it through the blood to the liver. In the liver, vitamin D₃ is hydroxylated at carbon 25 by vitamin D 25-hydroxylase, resulting in the formation of 25-hydroxyvitamin D₃. The vitamin D binding protein then binds this form of vitamin D₃ and transports it to the kidneys. In the kidneys, 25-hydroxyvitamin D₃ is then hydroxylated at carbon 1 of the A ring, which converts the vitamin D₃ to the active form, 1, 25-dihydroxyvitamin D₃.⁴

In order to control the amount of active vitamin D₃ found in target tissues, this active form of vitamin D₃ is also the substrate of the 24-hydroxylase enzyme. Elevated levels of vitamin D₃ cause it to bind to the 24-hydroxylase enzyme, forming 1, 24, 25-(OH)₃D₃, which is then converted to inactive calcitrolic acid. Vitamin D₃ can also produce 24, 25-(OH)₂D₃, which forms in order to regulate and decrease the amount of 25-(OH)D₃ available for carbon 1 hydroxylation.⁵⁻⁷ The metabolism of vitamin D is illustrated in Figure 2.

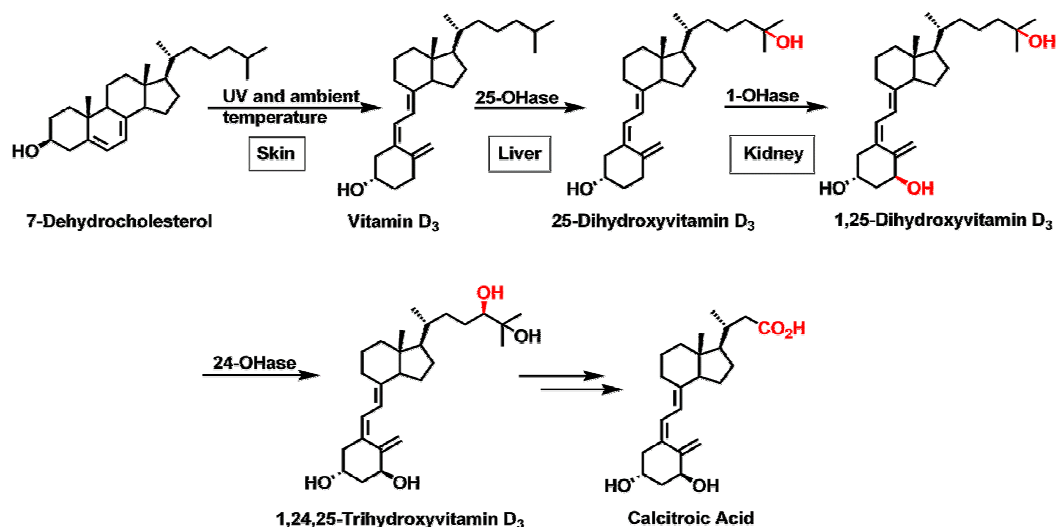


Figure 2: Vitamin D metabolism. Vitamin D, the precursor for calcitriol, or 1 α , 25-(OH)₂D₃, is synthesized from 7-dehydrocholesterol through photolysis occurring in the skin. The formation of 1, 25-(OH)₂D₃ occurs in the liver and kidneys.

VDR binds to its ligand, $1\alpha, 25\text{-(OH)}_2\text{D}_3$, with high affinity. This ligand binding causes the VDR-LBD to undergo a conformational change. The conformational change is essential to release corepressors bound to VDR, and also creates the VDR activation function-2 (AF-2) domain, which consists of a hydrophobic cleft of 3 helices and an amphipathic α -helix at the carboxyl terminal called helix 12, as seen in Figure 3.⁸

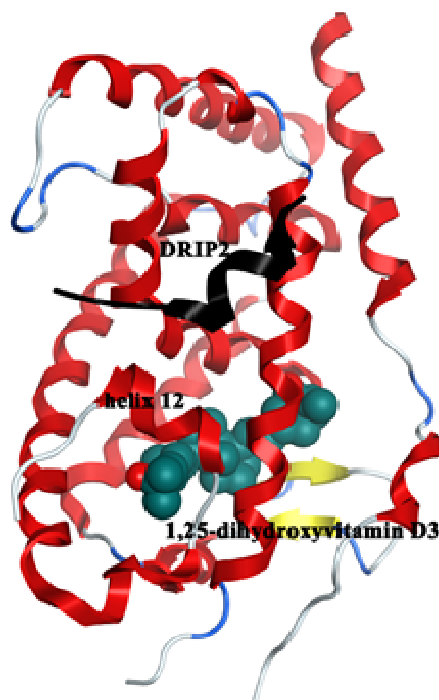


Figure 3: Ribbon structure of the VDR-LBD with the ligand, 1, 25-dihydroxyvitamin D₃, bound in the pocket. Helix 12 of the AF-2 and the DRIP interacting protein are also depicted.⁸

In an unligated state, VDR binds corepressor proteins, such as the nuclear receptor corepressor (NCoR) and the silencing mediator of retinoic acid and thyroid hormone receptor (SMRT), which repress the transcription of VDR target genes.⁹ NCoRs have short consensus sequences that are similar to that of coactivators, which are discussed later in this chapter. The consensus sequence of these corepressors is $\Phi xx\Phi\Phi$, where Φ is isoleucine or leucine, and x is any amino acid.^{10, 11} This sequence forms an α -helix, which is one turn longer than the coactivator helix. The formation of this helix allows for corepressor binding to the AF-2 domain without helix 12 contacting the VDR-LBD.

Helix 12 projects away from the core of the VDR-LBD, allowing corepressors to stay docked and to negatively control the transcriptional machinery by relaying a repressive signal to maintain a closed chromatin structure, leaving the histones in the amino terminal tails in a charged state, which is tightly associated with DNA.^{12, 13}

VDR binds corepressors to negatively modulate transcription through histone deacetylase activity. Deacetylase activity catalyzes the removal of acetyl groups from lysine residues to increase the positive charge on the histone, thus, strengthening the interactions between DNA and the histone. The deacetylation of the histones results in a compacted chromatin structure and prevents the RNA polymerase from initiating transcription.

The AF-2 domain is where coactivators are able to interact with the VDR multi-protein complex, which further modulates and activates VDR-mediated transcription by recruiting the assembly of transcriptional proteins. In the ligated state, helix 12 contacts the VDR-LBD, creating the AF-2 domain.

The creation of the AF-2 domain allows for positive modulation of transcription by modifying histone structure through acetyltransferases, which are recruited by coactivators, such as the steroid receptor coactivator (SRC), also known as the glutamate receptor interacting proteins (GRIP) family of coactivators, of which, the SRC-2 coactivator plays a critical role for the experiments in this thesis.¹⁴⁻¹⁶

Histone acetyltransferases (HATs) are a class of enzymes involved in gene transcription through remodeling chromatin structure. HATs target histones are bound to DNA and catalyze the acetylation of lysine residues in the amino terminal tail of histones. The DNA is unwound, and then targeted by VDR-interacting protein (DRIP) complex.¹⁷
¹⁸ DRIP is a protein complex which is required for the initiation of transcription.

VDR binds DNA gene response elements, so that when the coactivators are recruited, the histone structure of the target genes can be modified. Coactivators, which usually contain several LxxLL (L is leucine and x is any amino acid) consensus sequences with different flanking amino acid residues called NR boxes, bind in the hydrophobic cleft of the AF-2 domain. The LxxLL consensus sequences form an amphipathic α -helix which fits into the hydrophobic pocket of the AF-2 domain on the VDR-LBD.⁸

VDR coregulator binding inhibitors (VDR-CBIs) prevent the binding of corepressors or coactivators to the VDR. An inhibitor can bind to its target protein irreversibly through covalent bonding, or reversibly through either hydrophobic interactions, hydrogen bonds, or ionic interactions.

VDR ligand agonists have been developed to treat metabolic bone diseases and proliferative skin disorders; however, only a limited number of VDR ligand antagonists

have been determined to allosterically inhibit the interactions between VDR and its coactivators.¹⁹⁻²⁶ Direct inhibition of VDR-coactivator binding using small molecules was first reported by Mita et al.²⁷ This novel approach helps determine the role of coregulators in gene regulation in the presence 1, 25-(OH)₂D₃. CBIs have been discovered for the estrogen receptor (ER), thyroid receptor (TR), androgen receptor (AR), and the peroxisome proliferator activated receptor (PPAR).²⁸ The research described herein enabled the identification of the first irreversible and highly selective VDR-CBIs.²⁹

Small molecule inhibitors of protein-protein interactions are important tools in research and recently emerged as starting points for drug development. Identification of the molecular interaction between VDR and CBIs can provide insight to the development of novel and safer methods for nuclear hormone receptor ligand-based treatments, such as those for cancer; therefore, it is important to characterize these CBIs with regard to transcription and cytotoxicity.

The compounds were evaluated for the inhibition of transcription and cytotoxicity using a fluorescence resonance energy transfer (FRET)-based assay and a luciferase assay, respectively. In addition, a co-immunoprecipitation (co-IP) and an immune-detection pull-down assay were performed, in order to further prove the inhibition between VDR and SRC-2 coactivator was inhibited in a dose-dependent manner. One of the most promising inhibitors was based on the scaffold of 3-indolyl-methanamines.

In addition, newly synthesized analogs of 3-indolyl-methanamines were studied for transcriptional activity, as well as cytotoxicity, and produced the first selective and irreversible VDR-CBI, compound WL052410G (31b). The transcriptional regulation of these compounds was studied using the VDR target gene, *CYP24A1*, in mammalian cells.

The cell-based assay was developed in 1998 and has been used widely for NRs, including AR, progesterone receptor (PR), mineralocorticoid receptor (MR), glucocorticoid receptor (GR), and both ER- α and ER- β receptors.³⁰ These and other NRs bind various steroid-based ligands, which leads to the homodimerization of the NR and binding to specific promoter elements, in order to drive the expression of downstream NR genes, which control various cellular functions. Alterations in the function of these receptors lead to endocrine-related diseases, such as cancer and heart disease.

For VDR, a *Gal4*-DBD and VDR-LBD fusion protein was cloned into an upstream activation sequence (UAS) and stably transfected into *Hek 293T* cells. In addition, a β -lactamase reporter gene, under transcriptional control of an upstream activation sequence (UAS-*bla*), was stably transfected. The assay used known agonists and antagonists in a dose-response format as controls, which demonstrate selective NR modulation. The assay was also able to identify and differentiate mixed and partial agonists and antagonists.

The reason that partial agonists and antagonists have a more desirable drug effect than full agonists and antagonists is because they have fewer off-target side effects, due to their partial activity.³¹ These compounds can have different biological effects and alternative conformations of the receptor, which can result in differential recruitment or displacement of cofactors, as well as tissue-specific and promoter-selective expression of target genes.

A co-immunoprecipitation assay was performed as a secondary assay, in order to determine the inhibition between VDR and coactivators; therefore, *E. coli* cells were used for the expression and purification of the SRC-2 protein. Once the SRC-2 protein was

attached to a glutathione S-transferase (GST) bead, a pull-down assay was performed on varied concentrations of CBIs. This assay was then resolved using sodium dodecyl sulfate polyacrylamide gel electrophoresis (SDS-PAGE) gel, blotted to a Western membrane, and VDR was detected using a fluorescently tagged secondary antibody. The assay was performed in this manner, in order to demonstrate that the CBI showed a dose-response in competing with SRC-2 for VDR binding.

Chapter 2: Cell Culture and Gene BLAzer Assay

Chapter 2.1: HEP G2 Cells and Culture Methods of HEP G2 Cells

Cell culture practice began on the human hepatocellular liver carcinoma (*HEP G2*) cell line. This cell line is commonly used to determine liver toxicity of small molecules.³² First, the cells were thawed from liquid nitrogen, and a 1 mL fraction was pipetted into a cell culture flask containing 14 mL of recovery media, which was eagle's minimum essential medium (EMEM from ATCC). EMEM consists of a balanced salt solution, non-essential amino acids, 2 mM L-glutamine, 1 mM sodium pyruvate, and 1500 mg/L sodium bicarbonate. The cells were placed in the sterile incubator at 37°C and 5 percent carbon dioxide until they reached 60 to 90 percent confluency.

The cells were passaged by first aspirating the old growth media, and then by rinsing the cell flask with 10 mL of phosphate buffered saline (PBS), which rinsed away any dead cells. The cells were detached from the cell culture flask using 0.25 percent trypsin, which is described later in this chapter.³³ The flask was incubated with the trypsin for 3 to 5 minutes at 37°C and 5 percent carbon dioxide in a sterile incubator.

After incubation, the cell suspension was mixed by pipette, in order to achieve a single cell suspension, and 1 mL of the suspension was introduced into new flasks containing 15 mL of growth media, which was the same as the recovery media previously described, but with 10 percent fetal bovine serum (FBS) added to the recovery media. No further tests were conducted using this cell line.

Chapter 2.2: Description of the *Hek 293T* Cell Line

A commercially available, stably transfected, human embryonic kidney (*Hek 293T*) cell³⁴ line was cultured for use in the Gene BLAzer and Cell Titer-Glo assays.

The *Hek 293T* cells contained the simian vacuolating (SV) virus 40 T-antigen origin of replication,³⁵ which allowed for activated transient gene transcription and improved incorporation of foreign genes into the host genome.

The commercially available *Hek 293T* cell line also contained 2 stably transfected plasmid vectors. The first plasmid vector was a chimeric vector bearing the ligand binding domain of VDR and the DNA binding domain of the *Gal4* transcription factor (Figure 4).³⁶ The second vector contained chimeric DNA assembled from a UAS response element and a β -lactamase gene (*bla*) (Figure 5).

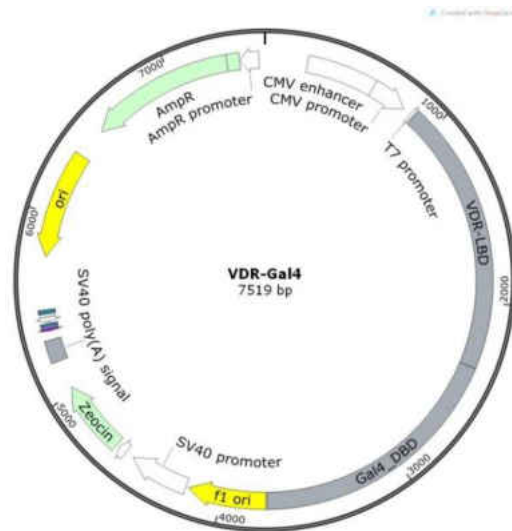


Figure 4: Chimeric plasmid vector of VDR-LBD and *Gal4*-DBD.

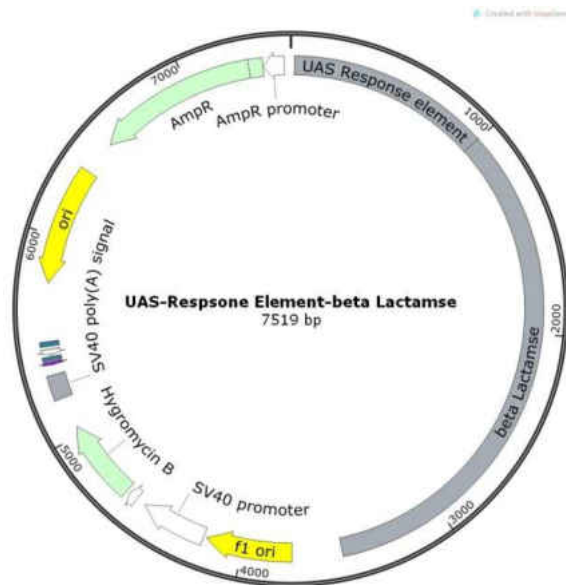


Figure 5: β -lactamase and UAS chimeric plasmid vector.

Gal4 is a yeast-specific transcription factor, which is a positive gene expression regulator of galactose-induced genes. *Gal4* encodes for enzymes which convert galactose to glucose. In order to ensure that this chimeric DNA was replicated continuously, the

vector contained antibiotic resistance to Zeocin, which was present in the cell culture medium at all times.³⁷

β -lactamase is an enzyme which is produced by some bacteria and causes resistance to β -lactam antibiotics.³⁸ The β -lactam antibiotics contain a four-member ring with three carbon atoms and one nitrogen atom. The β -lactamase enzyme breaks the ring open, which deactivates the antibacterial properties. The second vector also contained antibiotic resistance to Hygromycin B, which was also present in the cell culture medium at all times.

Culturing these cells in the presence of these 2 antibiotics ensured the transcription and translation of the VDR-LBD-*Gal4*-DBD and the availability of the reporter DNA bearing the *bla* gene (Figure 6).

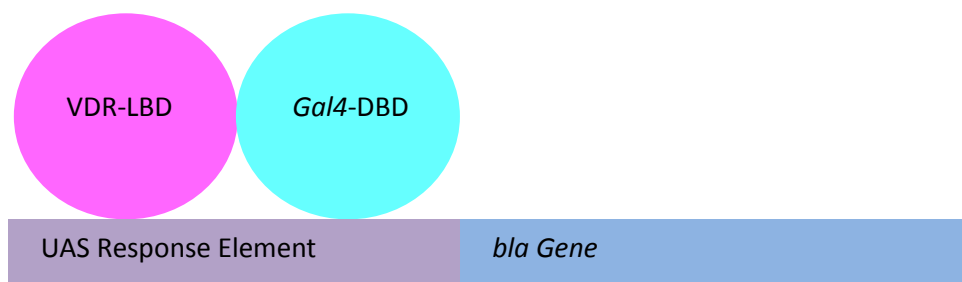


Figure 6: Binding of the first chimeric plasmid vector to the UAS of the second chimeric plasmid vector.

Chapter 2.3: Background and Description of the Gene BLAzer FRET Assay

This assay was used to detect the influence that CBIs have on the interference of transcription mediated by the VDR-LBD; therefore, cells were evaluated in the presence of calcitriol, which activated the VDR-LBD conformational change and allowed for the

recruitment of coactivators. The binding of the *Gal4*-DBD from the first chimeric plasmid vector to the UAS response element of the second chimeric plasmid vector triggered the transcription of the *bla* gene, which ultimately resulted in the generation of β -lactamase enzyme.

The expression of cellular β -lactamase was measured by the addition of a substrate (CCF4-AM) with the ability to create a FRET signal. CCF4-AM substrate has two fluorescent moieties, coumarin and fluorescein, which are linked by a β -lactam ring (Figure 7).⁴

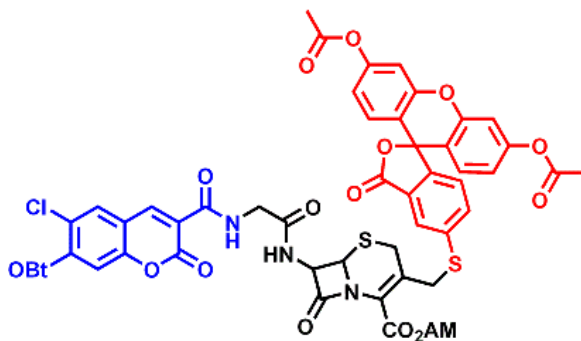


Figure 7: Structure of the CCF4-AM FRET substrate.

FRET is made possible by the presence of two fluorescent scaffolds in close proximity, that is, they are linked together in one molecule. Fluorescence is best explained with the Jablonski diagram in Figure 8.³⁹

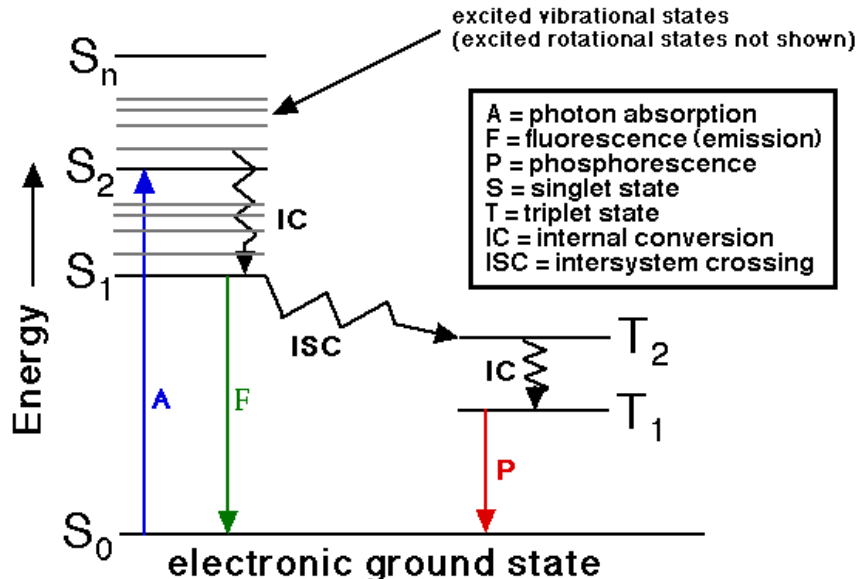


Figure 8: Jablonski diagram. An electron is excited by an energy source, and light is emitted when the electron returns to the ground state. This diagram shows possible routes that an excited electron can take when returning to the ground state. A rapid return to ground state results in fluorescence emission, and a slow return to ground state results in phosphorescence, after light crosses to the triplet state by intersystem crossing and undergoes internal conversion.

Using light of a certain wavelength, which corresponds to the absorbance wavelength of the molecule, an electron is excited from the ground state to any one of the singlet states, in this case, to the second singlet state. As the electron drops back to the ground state, not all the energy is emitted as light, but some of the energy is lost, usually as vibrational energy or heat. As a result, the emission wavelength is shifted to a higher wavelength than the excitation wavelength. If relaxation occurs by intersystem crossing, the electron can enter the triplet state and emit the energy as phosphorescence. ⁴⁰⁻⁴²

The FRET diagram (Figure 9) differs from the Jablonski diagram, in that a donor and acceptor are present in close proximity, because the donor and acceptor have to be in close proximity in order for significant energy transfer.

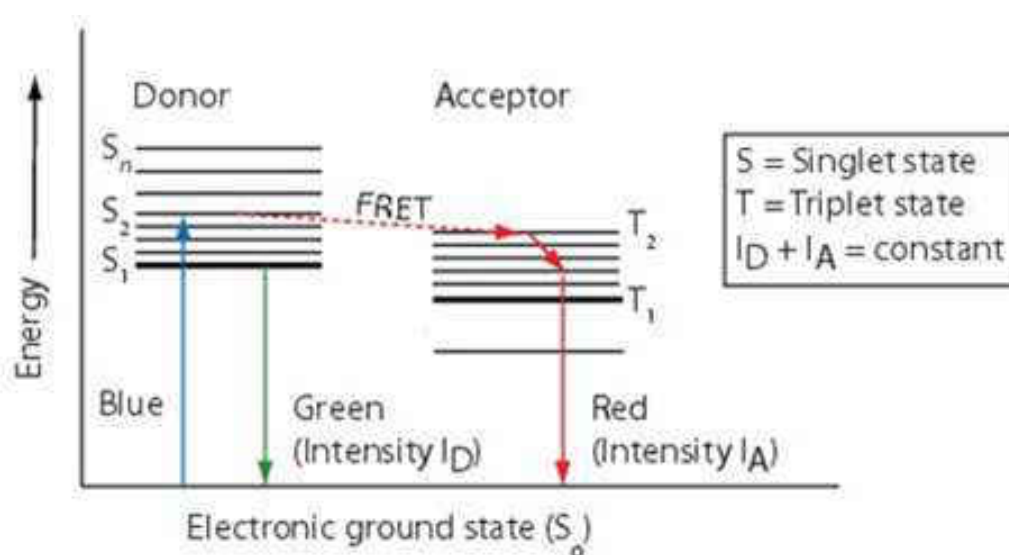


Figure 9: FRET diagram. The electron donor is excited to a singlet state, and energy is transferred to an electron acceptor through resonance transfer by overlapping emission spectra.

The donor is excited to a singlet state, and energy is transferred to the acceptor. This transfer is not radiative. The emission spectrum of the donor and the excitation spectrum of the acceptor must overlap, or cause resonance, in order for FRET to occur. As described in the following equation, the energy transfer is proportional to $(1/r)^6$, where r is the distance between the donor and the acceptor, which is typically around around 20-80 Å.⁴³

$$E = \frac{1}{1 + (r/R_0)^6}$$

The CCF4-AM FRET substrate is a membrane-permeable, non-fluorescent substrate, which crosses the plasma membrane and enters the cell cytoplasm, where esterases hydrolyze the esters in the substrate into carboxylic acids, causing the substrate to become fluorescent (Figure 10). The carboxylate groups of the substrate are derivatized as esters, in order to ensure the high permeability needed to cross cell membranes. In the absence of β -lactamase activity, the substrate remains intact.⁴ Excitation of the coumarin by 409 nm light results in FRET to fluorescein, which emits light at 530 nm (Figure 10).

In the presence of β -lactamase activity, the CCF4-AM substrate is cleaved at the β -lactam ring, which interrupts energy transfer, causes the fluorophores to separate, and terminates the FRET signal. Under these conditions, the excitation of coumarin results in the emission of fluorescence at 460 nm (Figure 10).⁴

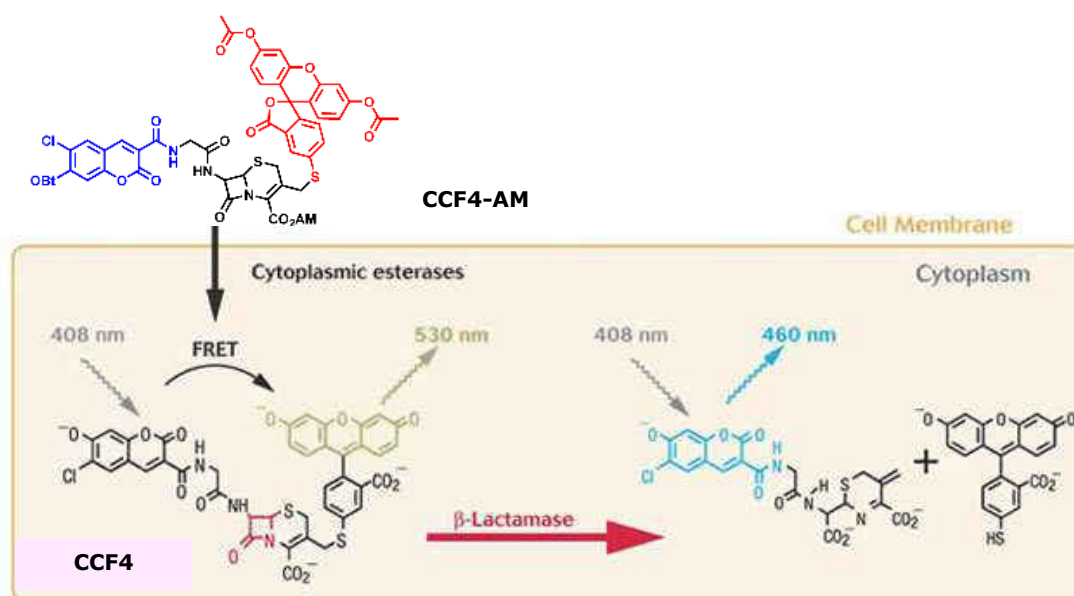


Figure 10: In-cell FRET diagram. The substrate permeates through the cell membrane and is cleaved by esterases to form a highly fluorescent compound, CCF4. Cleavage by β -lactamase releases the fluorescent coumarin derivative.

The expression of β -lactamase was quantified by measuring the ratio of the blue (460 nm) fluorescence to the green (530 nm) fluorescence.⁴ The CCF4-AM substrate works in conjunction with the *Hek 293T* cells, because the *Hek 293T* cells contain a β -lactamase reporter gene system. CBI inhibition of the VDR-coactivator interaction created a FRET signal, and showed that the β -lactamase was not formed. The opposite was true of VDR agonists, which activated the VDR-LBD and resulted in the transcription of the β -lactamase gene, which produced β -lactamase. The production of β -lactamase caused the substrate to be cleaved, and ultimately, a blue fluorescence emission.

Quantification of β -lactamase was accomplished by detecting the increase in FRET caused by inhibiting the enzymatic cleavage of the β -lactam-containing substrate, which was added after an incubation ranging from 5 to 24 hours. The cleaved substrate concentration was quantified by measuring the fluorescence emission at 460 nm, and the uncleaved substrate concentration was quantified by measuring the fluorescence emission at 530 nm.

Chapter 2.4: Gene BLAzer FRET Assay Methods

The *Hek 293T* cells were passaged using the methods described later in this chapter and resuspended in assay media at a concentration of 20,000 cells per well. The assay media contained 500 mL of phenol red-free Dulbecco's modified eagle medium (DMEM); 10 mL of charcoal-stripped FBS; 5 mL of sodium pyruvate; 5 mL of non-essential amino acids; and 5 mL of penicillin and streptomycin. The cells were counted by pipetting 30 μ L of cell suspension onto a hepatocytometer, giving the concentration of cells per mL.

The assay was performed with 30 μL per well, giving a concentration of 666,666 cells per mL, which was adjusted to 660,000 cells per mL.

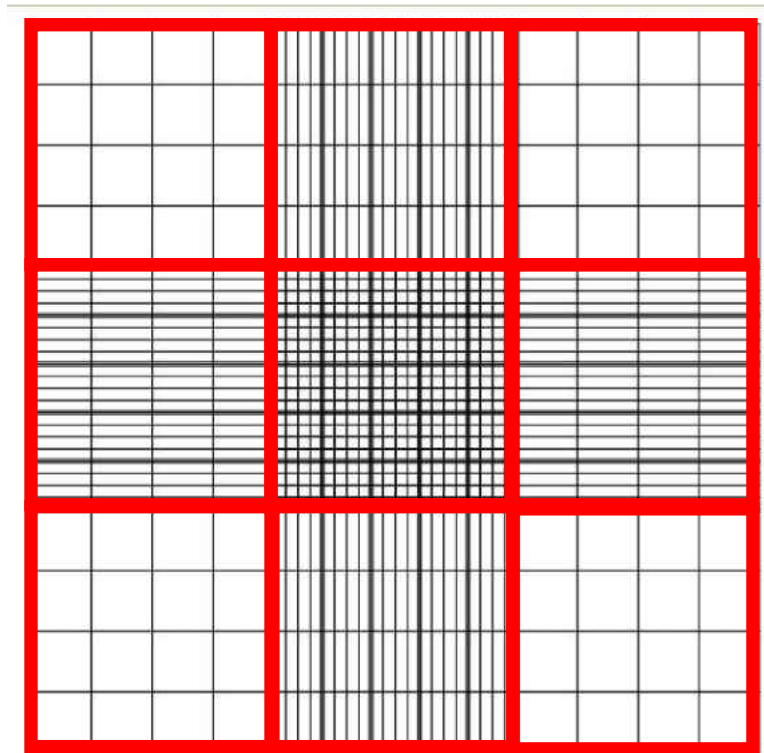


Figure 11: Hepatocytometer depiction. Approximately 30 μL of cell suspension was pipetted into this whole area. Cells were then counted in three separate red boxes and averaged. The volume of each of the red boxes was a 100 nL. Multiplication by 10,000 of the amount of cells counted gave the concentration of cells in cell per mL.

Matrigel solution was first pipetted into the 384-well black, clear bottom plate using a multi-channel pipette in the quantity of 30 μ L, and the 384-well plate was incubated at 37°C and 5 percent carbon dioxide for 15 minutes, in order to allow the cells to attach to the plate. The Matrigel solution is described later in this chapter. Then, 30 μ L of the cell suspension was pipetted into columns 1-23 of the same 384-well plate using a multi-channel pipette. Media only was pipetted into column 24 of the 384-well plate. The plate was incubated at 37°C and 5 percent CO₂ for times ranging from 2 to 24 hours.

The CBIs were transferred using a robotic pin tool transfer instrument, called the Tecan Freedom Evo liquid handler. This instrument allows for the transfer of 100 nL of liquid, which in this case, the liquid contained CBIs dissolved in DMSO. Controls for this assay were 1, 25-(OH)₂D₃ and LG 190178 (positives) and DMSO (negative). Two independent experiments were conducted in triplet or quadruplet for each of the Gene BLAzer assays.

After the 384-well plate containing the cells was incubated for 2 to 24 hours, 8 μ L of the FRET substrate was added to the wells for detection of the FRET signal using the Tecan Infinite M-1000 multi-label reader. The Tecan reader analyzed the excitation and emission of the blue and green fluorescence, and a ratio of the blue fluorescence to green fluorescence was determined.

Chapter 2.5: Fluorescence Detection

The excitation and emission of blue fluorescence were detected at 409 nm and 460 nm, respectively. The excitation and emission of green fluorescence were detected at 409 nm and 530 nm, respectively. The readings for the beginning assays were taken right after

centrifugation at 1 hour, 2 hours, 3 hours, and 4 hours after the addition of the FRET substrate. It was determined that the smallest standard deviation and highest signal window between the positive and negative controls were obtained after 3 hours of incubation at room temperature and in a dark environment. The fluorescence was read using the Tecan Infinite M-1000, which is a monochromator-based instrument.

The Tecan Infinite M-1000 spectrofluorimeter consists of the light source, the fluorescent top optics, the fluorescent bottom optics, and the fluorescence detector. The entire fluorescent optical system is illustrated in Figure 12.

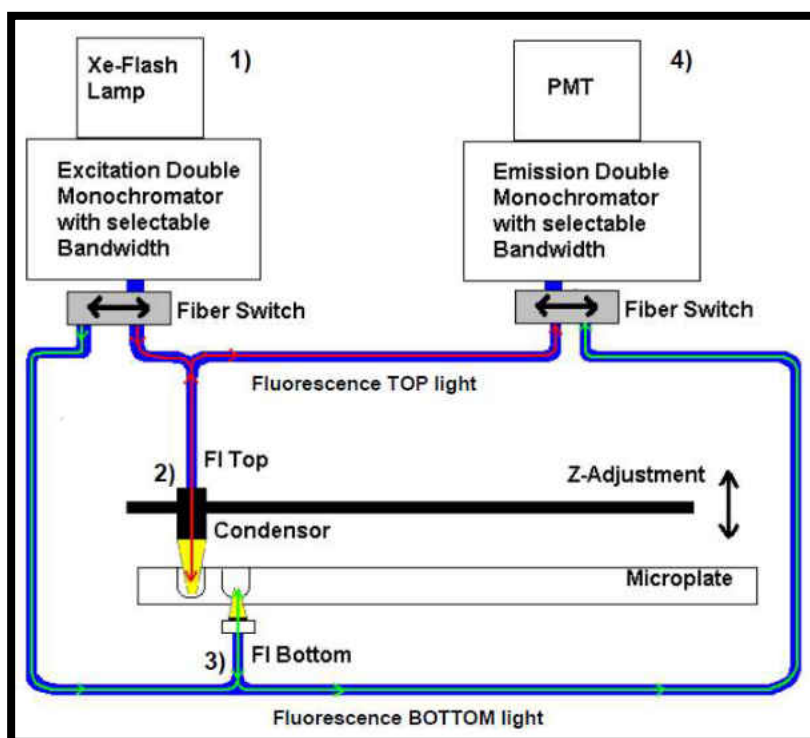


Figure 12: Entire fluorescent optical system, which consists of the light source, the fluorescent top and bottom optics, and the fluorescence detection unit.

The fluorescence optical path begins with the top light that continues from the light source to the top measurement head and to the photomultiplier tube (PMT). The

path of the fluorescent bottom light continues from the light source to the bottom measurement head, and to the PMT.

The light source system has the following components: flash lamp, condenser, order-sorting filter wheel, excitation double monochromator, fiber optic bundle, and flash lamp monitor. The flash lamp uses a high-energy xenon arc discharge lamp, where the flash sparks across a small gap between two electrodes and the lamp bulb, which contains a high pressure xenon atmosphere. The benefits of using a xenon flash lamp are high intensity from the deep ultraviolet region to the near infrared region, a long lifetime, and the ability to be used for a variety of applications.

The condenser focuses the light source onto the entrance slit of the excitation monochromator. A filter wheel is located between the condenser and the excitation monochromator and is set automatically, based on the programmed wavelength. The filter wheel contains wavelength-specific optical fibers, which are necessary to block undesired diffraction produced by the optical gratings (e.g. higher order energies). The excitation double monochromator is used to select desired wavelengths from the flash lamp spectrum in the range of 230 nm to 850 nm for fluorescence intensity.

A monochromator is an optical instrument that enables any wavelength to be selected from a defined optical spectrum, which consists of an entrance slit, a dispersive element, and an exit slit. The dispersive element diffracts the light and projects it onto the exit slit. A dispersive element can be realized by using a glass prism or an diffraction grating, which the later is used in the Tecan Infinite M-1000. Rotating the optical grating around its vertical axis moves the spectrum across the exit slit, and only a small part of the spectrum, or bandpass, passes through the exit slit. That means that when the

monochromator entrance slit is illuminated with white light, only light with a specific wavelength, or monochromatic light, passes through the exit slit. The wavelength of this light is set by the rotation angle of the optical grating. The bandwidth is set by the width of the exit slit.

Since monochromators only block undesired wavelengths to 10^3 , a second monochromator is needed in order to detect fluorescent light, because the detectable fluorescent light is much weaker than the excitation light. The second monochromator is connected in series, that is, the exit slit of the first monochromator acts as the entrance slit of the second monochromator, which allows for blocking to a factor of 10^6 . In this instrument, a double monochromator is on both the excitation and emission side.

The fiber optic bundle guides the light from the exit slit of the excitation monochromator, either to the top measuring optics or the bottom measuring optics. The bottom fluorescent optical system, which is identical to the top fluorescent optical system, is illustrated in Figure 13.

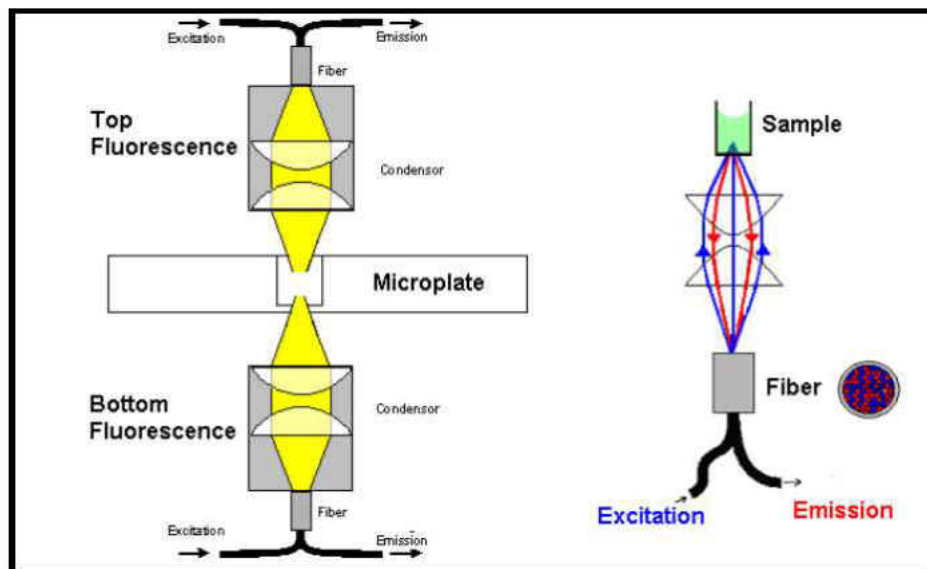


Figure 13: Schematic diagram of spectrofluorimeter showing the optics for reading both above and below the microplate. Fluorescence optics used for top and bottom reading of fluorescence intensity measurement. The right-hand side is an enlargement of the bottom fluorescence measurement, which is similar to the top fluorescence measurement.

The lower end of each fiber bundle acts as a color-specific light source. In both cases, a small portion of the light is guided to the flash lamp monitor diode. The flash lamp monitor is a silicon photodiode that takes single flash light variations into account and compensates for them.

The fluorescence fiber bundle that is plugged into the top and bottom measuring head contains both excitation and emission fibers. The emission fibers guide the fluorescent light to the emission monochromator head, where a lens system focuses the light onto the entrance slit of the emission monochromator.

The fluorescence detection system is used for measuring both fluorescence from above and fluorescence from below the microplate wells. The fluorescent light is focused onto the entrance slit of the emission monochromator. After passing through the

monochromator, the light passes through the filter wheel and is focused on the detector (PMT).

The emission monochromator is used to select any wavelength of fluorescent signal. It acts like an adjustable filter in wavelength and bandwidth to discriminate scatter of excitation light and non-specific fluorescence. The filter wheel contains wavelength specific optical fibers, which are necessary to block undesired diffraction produced by the optical gratings. The PMT is used for the detection of fluorescent low light levels, and electronic circuitry uses analog to digital conversion of PMT output current.

The Z-position of the fluorescence top optics helps to maximize the signal to noise ratio, as light is refracted at the sample's liquid surface. The fluorescence intensity lens system of both the top and bottom optics is designed to focus the excitation light at the exit side of the bundle, which acts as a color-specific light source, into the sample. The lens also collects the fluorescent light and focuses it back onto the fluorescence fiber bundle. The objective lenses are made from fused silica, which provides high ultraviolet transmission and eliminates most auto-fluorescence.

In summary, the flash light is focused by the condenser on the entrance slit of the excitation monochromator. The wavelength and bandwidth of the excitation light are selected within the monochromator. After passing through the monochromator, the excitation light is coupled into a fiber bundle guiding the light to the top or bottom measuring heads. The light is then focused into the sample by the top or bottom lens system. The fluorescent emission light is collected by the top or bottom lens system again, coupled into the fluorescence fibers bundle, and guided to the detection system.

The blue fluorescence emission, and then the green fluorescence emission, of the assay wells that were quantified by using the Tecan Infinite M-1000 instrument were displayed in an Excel spreadsheet across the row of the 384-well plate.

This raw data was applied to another spreadsheet in order to reorganize the data, to subtract the average of the background of the assay media from the wells, to determine the trend in blue fluorescence, to determine the trend in green fluorescence, to determine the ratio of blue to green fluorescence, to determine the averages of the positive and negative controls, to determine the standard deviation of the positive and negative controls and to determine the Z prime value as shown in Figure 14. The data was arranged into columns of descending concentrations for each CBI, and to group multiple plates for the same batch of cells in triplet or quadruplet.

The average values (n =3 or 4) were analyzed with Graph Pad Prism 5. Any data points that fell outside of three times the standard deviation were discarded. The two-dimensional graphs consisted of the ratio of blue to green fluorescence on the y-axis and the logarithm of the concentration of agonist or CBI on the x-axis. The best-fit non-linear regression was color-coded to match the legend for that molecule. The compounds that fit the sigmoidal graph shape were determined to be the most promising compounds, and an IC₅₀ value for each of these sigmoidal graphs was determined.

$$Z' = 1 - \left(\frac{3 * (\text{STD Positive Control} + \text{STD Negative Control})}{|\text{Average of the Positive Control} - \text{Average of the Negative Control}|} \right)$$

Figure 14: Z prime calculation. The Z prime value indicates the correlation of the experimental data. Z prime values from 0.50 to 1.0 indicate useful data sets.

Chapter 2.6: *Hek 293T* Cell Culture Methods

A 1 mL tube with commercially available *Hek 293T* cells was first thawed and pipetted into 10 mL of growth media. The growth and thawing media contained 500 mL of phenol red DMEM with Glutamax (L-glutamate); 50 mL of heat-inactivated and dialyzed FBS; 5 mL of 0.1 mM non-essential amino acids (glycine (750mg/L), L-alanine (890 mg/L), L-asparagine (1320 mg/L), L-aspartic acid (1330 mg/L), L-glutamic acid (1470 mg/L), L-proline (1150 mg/L), and L-serine (1050 mg/L)); 5 mL of HEPES buffer at pH 7.3, which maintains a physiological pH, despite carbon dioxide changes from respiration; and 5 mL of 100 µg/mL Penicillin and Streptomycin. The cell suspension was centrifuged at 1,000 rpm for 2 minutes. The supernatant was aspirated from the top, the cells were resuspended in 1 mL of media, and the cells were introduced into a tissue cell culture flask, which had been pre-coated with 3 mL of Matrigel matrix solution and contained 14 mL of growth media.

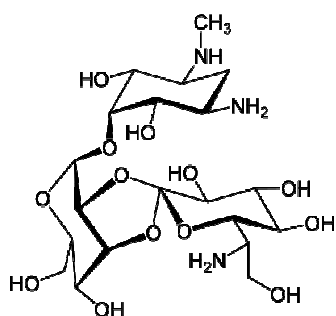
The Matrigel matrix solution contained 100 mL of phenol red-free DMEM and 250 µL of Matrigel concentrate and was used to coat the bottom of the tissue cell culture flasks and the 384-well plates prior to introducing the cells to the flasks and to the plates. Matrigel is a protein that is extracted from moose sarcoma cells and simulates the cell growth environment; therefore, Matrigel facilitates the attachment of the cells to the bottom of the tissue culture flasks. The 3 mL of Matrigel that had been added to the bottom of the tissue culture flasks coated the entire bottom surface of the flasks. The flasks with the Matrigel solution were incubated at 37°C and 5 percent carbon dioxide for 15 minutes. The Matrigel solution was aspirated, and the 14 mL of growth media was added to the flasks.

The amount of Zeocin added directly to the culture flasks was 12 μL , later changed to 15 μL , which corresponds to a final concentration of 80 $\mu\text{g/mL}$, later changed to 100 $\mu\text{g/mL}$. The same concentration was used for Hygromycin B, but 24 μL was added directly to the culture flasks, which was later changed to 30 μL of Hygromycin B to a concentration of 80 $\mu\text{g/mL}$, later changed to 100 $\mu\text{g/mL}$. This amount of antibiotics was added to the tissue culture flasks each time the cells were propagated.

Hygromycin B is an aminoglycosidic antibiotic which is produced by *Streptomyces hygroscopicus* (Figure 15A). The antibiotic inhibits protein synthesis by affecting mRNA translation, which is achieved by inducing the misreading of aminoacyl-tRNA through the distortion of the ribosomal active (A) site.

Zeocin is a copper-chelated glycopeptide which has been isolated from *Streptomyces verticillus* (Figure 15B). When the antibiotic enters the cell, the copper cation is reduced from Cu^{2+} to Cu^+ and binds to sulfhydryl-containing proteins in the cell. Removing the copper cation from the antibiotic complex activates Zeocin. Once Zeocin is activated, it binds to DNA and cleaves it, causing cell death.

A



B

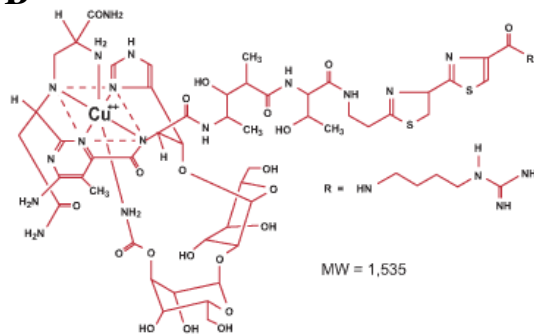


Figure 15: Hygromycin B (15A) and Zeocin (15B) antibiotic structures.

The cells were cultured to 70 to 95 percent confluency in the 15 mL solution of growth media and antibiotics from 2 to 5 days. Once the cells reached an appropriate confluency, the cells were washed with 10 mL of PBS without calcium ions and detached from the tissue culture flasks using 3 mL of 0.5 percent trypsin.

Trypsin is a protease enzyme which degrades proteins by hydrolysis and has an optimum working pH of 7 to 9. Trypsin is derived from trypsinogen in the pancreas by removing a terminal peptide from the trypsinogen. It is a highly discriminating protease, because it only cleaves amide and ester bonds at the carboxyl terminal side of arginines and lysines. Trypsin is inhibited by organophosphorous compounds which target serine in the active site of the enzyme. FBS contains a natural inhibitor of trypsin.

The cells were incubated for 3 to 5 minutes with the trypsin at 37°C and 5 percent carbon dioxide. The cell suspension was mixed by pipette and added to 7 mL of growth media in a conical tube, followed by 5 minutes of centrifugation at 1,000 rpm. The growth media was aspirated from the top of the cells, pelleted on the bottom of the conical tube, resuspended in 3 mL growth media, and 1 mL of this cell suspension was introduced to each new culture flask.

Chapter 2.7: Summary of the Results of the Gene BLAzer Assay

As discussed previously, *Hek 293T* cells were drugged with calcitriol ligand and CBIs, in order to determine the CBI's ability to inhibit VDR-mediated transcription using the described Gene Blazer assay. The summary of the structures of CBIs tested and their activities are compiled in Table 7 in Appendix A.

Figures 16 through 26 and Figure 28 represent the dose-response activity of all CBIs investigated. The graphs show the ratio of blue to green fluorescence, the blue fluorescent signal, and the green fluorescent signal for each compound. The reduced ratio of blue to green fluorescence is an indicator of the ability of CBIs to inhibit the transcription of VDR. The amount of blue fluorescent signal is directly related to the transcription of the *lactamase* gene, and consequently, to the activation of VDR. A blue fluorescent signal is an indication that the cleavage of the Gene BLAzer fluorescent substrate at the β -lactam ring by the β -lactamase enzyme occurs and that blue fluorescence is emitted by the Gene BLAzer fluorescent substrate.

The amount of green fluorescent signal is proportional to the amount of transcriptional inhibition of the *lactamase* gene mediated by VDR. The green fluorescent signal is an indication that no cleavage of the Gene BLAzer fluorescent substrate at the β -lactam ring by the β -lactamase enzyme occurs. The inhibition of the cleavage of the Gene BLAzer fluorescent substrate shows the ability of the CBIs to inhibit the transcription of VDR. Active CBIs will inhibit the VDR-mediated transcription of the *lactamase* gene, resulting in a lower blue fluorescent signal and a higher green fluorescent signal, as the concentration increases. The decrease in green fluorescent signal also shows the toxicity of the small molecules. Both signals should be inversely proportional; thus, giving a robust additive signal when divided, as described in the introduction. The IC_{50} values were determined using the following non-linear regression equation.

$$Y = \text{Bottom} + (\text{Top} - \text{Bottom}) / (1 + 10^{(\text{Log } IC_{50} - X) * \text{Hill Slope}}).$$

The IC_{50} value is half of the maximum inhibitory concentration that measures the effectiveness of a compound in inhibiting a biological function, in this case, transcription inhibition.

Chapter 2.8: Detailed Results and Figures of the Gene BLAzer Assay

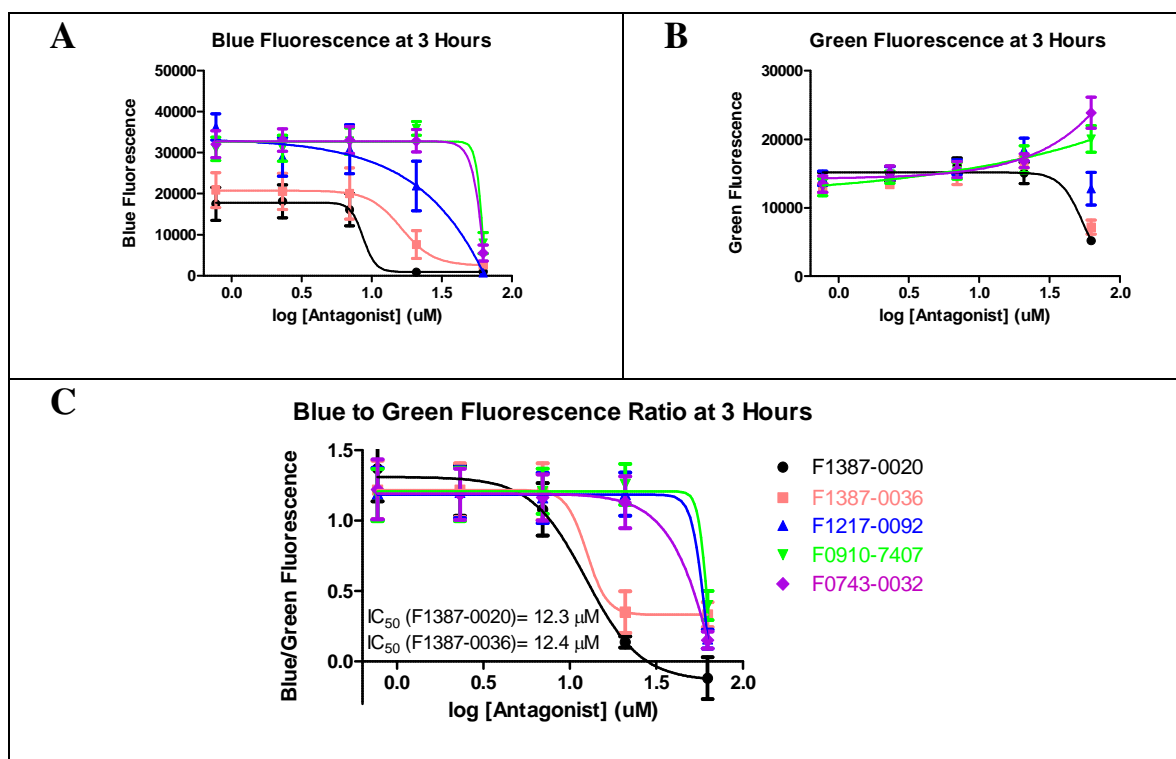


Figure 16: Inhibition of VDR-mediated transcription of compounds F1387-0020, F1387-0036, F1217-0092, F0910-7407, and F0743-0032.

Compounds F1387-0020, F1387-0036, F1217-0092, F0910-7407, and F0743-0032 all decreased in blue fluorescence after 3 hours at the highest concentration tested (Figure 16A). The activity can be interpreted that transcription increased with decreasing

concentration, thereby giving an increased blue signal as the graph goes from a higher to a lower concentration, and giving a decreased green signal as the graph goes from a higher concentration to a lower concentration. Compounds F0910-7407, F0743-0032, and F1217-0092 were less active than compounds F1387-0020 and F1387-0036. The IC_{50} values of compounds F1387-0020 and F1387-0036 were 12.3 μ M and 12.4 μ M, respectively (Figure 16C). In addition, compounds F1387-0020 and F1387-0036 were slightly more toxic than the other compounds in this compound set at higher concentrations, indicated by the decrease in green fluorescent signal (Figure 16B).

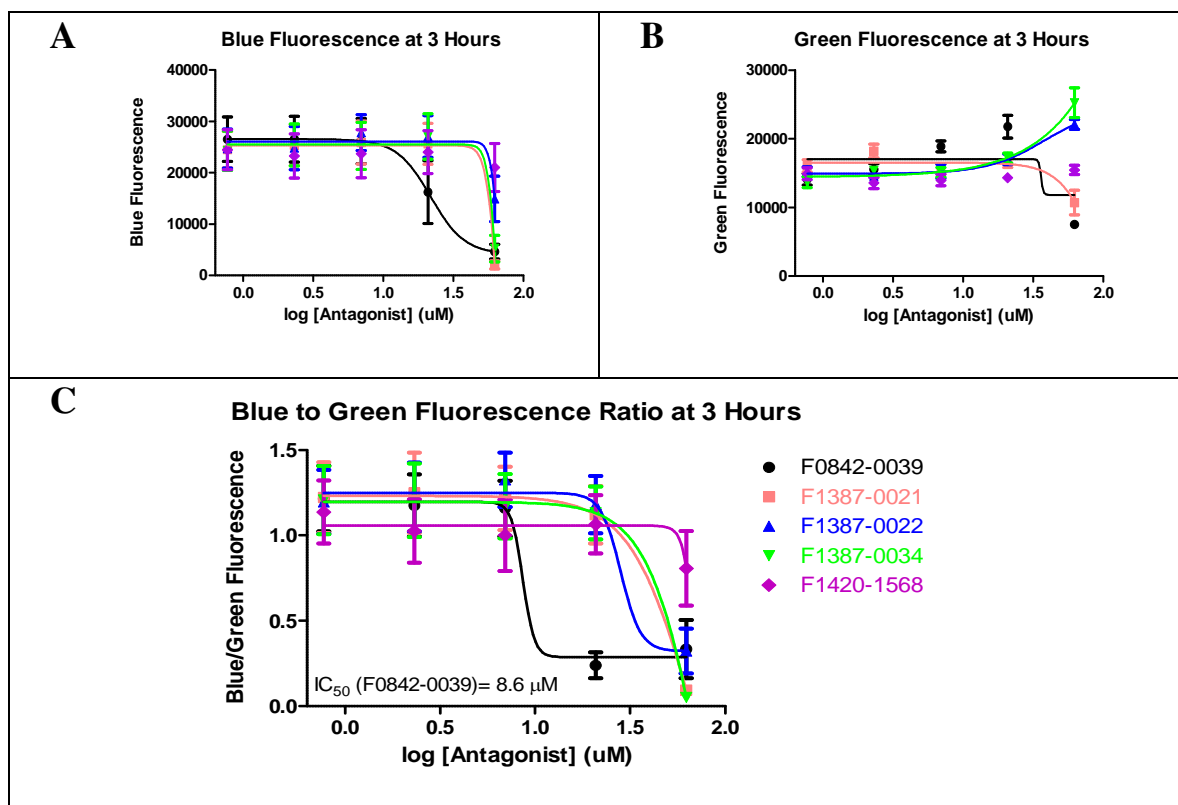


Figure 17: Inhibition of VDR-mediated transcription of compounds F0842-0039, F1387-0021, F1387-0022, F1387-0034, and F1420-1568.

Compounds F0842-0039, F1387-0021, F1387-0022, F1387-0034, and F1420-1568 all decreased in blue fluorescence after 3 hours at the highest concentration tested, which is equivalent to a decreased amount of β -lactamase transcribed by VDR (Figure 17A). Interestingly, only compounds F0842-0039, F1387-0022, and F1387-0034 exhibited an increased green fluorescent signal at higher concentrations, resulting from uncleaved substrate (Figure 17B). The most active compound of the 5 compounds in this compound set was compound F0842-0039, with an approximate IC_{50} value of 8 μ M. Compound F0842-0039 exhibited a decrease in the blue fluorescent signal and an increase in the green fluorescent signal (Figure 17C). Additionally, signs of high toxicity were observed at the highest concentration of 62.5 μ M for all compounds, except compound F1420-1568, which is depicted by the decreased green fluorescent signal at that concentration (Figure 17B).

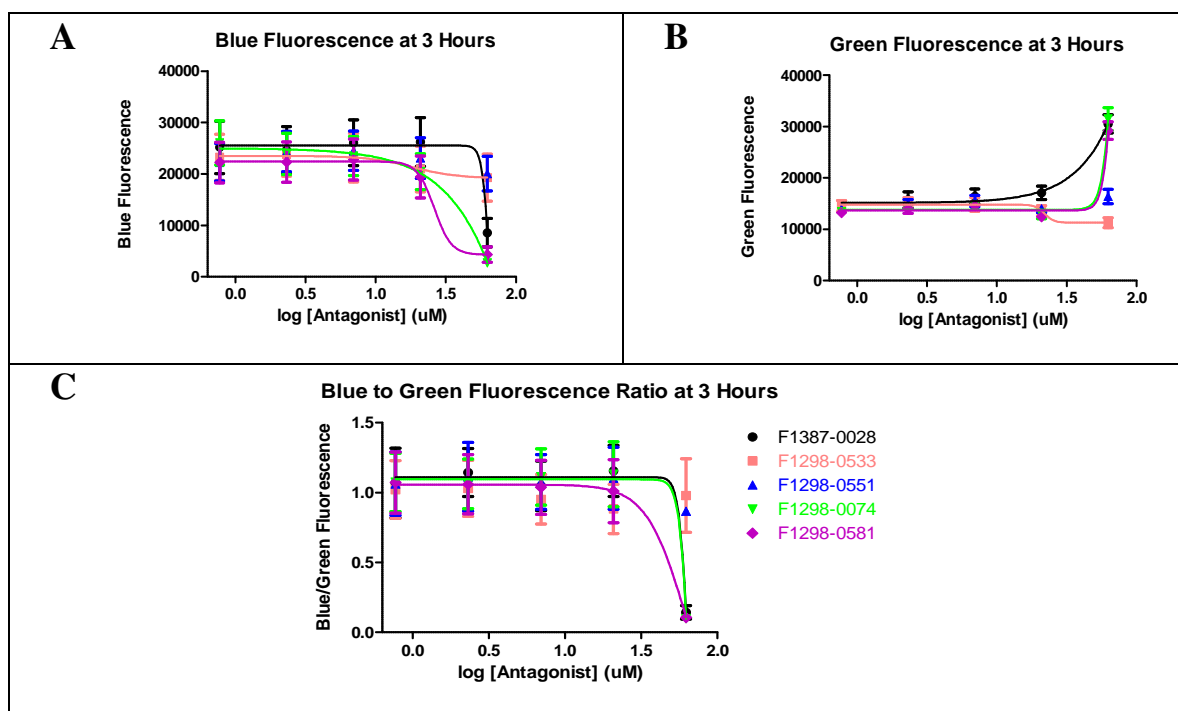


Figure 18: Inhibition of VDR-mediated transcription of compounds F1387-0028, F1298-0533, F1298-0551, F1298-0074, and F1298-0581.

Compounds F1387-0028, F1298-0533, F1298-0551, F1298-0074, and F1298-0581 all decreased in blue fluorescence after 3 hours at higher concentrations (Figure 18A). Only compounds F1387-0028, F1298-0074, and F1298-0581 exhibited an increased green fluorescent signal at the highest concentrations tested (Figure 18B). Because only the highest concentration showed a change of signal for all five compounds, it was not possible to calculate reliable IC_{50} values for these compounds.

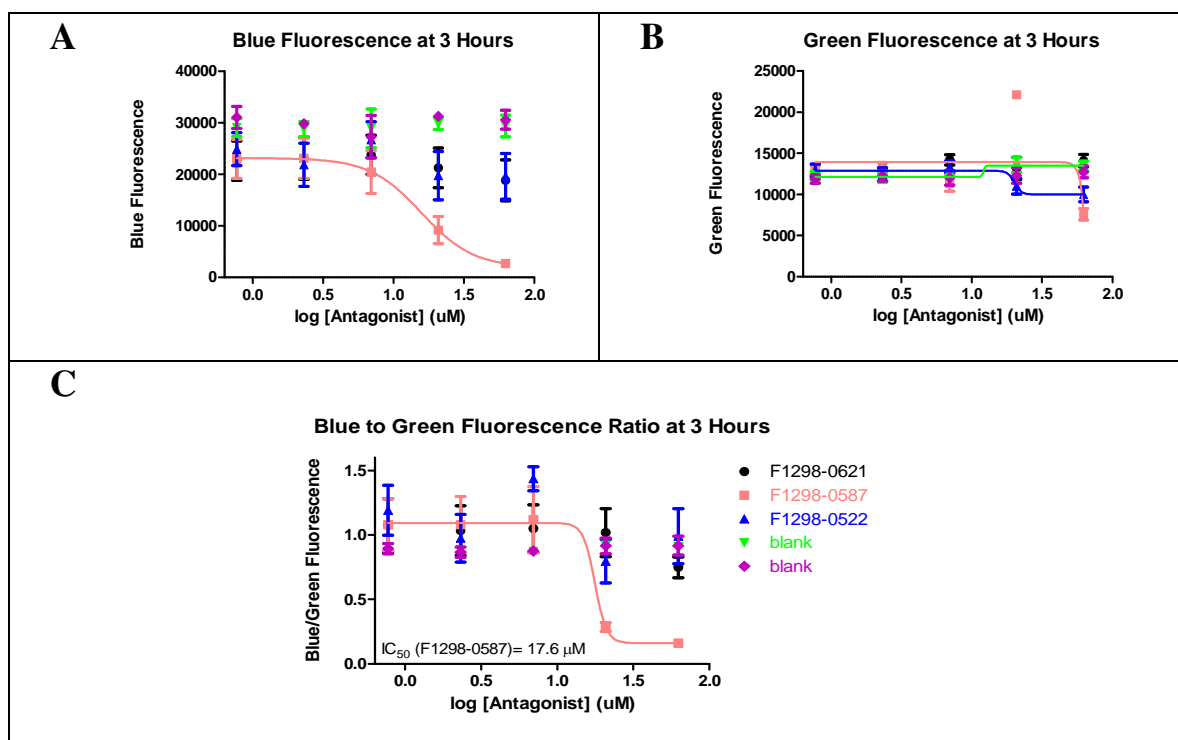


Figure 19: Inhibition of VDR-mediated transcription of compounds F1298-0621, F1298-0587, and F1298-0522.

Among the 3 compounds tested in this compound set, F1298-0621, F1298-0587, and F1298-0522, only compound F1298-0587 decreased in blue fluorescence after 3 hours at higher concentrations (Figure 19A). Additionally, two experiments with vehicle DMSO were added as a negative control. Only compound F1298-0587 showed an increased green fluorescent signal at a concentration of 21 μ M, which decreased at the highest concentration tested. It can be concluded that only compound F1298-0587 was able to inhibit VDR-mediated transcription, because it had an IC_{50} value of 17.6 μ M and was toxic at 62.5 μ M (Figure 19C).

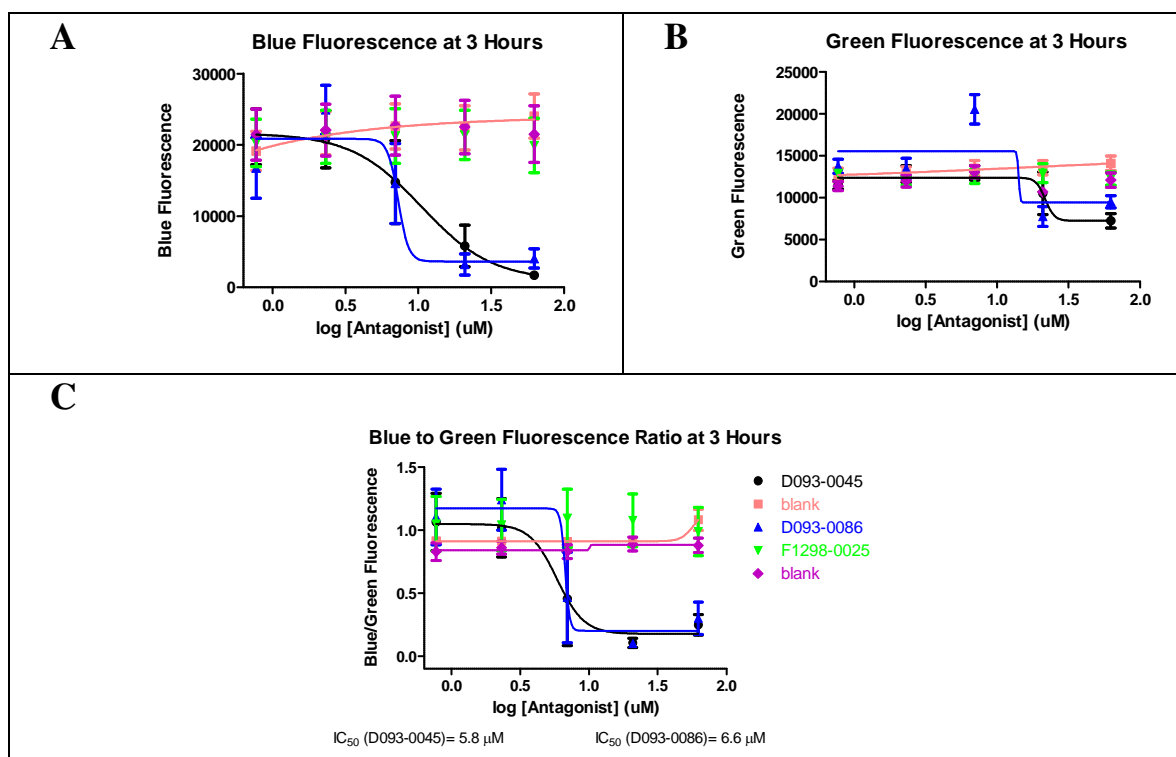


Figure 20: Inhibition of VDR-mediated transcription of compounds D093-0045, D093-0086, and F1298-0025.

Compounds D093-0045 and D093-0086 decreased in blue fluorescence after 3 hours at higher concentrations (Figure 20A). Additionally, two experiments with vehicle DMSO were added as a negative control. Although there was a decrease in blue fluorescent signal for compound D093-0086, it can be concluded that it was not an active compound. The IC₅₀ values for compounds D093-0045 and D093-0086 were 5.8 μ M and 6.6 μ M, respectively (Figure 20C).

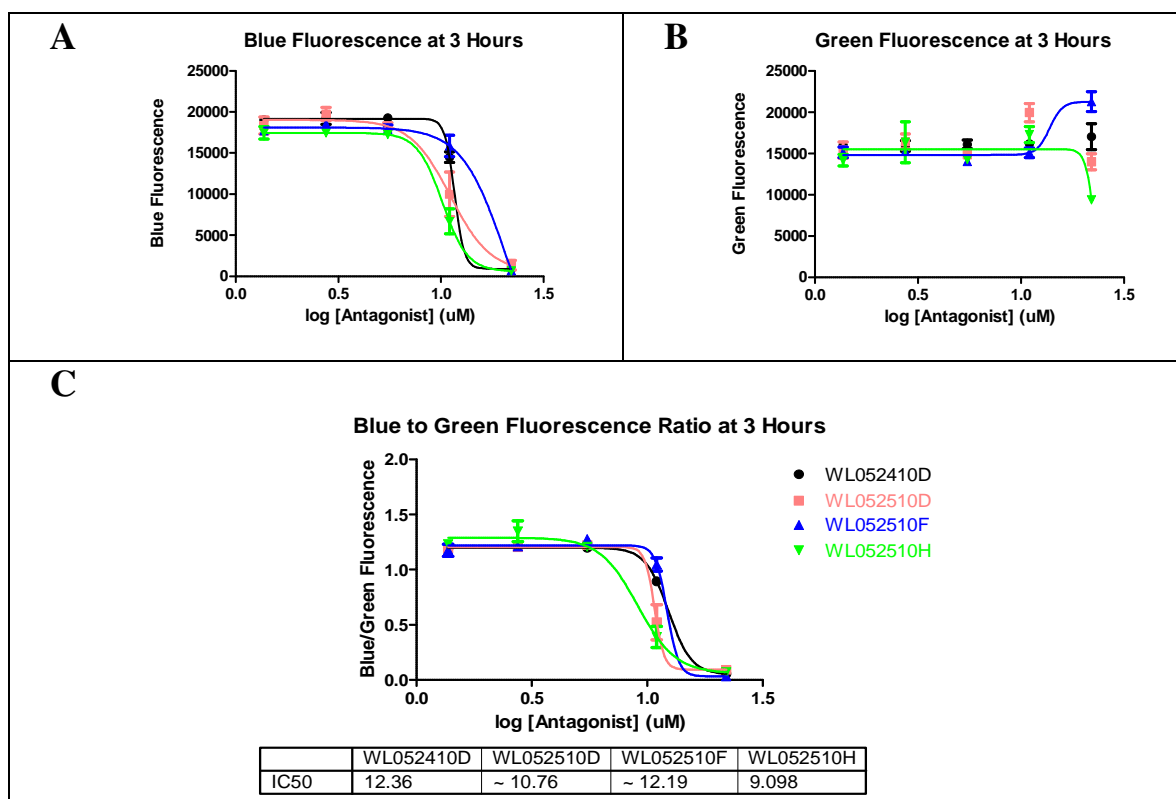


Figure 21: Inhibition of VDR-mediated transcription of compounds WL052410D, WL052510D, WL052510F, and WL052510H.

Compounds WL052410D, WL052510D, WL052510F, and WL052510H, which were all based on the same chemical scaffold, decreased in blue fluorescence after 3 hours at higher concentrations (Figure 21A). Compounds WL052510D and WL052510H were more active than compounds WL052410D and WL052510F. Consequently, for compounds WL052510D and WL052510H, an increased green fluorescent signal was observed at 3.3 μ M, which indicated inhibition of VDR-mediated transcription (Figure 21B). Toxicity at the highest concentrations was observed for all compounds. The IC₅₀ values for all 5 compounds ranged from 9.1 to 12.4 μ M (Figure 21C).

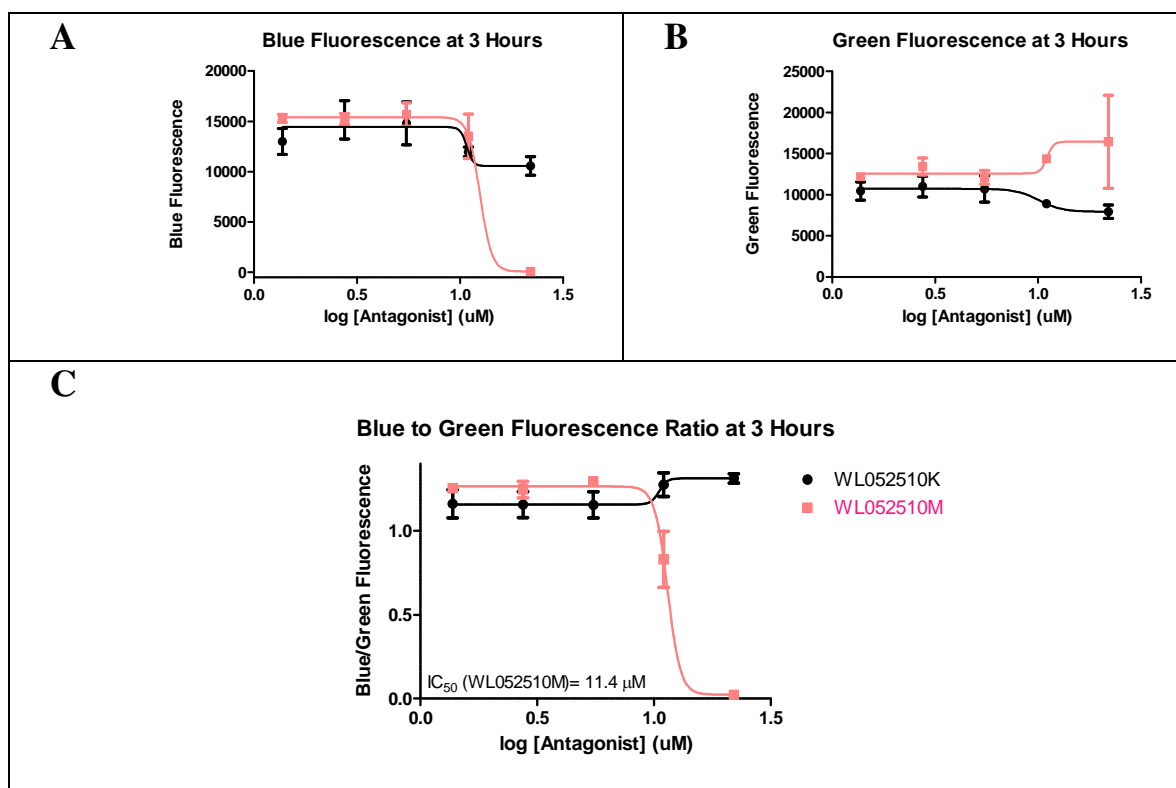


Figure 22: Inhibition of VDR-mediated transcription of compounds WL052510K and WL052510M.

From the 2 compounds tested in this compound set, only compound WL052510M exhibited a decrease in blue fluorescence after 3 hours at the higher concentrations (Figure 22A). As expected, the green fluorescent signal of compound WL052510M increased with higher concentration (Figure 22B). The IC₅₀ value for compound WL052510M was 11.4 μ M, and compound WL052510K was not an active compound (Figure 22C).

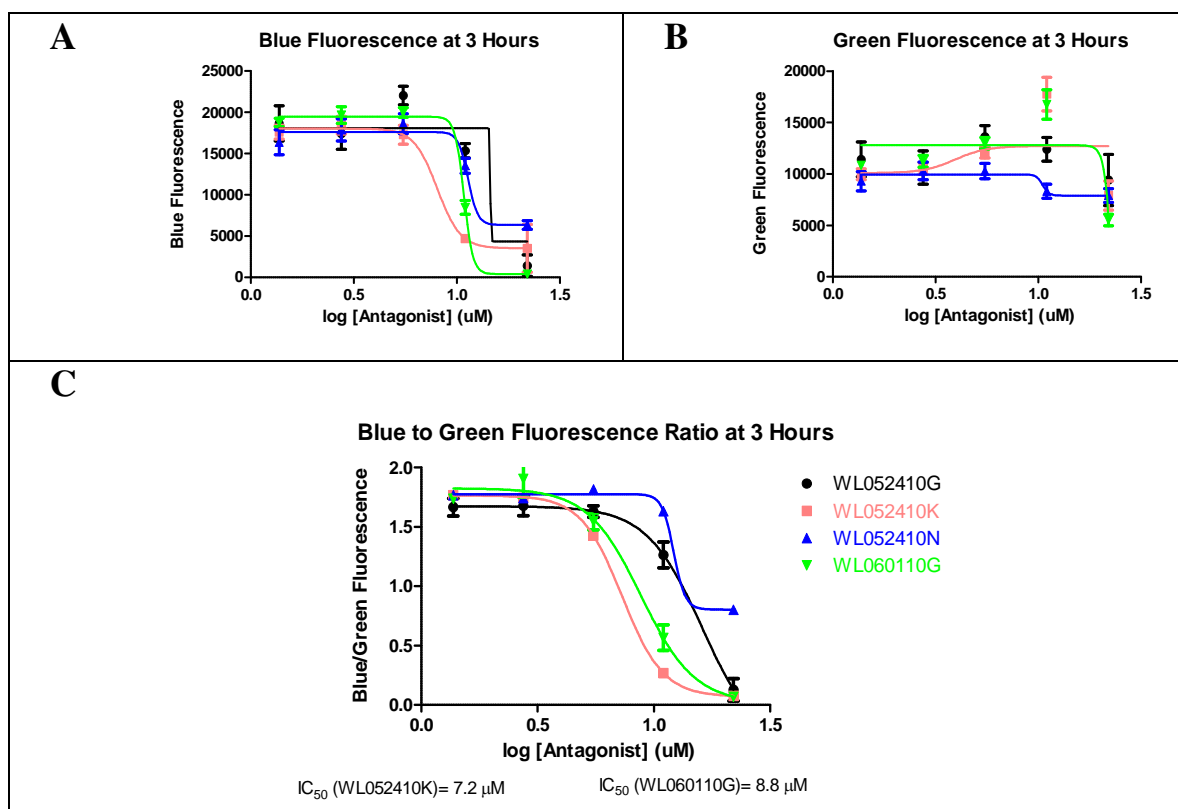


Figure 23: Inhibition of VDR-mediated transcription of compounds WL052410G, WL052410K, WL052410N, and WL060110G.

Compounds WL052410G, WL052410K, WL052410N, and WL060110G all decreased in blue fluorescence after 3 hours at higher concentrations (Figure 23A). The green fluorescent signal was significantly increased for compounds WL052410K and WL060110G at a concentration of 3.3 μ M, but reduced at 10 μ M, due to toxicity. Compounds WL052410G and WL052410N showed no increase at all in green fluorescent signal, which is most likely due to a very small window between activity and toxicity; therefore, no IC₅₀ values are given for these compounds. However, the IC₅₀ values of compounds WL052410N and WL060110G were 7.2 μ M and 8.8 μ M, respectively (Figure 23C).

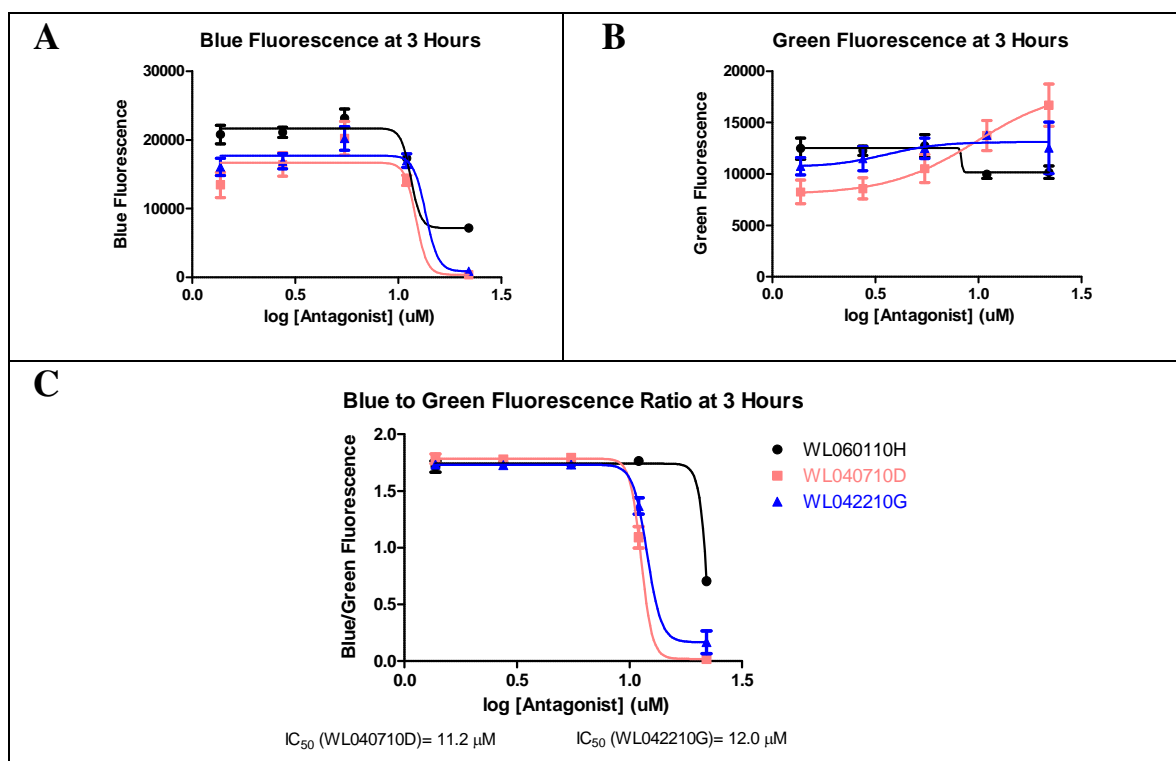


Figure 24: Inhibition of VDR-mediated transcription of compounds WL060110H, WL040710D, and WL042210G.

Compounds WL060110H, WL040710D, and WL042210G all decreased in blue fluorescence after 3 hours at higher concentrations (Figure 24A). The green fluorescent signal was increased for compound WL040710D (Figure 24B). It can be concluded that both compounds WL040710D and WL042210G were very active, with IC₅₀ values of 11.2 μM and 12.0 μM, respectively (Figure 24C).

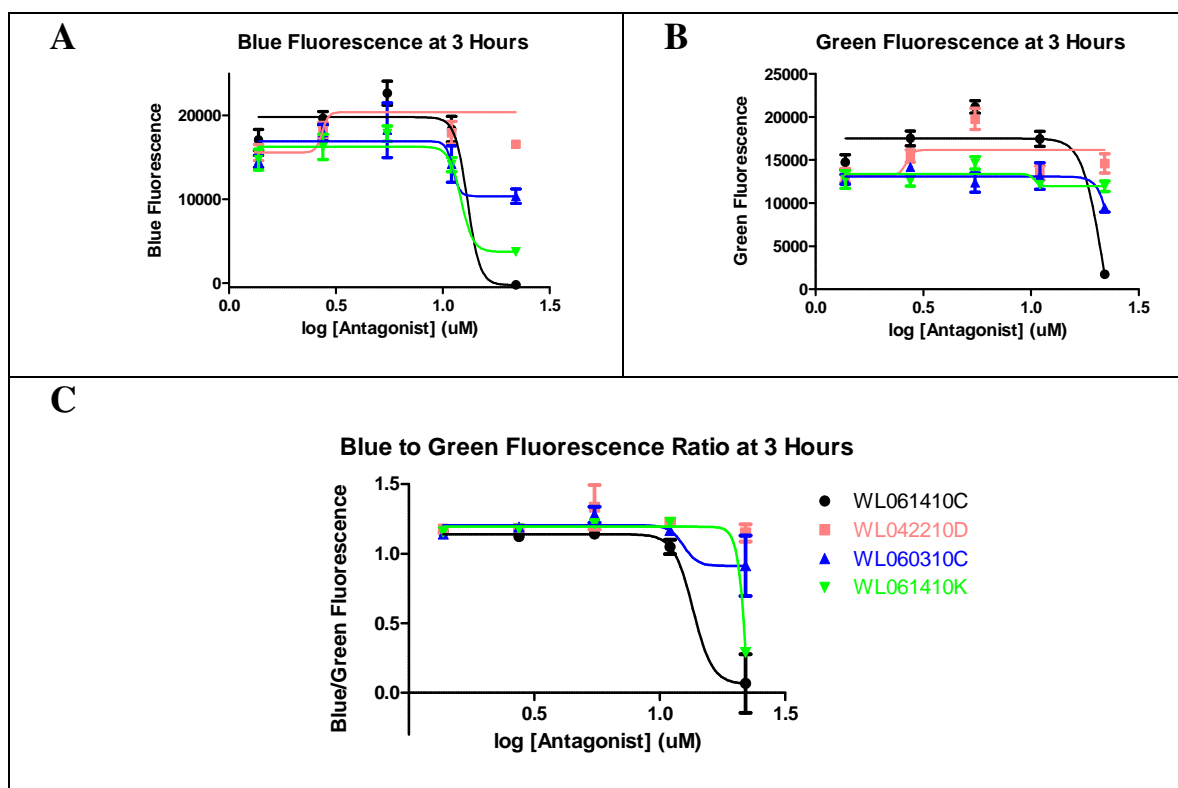


Figure 25: Inhibition of VDR-mediated transcription of compounds WL061410C, WL042210D, WL060310C, and WL061410K.

Among all of the compounds tested in this compound set, only compounds WL061410C, WL060310C, and WL061410K decreased in blue fluorescence after 3 hours at the highest concentration tested (Figure 25A). None of the compounds showed an increase in green fluorescent signal, but rather, a decrease in green fluorescent signal; therefore, accurate IC_{50} values for these four compounds were unable to be determined (Figure 25B).

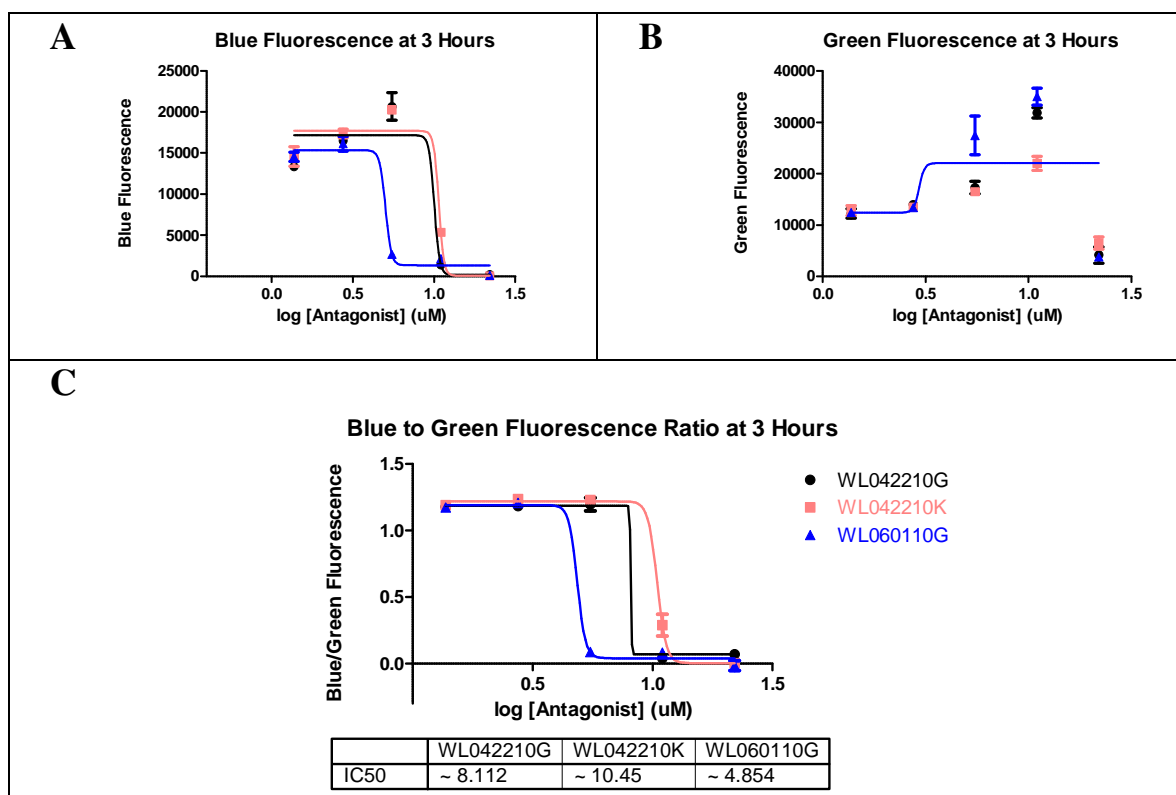


Figure 26: Inhibition of VDR-mediated transcription of compounds WL042210G, WL042210K, and WL060110G.

Compounds WL042210G, WL042210K, and WL060110G all decreased in blue fluorescence after 3 hours at the higher concentrations (Figure 26A). Accordingly, the green fluorescent signal increased for all compounds, except for the highest concentration of 25 μ M; thus, all 3 compounds were active, with IC₅₀ values of 8.1 μ M, 10.4 μ M, and 4.8 μ M, respectively (Figures 26B and 26C).

Another compound identified by HTS as a potential CBI of VDR was compound GW 0742 (Figure 27). The inhibition of transcription mediated by VDR was determined twice in quadruplet, as depicted in Figure 28.

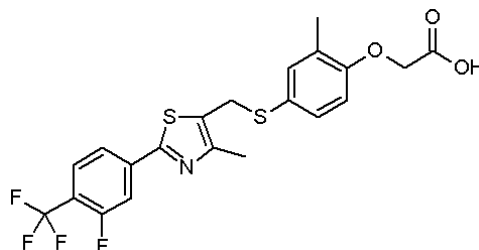


Figure 27: Structure of compound GW 0742.

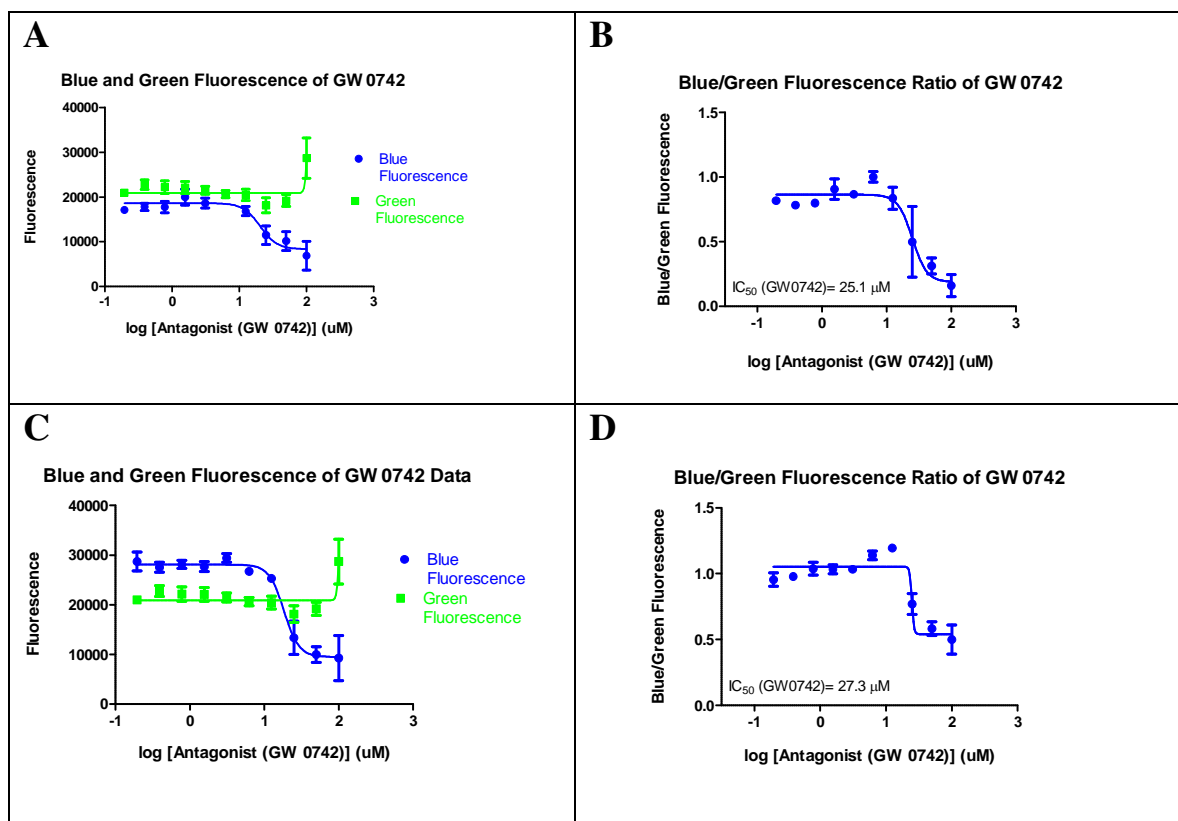


Figure 28: Inhibition of VDR-mediated transcription of compound GW 0742.

The 2 measurements for compound GW0742 show reproducible data. The blue fluorescent signal decreased at higher concentrations after 3 hours, whereas the green fluorescent signal was the highest at the highest concentration tested at 3 hours, as seen in Figures 28A and 28C. Both results show that compound GW 0742 inhibited VDR-mediated transcription, with IC₅₀ values between 25.1 μ M and 27.3 μ M.

Compound GW 0742 was introduced by GlaxoSmithKline in 2003 as a highly selective agonist for PPAR δ .⁴⁴ Since then, compound GW 0742 has been investigated in cell-based assays and *in vivo*, in order to understand the role of PPAR δ in hypertension,⁴⁵ diabetes,⁴⁶ inflammation,^{47, 48} obesity,^{49, 50} and cancer.⁵¹ Interestingly, PPAR agonists have been shown to inhibit the transcription of the VDR target gene, *CYP24A1*, in the presence of 1, 25-(OH)₂D₃;⁵⁵ therefore, compound GW 0742 was tested for transcription inhibition and cytotoxicity. It was determined that at micromolar concentrations, compound GW 0742 behaved as an antagonist of VDR.⁵⁶

Chapter 2.9: Discussion of the Results of the Gene BLAzer Assay

In total, 39 compounds were investigated with respect to their ability to inhibit transcription mediated by VDR. Interestingly, many different scaffolds were able to modulate gene regulation; however, high toxicity was a concern with some of these molecules. The class of 3-indolyl methanamines (compounds F0842-0039, F1217-0092, F1387-0028, F1387-0021, F1387-0036, F0743-0032, F1387-0020, F1387-0034, and F1387-0022) was identified as the superior class of irreversible inhibitors of the VDR-coactivator interaction. These compounds were shown to inhibit this interaction in *Hek*

293T cells, which led to inhibition of transcription. The results presented previously in this chapter are published in Nandhikonda et al.²⁹

The 3-indolyl methanamine class varied in aromatic substituents. Compound F0842-0039 had a phenol group; compound F1217-0092 had a para toluene group; compound F1387-0028 had a meta anisole group; compound F1387-0021 had a meta bromobenzene group; compound F1387-0036 had a para bromobenzene group; compound F0743-0032 had a para fluorobenzene group; compound F1387-0020 had a para xylene group; compound F1387-0034 had a meta chlorobenzene group; and compound F1387-0022 had a meta fluorobenzene group.

Of these compounds, compound F0842-0039, which had a phenol group and an IC₅₀ value of 8.6 μ M; compound F1387-0036, which had a para bromobenzene group and an IC₅₀ value of 12.4 μ M; and compound F1387-0020, which had a para xylene group and an IC₅₀ value of 12.3 μ M, were the most active. The rest of the compounds in this class showed little to no transcriptional inhibition. Of the remaining commercially available compounds, only compound F1298-0587 and compound D093-0045 had only a slight potential for transcription inhibition.

Of the compounds synthesized from the 3-indoyl methanamines, compounds WL052410D (30c), which had an anisole group and an IC₅₀ value of 12.4 μ M; WL052510D (30a), which had a benzene group and an IC₅₀ value of 10.8 μ M; WL052510F (30d), which had a toluene group and an IC₅₀ value of 12.2 μ M; WL052510H (30b), which had a chlorobenzene group and an IC₅₀ value of 9.1 μ M; WL052510M (30f), which had a nitrobenzene group and an IC₅₀ value of 11.4 μ M; WL052410K (31c), which had a para methoxybenzene group and an IC₅₀ value of 7.2

μM ; WL060110G (31d), which had a toluene group and an IC_{50} value of 8.8 μM ; WL040710D (31a), which had a benzene group and an IC_{50} value of 11.2 μM ; WL042210G (31h), which had an ortho methoxybenzene group and an IC_{50} value of 12.0 μM ; WL042210K (30h), which had a naphthylbenzene group and an IC_{50} value of 10.5 μM ; and WL052410G (31b), which had a chlorobenzene group and an IC_{50} value of 4.9 μM , were the most active compounds.

When considering small molecules for therapeutic use, the compounds that are most active and are partially toxic have the greatest potential. Of the above listed compounds, compound WL042210K (30h), which had a naphthylbenzene group and an IC_{50} value of 10.5 μM ; compound WL052410G (31b), which had a chlorobenzene group and an IC_{50} value of 4.9 μM ; compound WL052410K (31c), which had a para methoxybenzene group and an IC_{50} value of 7.2 μM ; and compound WL060110G (31d), which had a toluene group and an IC_{50} value of 8.8 μM , have the greatest potential for therapeutic uses. The characteristic that all of these compounds have in common, besides being 3-indolyl methanamines, is that they have electron-donating aryl substituents or ortho, para directing groups, such as chlorine, which appears to be effective in inhibiting VDR-mediated transcription.

Chapter 3: Cell Titer-Glo Luciferase Assay

Chapter 3.1: Background and Description of the Cell Titer-Glo Luciferase Assay

The cytotoxicity of CBIs was determined by luminescence using Cell Titer-Glo reagent (Promega). This reagent determines the number of viable cells in a well-based assay by the quantification of adenosine triphosphate (ATP), which is an indicator of metabolically active cells. The Cell Titer-Glo reagent contains a surfactant, which causes cell lysis for ATP liberation, and through an enzymatic reaction, generates a luminescent signal that is proportional to the amount of ATP liberated. The thermally stable luciferase enzyme used in this assay produces the stable luminescent signal, while the reagent inhibits enzymes released during cell lysis, such as ATPases, which will interfere with obtaining an accurate ATP measurement.⁵⁷ In summary, the Cell Titer-Glo reagent lyses cell membranes to release ATP, inhibits endogenous ATPases, and provides the purified luciferin and luciferase necessary to measure ATP using a bioluminescent reaction. The luciferase used in this assay is based on the gene from the firefly, *Photuris pennsylvanica*.

Luciferase is a great detection enzyme, because it is absent in mammals, and it has a luminescent quality which can be quantified by a luminescent reader. ATP is a required cofactor of the luciferase reaction. The luciferase enzyme acts on luciferin in the presence of magnesium cations and oxygen, and releases energy in the form of luminescence, that is, light is produced by the oxidation of luciferin (Figure 29).

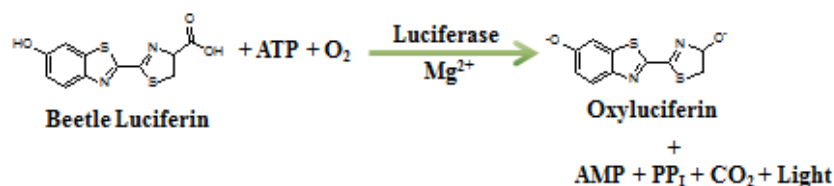


Figure 29: Enzymatic reaction of luciferase.

Luciferin and ATP combine to form adenylyl-luciferin, in the presence of luciferase and magnesium cations (Figure 30).⁵⁸ Adenylyl-luciferin is then oxidized to produce oxyluciferin, carbon dioxide, and water, while the energy released is in the form of luminescence. The luminescent signal that is produced is proportional to the amount of ATP present in the cell, and the amount of ATP is, therefore, directly proportional to the number of metabolically active cells.

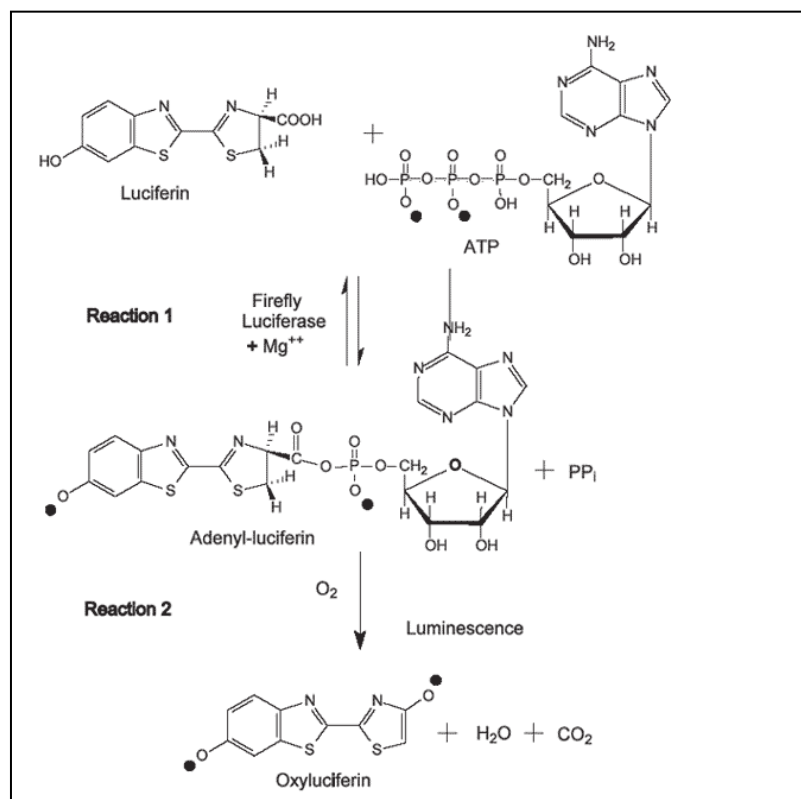


Figure 30: The interaction between ATP and luciferin in the presence of luciferase, magnesium cations, and oxygen.

Chapter 3.2: Luminescence

Luminescence is a term applied to all forms of cool light, or light that is emitted by sources other than a hot and incandescent source, such as chemical energy or U.V. radiation. Generally, luminescence is caused by electrons falling from excited states to less excited states. The types of luminescence are usually named after the source of energy that excites the electron. For example, chemiluminescence is mainly produced by oxidation reactions at low temperatures, and bioluminescence is an enzymatic reaction that is produced by living organisms by some form of chemiluminescence.

Bioluminescence is unique in that the excitation of the electrons comes from a reaction inside the living system, rather than from some external source; however, the distinguishing terms used for the different types of luminescence are used for convenience, because luminescent phenomena have the same mode of excitation, regardless of the source.

There are two classifications of luminescence. Fluorescent luminescence stops shortly after the excitation process ceases and has an afterglow duration that is temperature-independent, whereas phosphorescent luminescence phosphorescence also continues after the excitation process ends but the emission lifetime is of much longer duration. Phosphoresence produces and afterglow with a duration that becomes increasingly shorter with increasing temperature. .

Chapter 3.3: Luminescence Detection

To detect the luminescent signal, the luminometer, illustrated in Figure 31, uses the single photon counting measurement technique, which is based on a photomultiplier tube (PMT). The luminescence system consists of the following parts: luminescence fiber bundle, filter wheel, and PMT detector. The luminescence fiber bundle guides the light from the sample, to the filter wheel, and finally to the detector.

The filter wheel has six filter positions better isolate the analytical signal. The photon counting module (PCM) is designed to read chemi- and bioluminescence and contains a channel photomultiplier, which provides luminescence measurement with strong variations in light levels. The PCM also provides high sensitivity and low noise to allow luminescence detection at very low light levels.

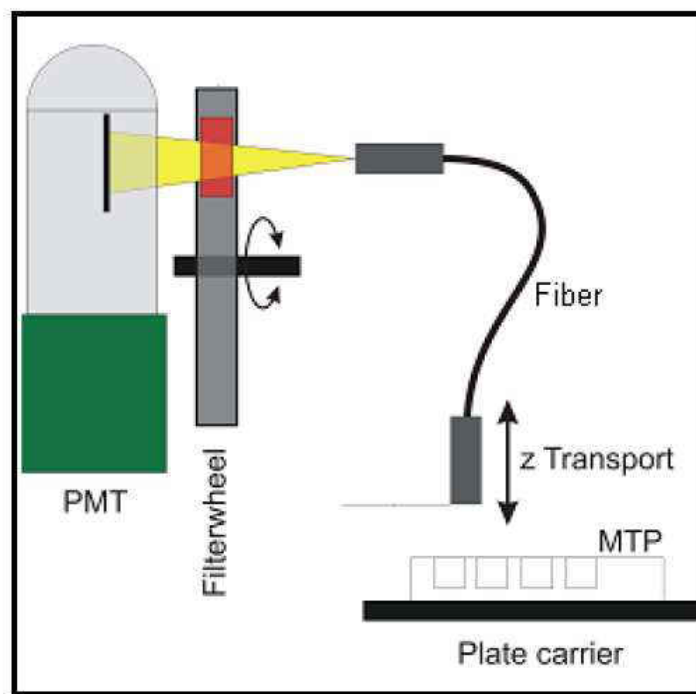


Figure 31: Luminometer detection system.

The Z-position of the luminescence fiber bundle helps to maximize the signal to noise ratio and minimize cross-talk, as light is refracted by the sample's liquid surface. The luminescence fiber bundle guides the light from the sample to the PMT detector. Luminescence is read from the top of the well and collects as much light as possible, in order to maximize the luminescent signal. "Cross-talk" is also minimized by the neighboring wells not receiving substantial amounts of light from other neighboring wells.

Chapter 3.4: The Cell Titer-Glo Luciferase Assay

Hek 293T cells were also used for this assay and were cultured, plated, and drugged in the same manner as described in the "Cell Culture and Gene BLAzer Assay" chapter. The

Gene BLAzer assay was completed first, followed by the addition of the Cell Titer-Glo reagent. Controls for cell viability were 3-dibutylamino-1-(4-hexyl-phenyl)-propan-1-one⁵⁹ (CBT-1; 100 μ M in DMSO, positive control, toxic) and 1, 25-(OH)₂D₃ or LG 190178⁶⁰ (negative control, not toxic). Two independent experiments were conducted in triplet or quadruplet for each of the Cell Titer-Glo luminescence assays performed.

To perform the luciferase assay, 30 μ L of the Cell Titer-Glo reagent was added to each well of the 384-well plate that contained the cells, the positive and negative controls, and the assay media, using a multi-channel pipette. The plate was centrifuged for 2 minutes at 1,000 rpm and allowed to sit for 15 to 20 minutes. The Tecan Infinite M-1000 multi-label reader was used to measure the amount of luminescence generated from each well.

The 384-well clear bottom plate was read with and without a white bottom sticker to compare the influence of escaping light through the bottom of the plate. Surprisingly, it was discovered that both experiments were the same quality, which was quantified by the Z prime factor (Figure 32). Table 1 demonstrates an example of an experiment with compound GW 0742 from exactly identical experimental conditions. These results were consistently observed after recording both observations.

Additionally, it was determined that this assay could be multi-plexed with the Gene BLAzer assay for the same reason that the signals from each of the readings of the non-multi-plexed and multi-plexed signals were determined; thus, discovering a time-saving and cost-saving shortcut (Table 1).

$$Z' = 1 - \left(\frac{3 * (\text{STD Positive Control} + \text{STD Negative Control})}{|\text{Average of the Positive Control} - \text{Average of the Negative Control}|} \right)$$

Figure 32: Z prime calculation. The Z prime value indicates the correlation of the experimental data. Z prime values from 0.50 to 1.0 indicate useful data sets.

Compound Set	With Sticker Z' Value	Without Sticker Z' Value	Not Multi-Plexed Z' Value	Multi-Plexed Z' Value
GW 0742 (Plate UWM 6515)	0.911306	0.911340	0.911306	N/A
GW 0742 (Plate UWM 6517)	0.218768	0.373101	N/A	0.218768
GW 0742 (Plate UWM 6519)	0.999436	0.997010	N/A	0.999436
GW 0742 (Plate UWM 6521)	0.994719	0.996952	N/A	0.996952

Table 1: Comparison of the Z prime values of 384-well plates containing compound GW 0742, which were run with and without a bottom sticker and of 384-well plates that were not multi-plexed with the Gene BLAzer assay and that were multi-plexed with the Gene BLAzer assay.

The luminescence readings of the wells were displayed in an Excel spreadsheet across the row of the 384-well plate. The average of the background of the assay media from the wells was subtracted from the raw data. The averages of the positive and negative controls were used to determine the standard deviation of the positive and negative controls and to determine the Z prime values of the data.

The arranged triplet or quadruplet luminescence values were graphed using Graph Pad Prism 5. Any data points that fell outside of three times the standard deviation were discarded. The two-dimensional graphs consisted of the crude or normalized

luminescence values on the y-axis and the logarithm of the concentration of agonist or CBI on the x-axis (Figures 33 through 43 and Figure 45). The data were fit to a sigmoidal curve of variable slope.

Chapter 3.5: Summary of the Results of the Cell Titer-Glo Luciferase Assay

As discussed previously, *Hek 293T* cells were drugged with calcitriol ligand and CBIs to determine the CBI's ability to inhibit VDR-mediated transcription using the previously described GeneBLAzer assay. The Cell Titer-Glo luciferase assay was used to determine the toxicity of the CBIs in *Hek 293T* cells, by measuring the chemiluminescent signal released by a luciferase-mediated reaction, which quantifies the amount of ATP in living cells.

The following figures represent the crude luminescence signal, as well as the normalized data for each compound. The amount of luminescent signal is proportional to the amount of ATP emitted from the living cells. The higher the luminescent signal the more ATP that is present, which is indicative of a higher amount of metabolically active cells.

The LD₅₀ values are given for the most toxic compounds, which were calculated by the following non-linear regression equation.

$$Y = \text{Bottom} + (\text{Top} - \text{Bottom}) / (1 + 10^{(\text{Log IC}_{50} - X) * \text{Hill Slope}})$$

The LD₅₀ value is half of the maximum lethal dosage, which measures the effectiveness of CBI toxicity. For weakly toxic compounds, the percentage of non-living cells is given for the highest concentration tested.

Figures 33 through 43 and Figure 45 show the results of the Cell Titer-Glo luminescence cytotoxicity assay. The luminescent signal in all of these figures is equivalent to the amount of ATP released from living cells. The normalized data in all of these figures uses CBT-1, which is the same toxic compound in high concentration as a positive control, and 1, 25-(OH)₂D₃ or LG 190178 as the negative control. The positive and negative controls allow for the calculation of the percent toxicity. The degree of toxicity was quantified by the LD₅₀ values, which are given for the most toxic compounds.

Chapter 3.6: Detailed Results and Figures of the Cell Titer-Glo Luciferase Assay

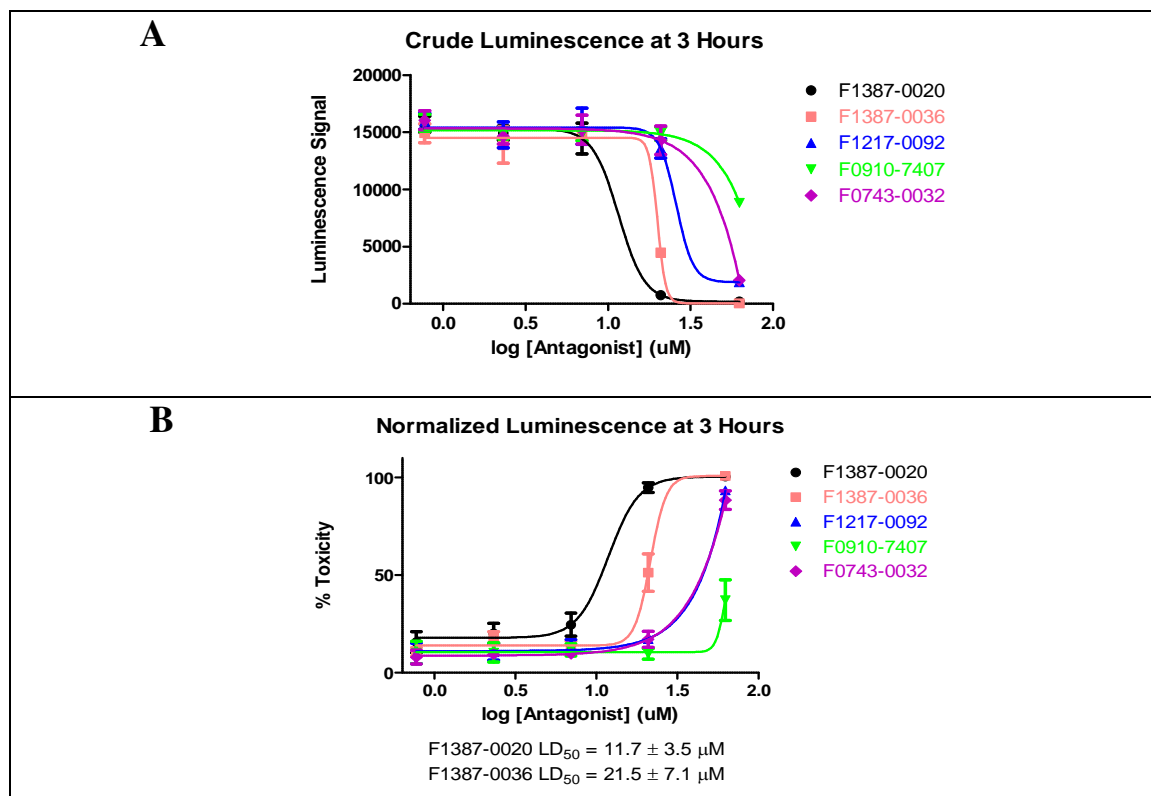


Figure 33: Toxicity of compounds F1387-0020, F1387-0036, F1217-0092, F0910-7407, and F0743-0032.

Compounds F1387-0020, F1387-0036, F1217-0092, F0910-7407, and F0743-0032 all decreased in the crude luminescent signal after 3 hours at higher concentrations (Figure 33A). It can be interpreted that the compounds tested had varying degrees of toxicity at higher concentrations, because the luminescent signal was equivalent to the amount of ATP released from living cells. The normalized data using a toxic compound (CBT-1) in high concentration as a positive control, and 1, 25-(OH)₂D₃, as a negative control, allowed for the calculation of the percent toxicity given in Figure 33B.

Compound F1387-0020 was the most toxic compound in this compound set, followed by compounds F1387-0036, F1217-0092, F0910-7407, and F0743-0032. The insufficient data for the saturated values, or the higher concentrations, for compounds F1217-0092, F0910-7407, and F0743-0032 resulted in the absence of LD₅₀ values for these compounds; however, compound F1387-0020 had an accurate LD₅₀ value of $11.7 \pm 3.5 \mu\text{M}$, whereas compound F1387-0036 had an LD₅₀ value of $21.5 \pm 7.1 \mu\text{M}$.

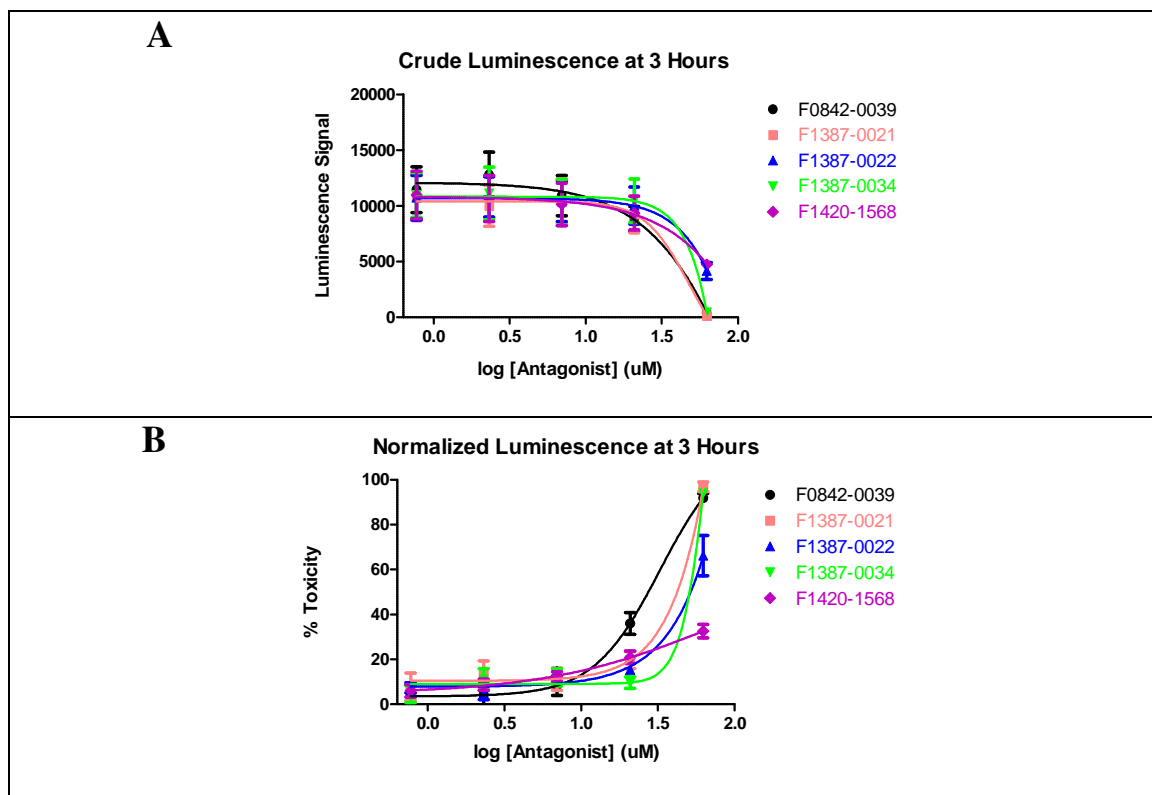


Figure 34: Toxicity of compounds F0842-0039, F1387-0021, F1387-0022, F1387-0034, and F1420-1568.

Compounds F0842-0039, F1387-0021, F1387-0022, F1387-0034, and F1420-1568 all decreased in the crude luminescent signal after 3 hours at higher concentrations (Figure 34A). The normalized data, depicted in Figure 34B, was based on the positive and negative controls in the same plate. The activity can be interpreted that compounds F0842-0039, F1387-0021, and F1387-0034 were toxic, and compounds F1387-0022 and F1420-1568 were somewhat toxic at the highest concentration tested. This interpretation can be made, because the luminescent signal decreased sharply for all of the compounds at this concentration, but compounds F0842-0039, F1387-0021, and F1387-0034 had the sharpest decrease (Figure 34A). In the normalized graph, the signal increased more sharply for compounds F0842-0039, F1387-0021, and F1387-0034, because the graph

was indicative of the percent toxicity at varying concentrations (Figure 34B). No LD₅₀ values could be calculated for any of these compounds, because of insufficient data for higher compound concentrations.

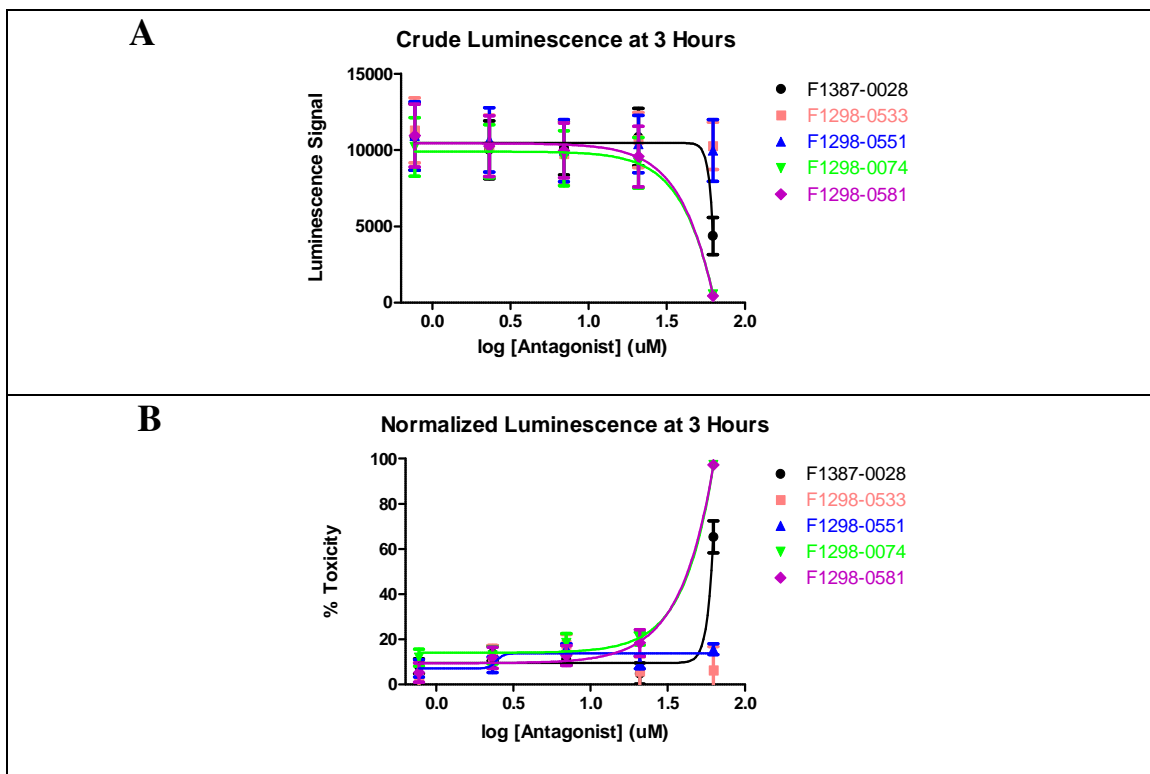


Figure 35: Toxicity of compounds F1387-0028, F1298-0533, F1298-0551, F1298-0074, and F1298-0581.

Compounds F1387-0028, F1298-0074, and F1298-0581 all decreased in the crude luminescent signal after 3 hours at the higher concentrations, whereas compounds F1298-0533 and F1298-0551 showed no signal change (Figure 35A). The activity can be interpreted that compounds F1298-0074 and F1298-0581 were toxic, compound F1387-0028 was somewhat toxic, and compounds F1298-0533 and F1298-0551 were not toxic at the highest concentration tested. This interpretation can be made, because the

luminescent signal decreased sharply for compounds F1298-0074 and F1298-0581, somewhat sharply for compound F1387-0028, and not at all for compounds F1298-0533 and F1298-0551 (Figure 35A). In the normalized graph, the signal increased more sharply for compounds F1298-0074 and F1298-0581, because the graph was indicative of the percent toxicity at varying concentrations (Figure 35B). The least toxic compounds were compounds F1298-0533 and F1298-0551, which was indicated by the nearly linear graphs for these compounds in the percent toxicity graph (Figure 35B).

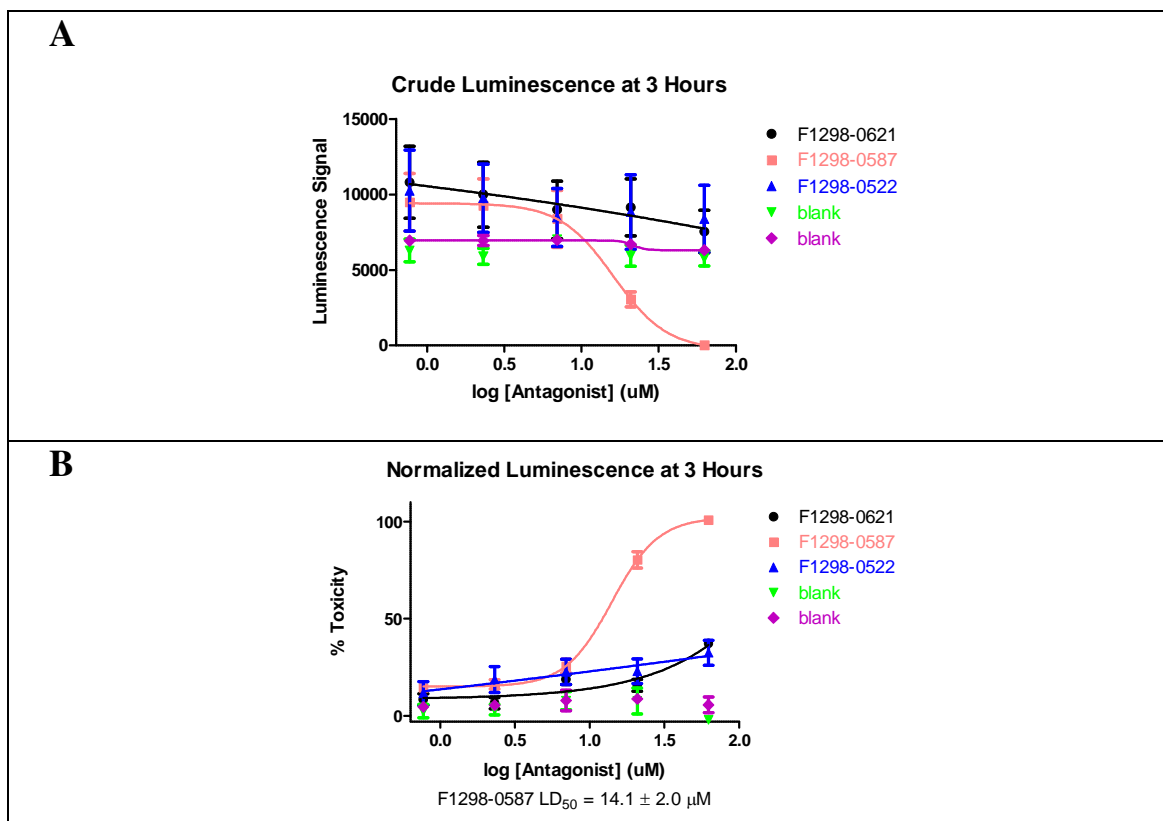


Figure 36: Toxicity of compounds F1298-0621, F1298-0587, and F1298-0522.

Only compound F1298-0587 decreased in the crude luminescent signal after 3 hours at the highest concentration tested, whereas compounds F298-0621 and F1298-

0522 showed no signal change (Figure 36A). The blanks, which did not contain any CBIs, were consistent with a lack of toxicity. The activity can be interpreted that compound F1298-0587 was toxic, with an LD₅₀ value of $14.1 \pm 2.0 \mu\text{M}$, and compounds F298-0621 and F1298-0522 were very mildly toxic at the highest concentration tested. This interpretation can be made, because the luminescent signal decreased sharply for compound F1298-0587, and very slightly for compounds F298-0621 and F1298-0522 (Figure 36A). In the normalized graph, the signal increased more sharply for compound F1298-0587, because the graph was indicative of the percent toxicity at varying concentrations (Figure 36B).

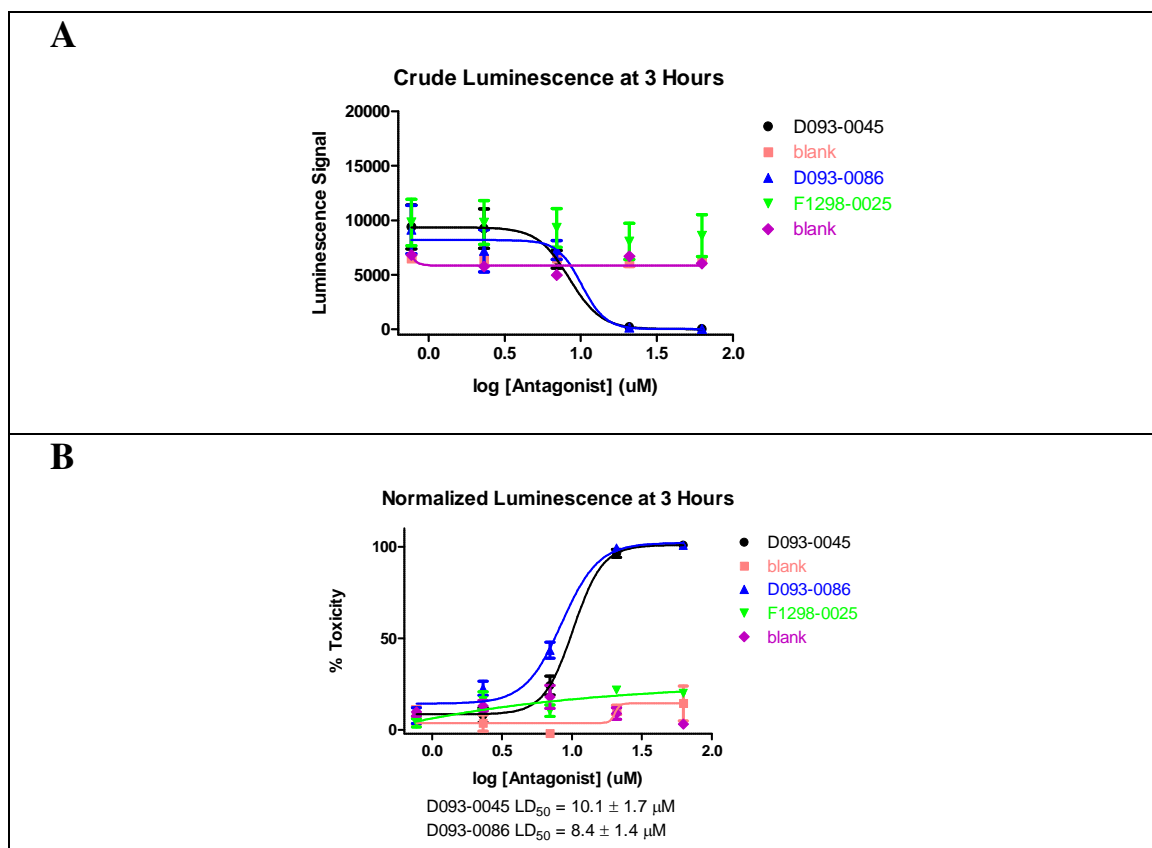


Figure 37: Toxicity of compounds D093-0045, D093-0086, and F1298-0025.

Compounds D093-0045 and D093-0086 decreased in the crude luminescent signal after 3 hours at higher concentrations, while compound F1298-0025 remained relatively consistent, even at higher concentrations (Figure 37A). Additionally, two graphs were added with vehicle DMSO treatment only as a control. The normalized data showed 100 percent toxicity at higher concentrations for compounds D0093-0045 and D093-0086, and only 10 to 20 percent toxicity for compound F1298-0025 (Figure 37B). The LD₅₀ values could be calculated accurately for compounds D0093-0045 and D093-0086, which were $10.1 \pm 1.7 \mu\text{M}$ and $8.4 \pm 1.4 \mu\text{M}$, respectively.

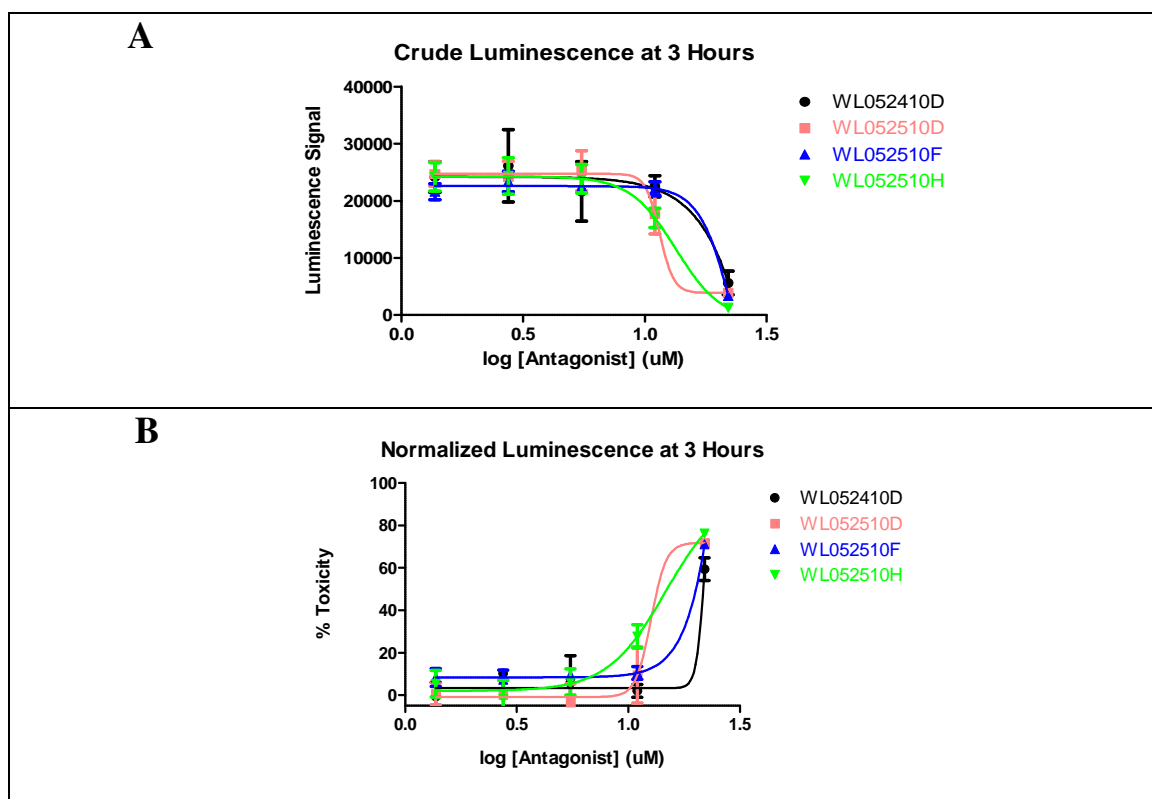


Figure 38: Toxicity of compounds WL052410D, WL052510D, WL052510F, and WL052510H.

Compounds WL052410D, WL052510D, WL052510F, and WL052510H all decreased in crude luminescent signal after 3 hours at the highest concentration tested (Figure 38A). It can be concluded that these compounds showed low toxicity at a concentration of 11 μ M, but were toxic at 22.5 μ M (Figure 38B). Due to insufficient data points at higher concentrations, accurate LD₅₀ values were unable to be calculated.

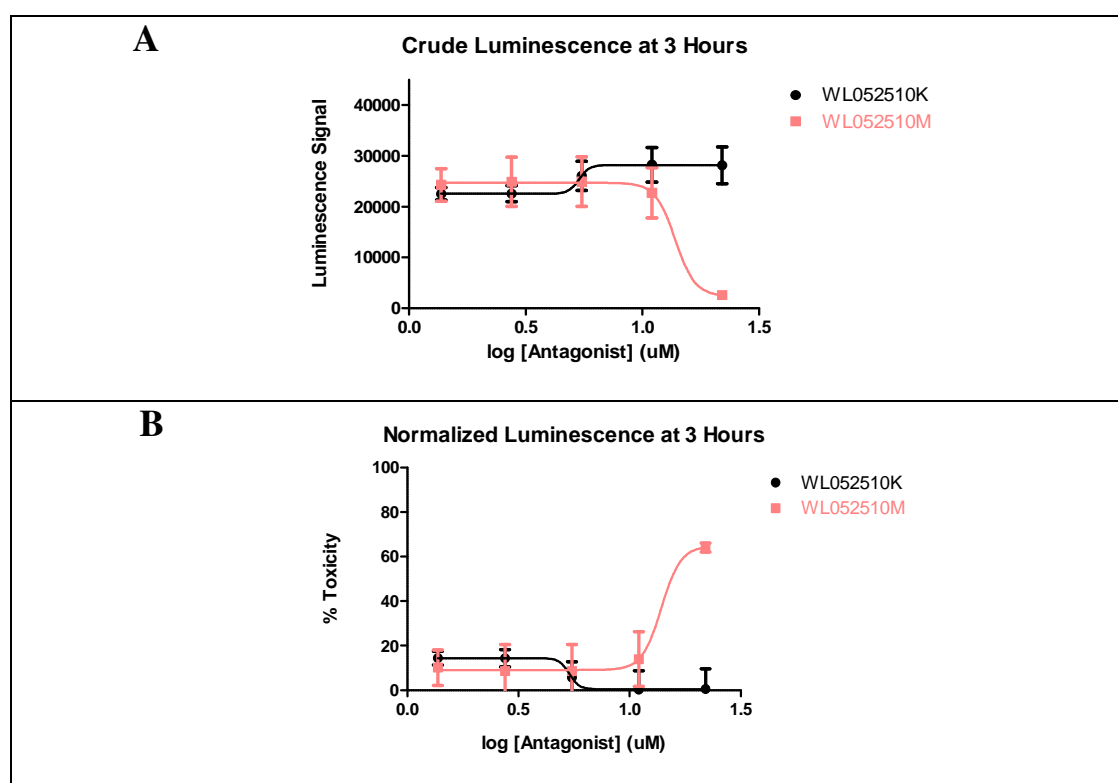


Figure 39: Toxicity of compounds WL052510M and WL052510K.

Compound WL052510M, but not compound WL052510K, decreased in the crude luminescent signal after 3 hours at the highest concentration tested (Figure 39A). This result was confirmed by the normalized data in Figure 39B. Because of the insufficient

data at higher concentrations, no accurate LD₅₀ values could be calculated for compound WL052510M, but toxicity was established at a concentration of 22.5 μ M.

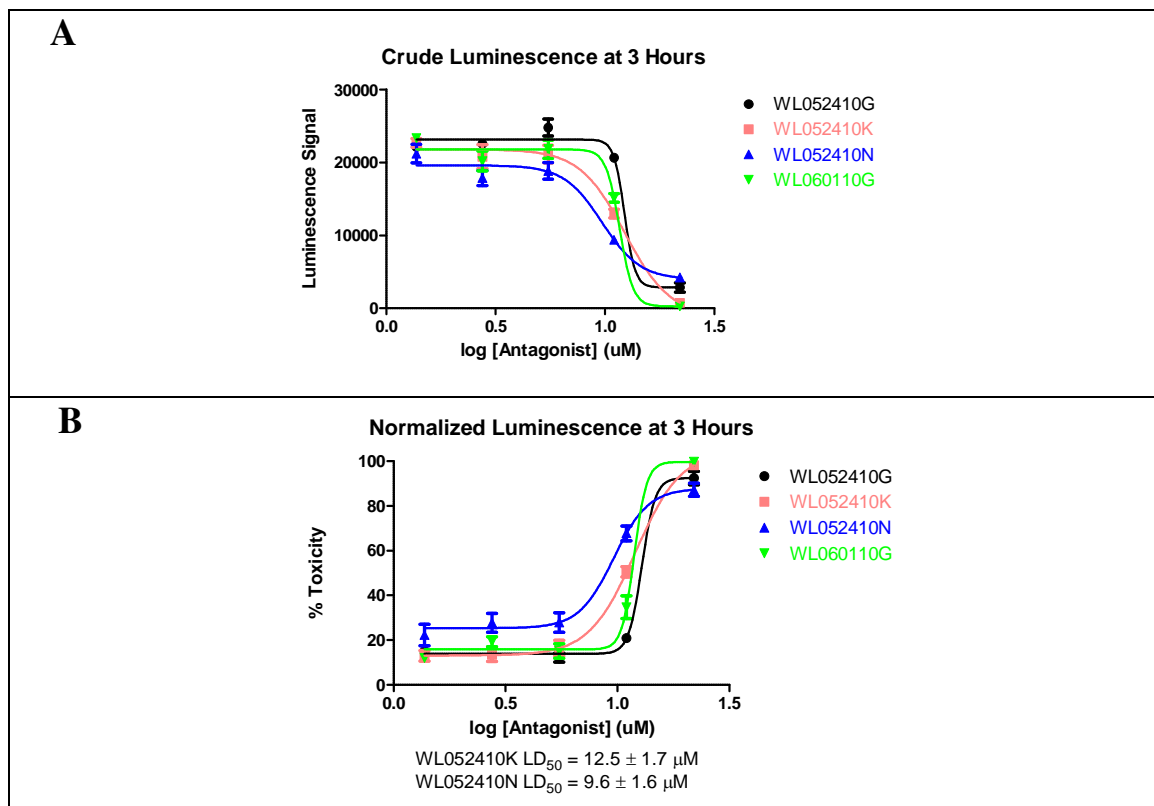


Figure 40: Toxicity of compounds WL052410G, WL052410K, WL052410N, and WL060110G.

Compounds WL052410G, WL052410K, WL052410N, and WL060110G all decreased in the crude luminescent signal after 3 hours at higher concentrations (Figure 40A). The normalized data confirmed that the toxicity was more than 90 percent, with respect to the controls for all compounds tested at a concentration of 22.5 μ M (Figure 40B). The calculation of the LD₅₀ values was compromised, due to the missing data at higher compound concentrations for compounds WL052410G and WL060110G (Figures

40A and 40B). However, the LD₅₀ values for compounds WL052410K and WL052410N were $12.5 \pm 1.7 \mu\text{M}$ and $9.6 \pm 1.6 \mu\text{M}$, respectively.

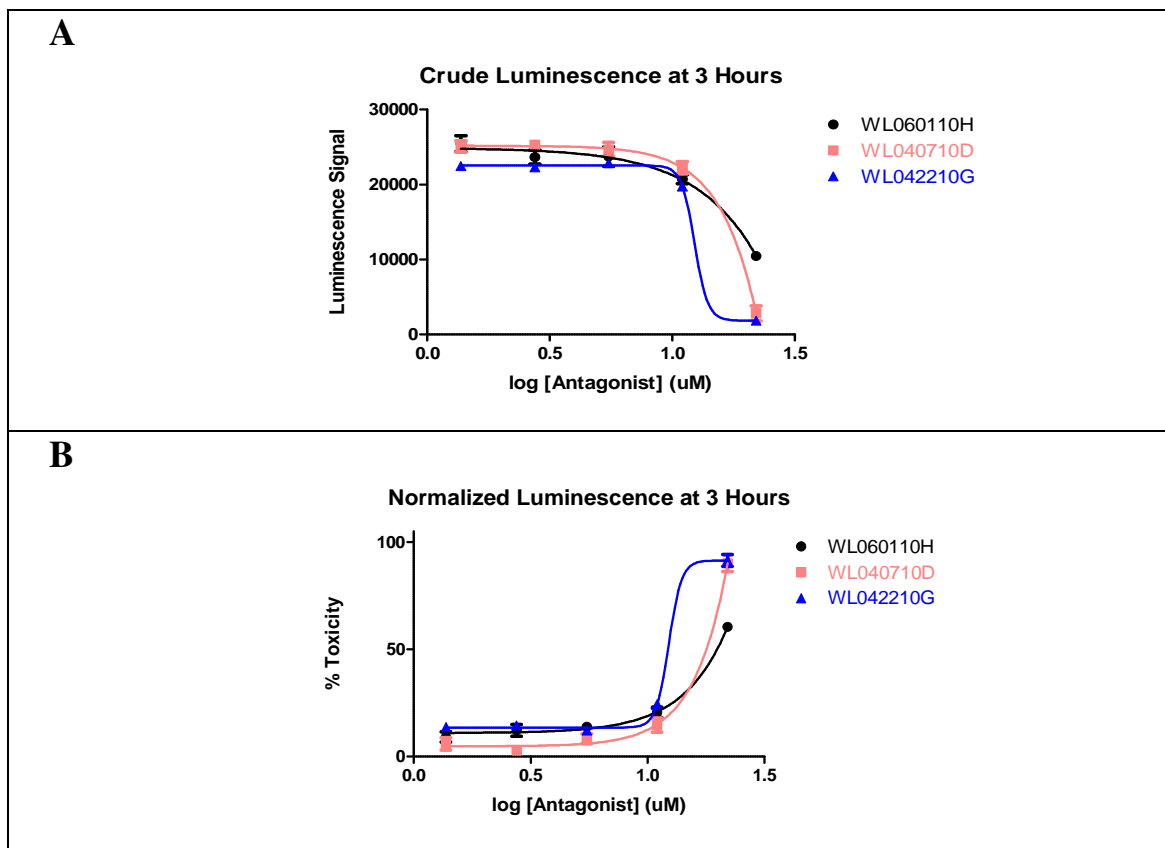


Figure 41: Toxicity of compounds WL060110H, WL040710D, and WL042210G.

Compounds WL060110H, WL040710D, and WL042210G all decreased in the crude luminescent signal after 3 hours at the highest concentration tested (Figure 41A). The normalized data showed a toxicity for compounds WL040710D and WL042210G of higher than 90 percent at 22.5 μM . In addition, the toxicity of compound WL060110H was approximately 60 percent at 22.5 μM . As mentioned before, the accurate calculation of the LD₅₀ values was not possible, due to insufficient data.

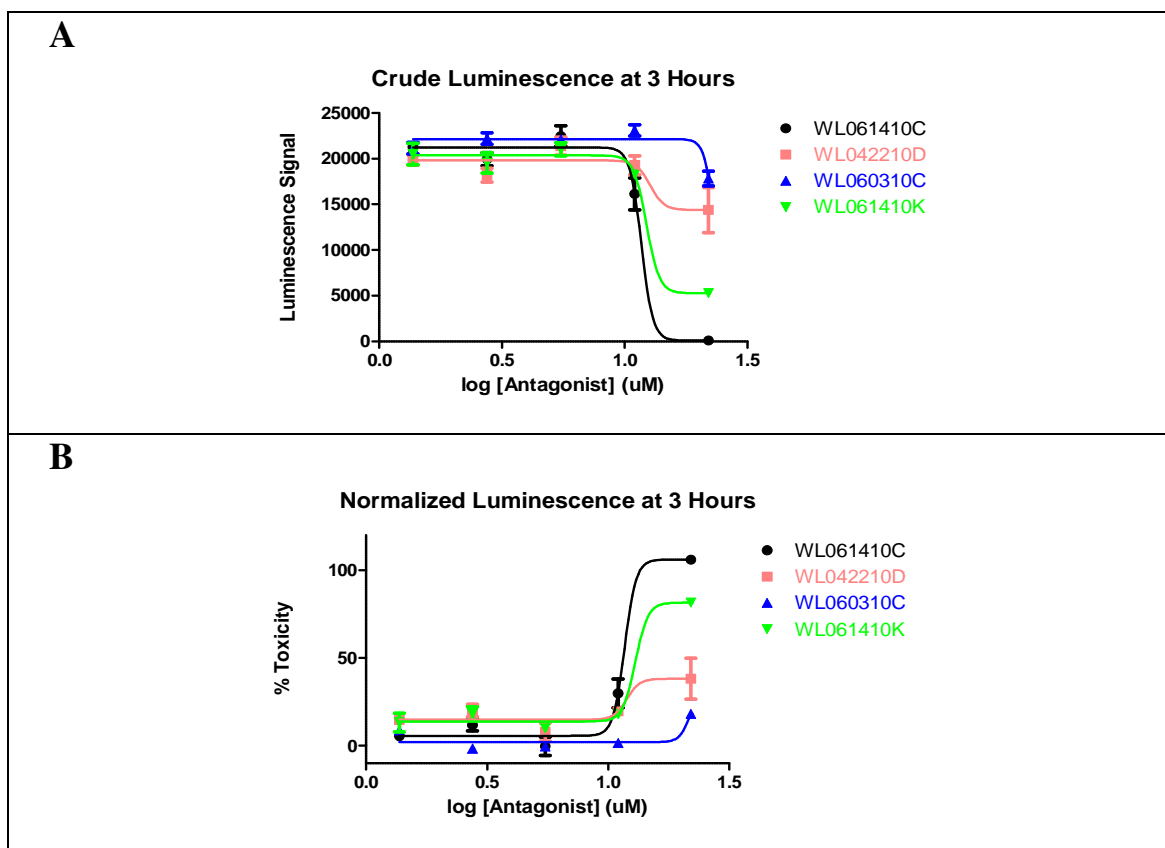


Figure 42: Toxicity of compounds WL061410C, WL042210D, WL060310C, and WL061410K.

Compounds WL061410C, WL042210D, WL060310C, and WL061410K all decreased in the crude luminescent signal after 3 hours at the highest concentration tested (Figure 42A); however, the crude luminescent signal for compounds WL042210D and WL060310C only slightly decreased at the highest concentration, indicating that these compounds were only weakly toxic. The normalized data confirmed this observation that compounds WL061410C and WL061410K were more toxic than compounds WL042210D and WL060310C (Figure 42B). Compound WL061410C was the only compound that reached 100 percent toxicity at the highest concentration, making it the

most toxic compound in the compound set (Figure 42B). Compound WL042210D had about 30 percent toxicity at the highest concentration tested, compound WL060310C had about 10 percent toxicity at the highest concentration tested, and compound WL061410K had about 70 percent toxicity at the highest concentration tested (Figure 42B).

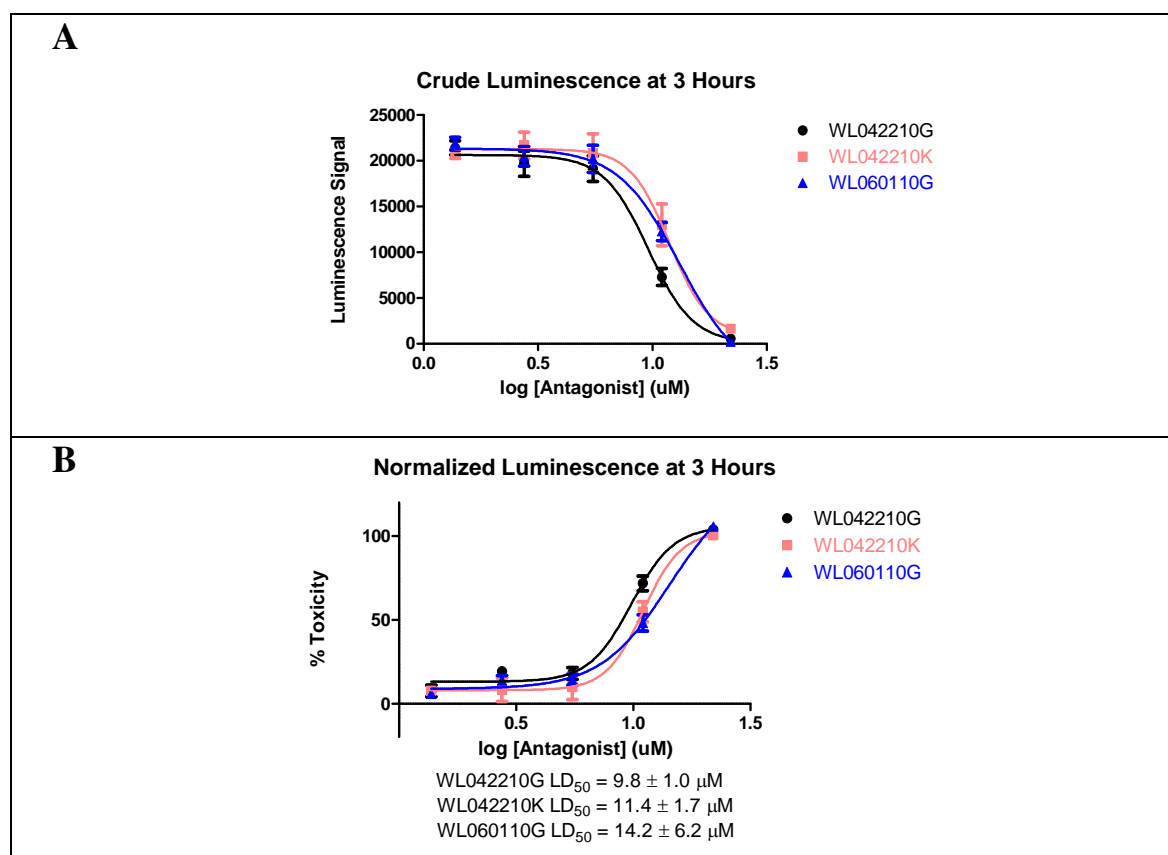


Figure 43: Toxicity of compounds WL042210G, WL042210K, and WL060110G.

Compounds WL042210G, WL042210K, and WL060110G decreased in the crude luminescent signal after 3 hours at the highest concentration tested (Figure 43A). From the normalized data, it can be concluded that compounds WL042210G, WL042210K, and

WL060110G were significantly toxic. The LD₅₀ values were 9.8 ± 1.0 μ M, 11.4 ± 1.7 μ M, and 14.2 ± 6.2 μ M, respectively.

Another compound identified by HTS was compound GW 0742 (Figure 44). The toxicity of compound GW 0742 was determined twice in quadruplet, as depicted in Figure 45.

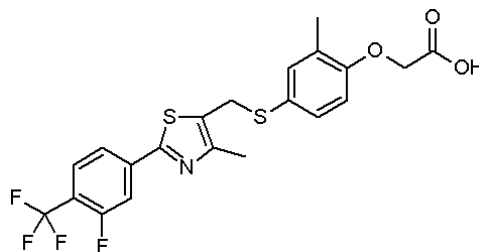


Figure 44: Structure of compound GW 0742.

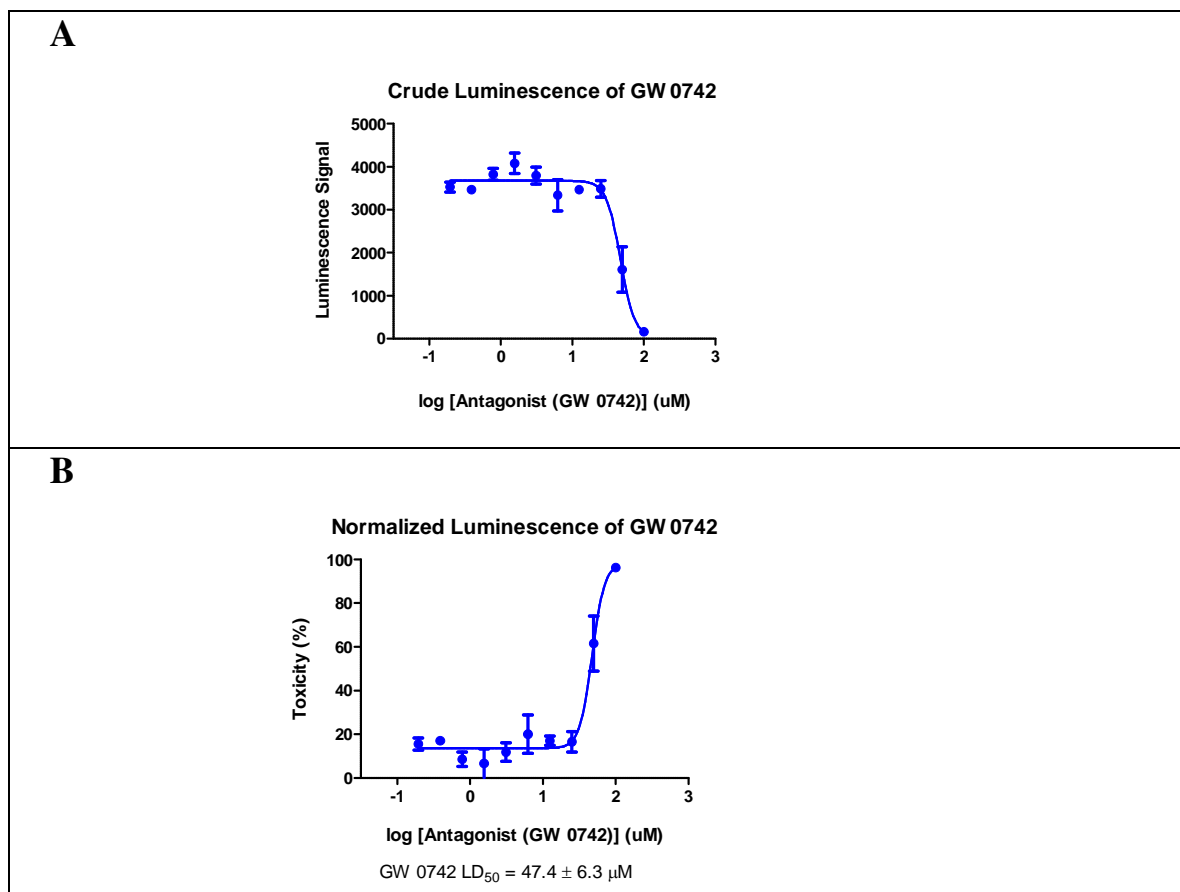


Figure 45: Toxicity of compound GW 0742.

The 2 measurements for compound GW 0742 show reproducible data. Figure 45 consists of crude and normalized luminescence performed under identical conditions for compound GW 0742. The concentrations tested range from 100 μM to 0.195 μM . Both results showed that compound GW 0742 was only toxic at higher concentrations. The LD_{50} value determined was $47.5 \pm 6.3 \mu\text{M}$.

The results of all compounds are summarized in Table 7 in Appendix A, which categorizes all of the tested compounds with respect to their toxicity and their corresponding activity in the transcription assay.

Chapter 3.7: Discussion of the Results of the Cell Titer-Glo Luminescence Assay

In total, 39 compounds were investigated with respect to their toxicity. Many different scaffolds were toxic, which is a concern with some of these molecules. As seen in the Gene BLAzer transcription inhibition assay, the class of 3-indolyl methanamines (compounds F0842-0039, F1217-0092, F1387-0028, F1387-0021, F1387-0036, F0743-0032, F1387-0020, F1387-0034, and F1387-0022) was also identified as the superior class of irreversible inhibitors of the VDR-coactivator interaction and of partial toxicity. The results presented previously in this chapter are published in Nandhikonda et al.²⁹

The 3-indolyl methanamine class varied in aromatic substituents. Compound F0842-0039 had a phenol group; compound F1217-0092 had a para toluene group; compound F1387-0028 had a meta anisole group; compound F1387-0021 had a meta bromobenzene group; compound F1387-0036 had a para bromobenzene group; compound F0743-0032 had a para fluorobenzene group; compound F1387-0020 had a

para xylene group; compound F1387-0034 had a meta chlorobenzene group, and compound F1387-0022 had a meta fluorobenzene group.

Of these compounds, compound F1387-0036, which had a para bromobenzene group and an LD₅₀ value of 21.5 μ M, and compound F1387-0020, which had a para xylene group and an LD₅₀ value of 11.7 μ M, were the most active compounds with partial toxicity. The rest of the compounds in this class showed a high toxicity with low transcriptional activity. Of the remaining initial compounds, only compound F1298-0587 and compound D093-0045 have only a slight potential, due to their transcriptional inhibition abilities and partial toxicity. Compound D093-0086 demonstrated high toxicity with an LD₅₀ value of 8.4 μ M.

Of the compounds synthesized from the 3-indoyl methanamines, compounds WL052410K (31c), which had a para methoxybenzene group and an LD₅₀ value of 12.5 μ M; WL060110G (31d), which had a toluene group and an LD₅₀ value of 16.9 μ M; WL042210G (31h), which had an ortho methoxybenzene group and an LD₅₀ value of 9.8 μ M; WL042210K (30h), which had a naphthylbenzene group and an LD₅₀ value of 11.4 μ M; and WL052410G (31b), which had a chlorobenzene group and an LD₅₀ value of 14.2 μ M were the most active compounds.

Compounds WL052410D (30c), which had an anisole group; WL052510D (30a), which had a benzene group; WL052510F (30d), which had a toluene group; WL052510H (30b), which had a chlorobenzene group; WL052510K (30e), which had a dimethylaniline group; WL052410G (31b), which lacked a methyl on the indoyl group; WL060110H (31f), which had a nitrobenzene group; WL061410C (32c), which had a thiobenzene group; WL061410K (30g), which had a methyl group; WL052510M (30f),

which had a nitrobenzene group; and WL040710D (31a), which had a benzene group, were highly toxic compounds. The rest had little to no toxicity and little to no transcriptional activity.

When considering small molecules for therapeutic use, the compounds that were most active in transcriptional inhibition and had partial toxicity have the greatest potential. Of the above listed compounds, compounds WL052410K (31c), which had a para methoxybenzene group and an LD₅₀ value of 12.5 μ M; WL060110G (31d), which had a toluene group and an LD₅₀ value of 16.9 μ M; WL042210G (31h), which had an ortho methoxybenzene group and an LD₅₀ value of 9.8 μ M; WL042210K (30h), which had a naphthylbenzene group and an LD₅₀ value of 11.4 μ M; and WL052410G (31b), which had a chlorobenzene group and an LD₅₀ value of 14.2 μ M have the greatest potential for therapeutic uses. The characteristic that these compounds have in common, besides being 3-indolyl methanamines, is that they have electron-donating aryl substituents, or ortho, para directing groups, such as chlorine, which appear to be effective in inhibiting VDR-mediated transcription and appear to have partial cytotoxicity.

Chapter 4: VDR, SRC-2, and SRC-2-3 Protein Expression and Purification

Chapter 4.1: Protein Expression

Protein expression and purification were completed, in order to obtain the VDR-LBD, SRC-2, and SRC-2-3 proteins that were used for the co-IP and pull-down assays. To begin the protein expression, carbenicillin agar plates were prepared by mixing 20 grams of agar mix in 500 mL of water in a 2,000 mL autoclavable Erlenmeyer flask. The Erlenmeyer flask was then autoclaved. Once the liquid had cooled to room temperature, 0.5 mL of carbenicillin was added to the flask, and the liquid was poured into the agar plates. The liquid in the plates was allowed to set, and the plates were stored in the refrigerator until needed.

Escherichia coli cells, strain database number AMKB037-B, containing plasmids for the *vdr-LBD* gene and carbenicillin resistance, were streaked onto the agar plates, and the plates were inverted and placed in an incubator at 37°C overnight. These *E. coli* then produced the VDR protein with only its ligand binding domain. The VDR-LBDmt DNA was kindly provided by D. Moras and cloned into pMAL-c2X vector (New England Biolabs).

BL-21 E. coli cells were heat shocked, in order to insert the SRC-2 and SRC-2-3 genes into the cells. The vials of *BL 21* cells were obtained from the -80°C freezer and thawed on ice for about 10 minutes. The 200 µL cell solution was mixed into a suspension, divided in half, and pipetted into 2 separate 1.5 mL microfuge tubes. To each of the microtubes, 1 µL of purified plasmid DNA to be uptaken was added. One

microtube contained the plasmid DNA for the SRC-2 protein, and the other microtube contained the plasmid DNA for the SRC-2-3 protein. The microtubes were incubated on ice for 30 minutes and heat shocked for exactly 40 seconds in an exactly 42°C tempered water bath. After the microtubes were removed from the water bath, they were incubated on ice again for another 2 minutes.

Under sterile conditions in the biological fume hood, 900 µL of super optimal broth (SOC) growth medium with glucose added for catabolite repression was pipetted into each microtube. The microtubes were taped to a flask holder in the incubation shaker, and the cells were allowed to propagate for 1 hour at 37°C and 250 rpm. After the 1 hour incubation, the cells were concentrated by microfugation for 1 minute at 6,000 rpm. The supernatant was removed by pipette and discarded. The cells were resuspended in the remaining 100 µL of solution.

A 100 µL aliquot of each cell suspension, that is, SRC-2 and SRC-2-3, was used to inoculate 2 separate agar plates, one for the SRC-2 gene and the other for the SRC-2-3 gene, for the desired expression in *E. coli*. The inoculated agar plates were sealed with parafilm, inverted, and placed in the incubation shaker at 37°C at the lowest shaking setting (25 rpm) overnight. Once the growth of the cell colonies was verified on the agar plates, a colony of the cells was used to inoculate a seed culture in Erlenmeyer flasks containing Luria Bertani (LB) broth and carbenicillin antibiotics. The inoculated seed culture was placed on the incubation shaker overnight at 37°C and 325 rpm. The LB broth growth media was prepared by adding 1,000 mL of tap water and 2 LB broth capsules to a 2,000 mL autoclavable Erlenmeyer flask and autoclaved. A quantity of 1

mL of carbenicillin antibiotics was added to the flasks when they cooled, in order to promote growth of bacteria with carbenicillin resistance only.

Approximately 25 mL of the VDR-LBD seed culture was pipetted into 8 separate 2,000 mL Erlenmeyer flasks containing 1,000 mL of LB broth growth media and carbenicillin antibiotics. Only 2 separate 2,000 mL Erlenmeyer flasks were prepared with 25 mL of the SRC-2 protein, and 2 for the SRC-2-3 protein. These flasks were placed in the incubator-shaker at 25°C and 325 rpm until an optical density of 0.3 to 0.6 was read on the spectrophotometer at 600 nm in a cuvette containing 1 mL of cell mixture.

Once this optical density was reached, some 1 mL aliquots of the culture were frozen with 10 percent DMSO, placed in the -80°C freezer, and used in future protein expressions to prevent starting the protocol with *E. coli* colonies. After removing some aliquots of the cell culture, the cultures were induced with 1 mL of 0.2 mM of isopropyl β -D-1-thiogalactopyranoside, or IPTG, (10 mL of Milli-Q water in 0.478 grams of IPTG) and allowed to shake in the incubator-shaker overnight at 25°C and 325 rpm.

IPTG triggers transcription of the lac operon, because it mimics the action of allolactose. IPTG is not degraded, allowing the concentration to remain constant, which allows transcription to occur at a steady rate.

The cells were harvested by centrifugation (JA-9.1000 rotor at 4°C at 6,000 rpm for 20 minutes). The pellet that remained after centrifugation was the *E. coli* cells containing the desired protein. The cells were placed into a 50 mL conical tube and frozen in the -80°C freezer until the protein purification process could be started.

Chapter 4.2: Protein Purification

The first step in the protein purification process was the sonication of the cell pellet obtained from the protein expression. First, protease inhibitor was made by adding 1 EDTA-free protease inhibitor cocktail tablet (Roche Diagnostics) for every 50 mL of 1X dialysis buffer (20 mM Tris-base (pH 7.4), 100 mM NaCl, 1 mM EDTA, 1 mM sodium azide, 1 mM dithiothreitol (DTT), 10 percent glycerol, and 0.01 percent NP-40 detergent).

Protease inhibitors prevent proteolytic activity of enzymes, which are also known as proteases, present in *E. coli*. Proteases cleave the peptide bonds that link amino acids in proteins. In this particular protease inhibitor, serine, threonine, cysteine, aspartate, and glutamic acid proteases were inhibited, as well as metalloproteases.

The cells were allowed to thaw on ice, and 30 mL of the protease inhibitor solution was pipetted into each of the conical tubes containing the cell pellet. The slurry was mixed until all of the cells were in suspension. The cell solution was placed into an ice and salt mixture and sonicated 3 times for 30 seconds each time at 40 percent amplitude, with a waiting period of at least 2 minutes between each sonication. After sonication, the cells were lysed by centrifugation using the JA-20 rotor, at 4°C and 18,000 rpm for 45 minutes. The lysate was separated and cleared from the supernatant, which contained the desired VDR, SRC-2, or SRC-2-3 proteins from the cells.

The protein solutions were incubated with 3 mL per 50 mL of protein solution with affinity-tagged beads overnight on the rotisserie turner at 4°C. For VDR, maltose beads were used, for SRC-2, glutathione S-transferase (GST) beads were used, and for SRC-2-3, nickel-chelated beads were used (Figures 46 through 48).



Figure 46: Maltose binding protein (MBP) attached to an amylose resin. MBP is a member of the maltose and maltodextrin system of *E. Coli*, which is responsible for the catabolism of maltodextrins. Maltose can be immobilized by cross-linking to a solid-support amylose resin. The purified MBP fusion protein can be dissociated and eluted by the addition of excess maltose (10 mM).

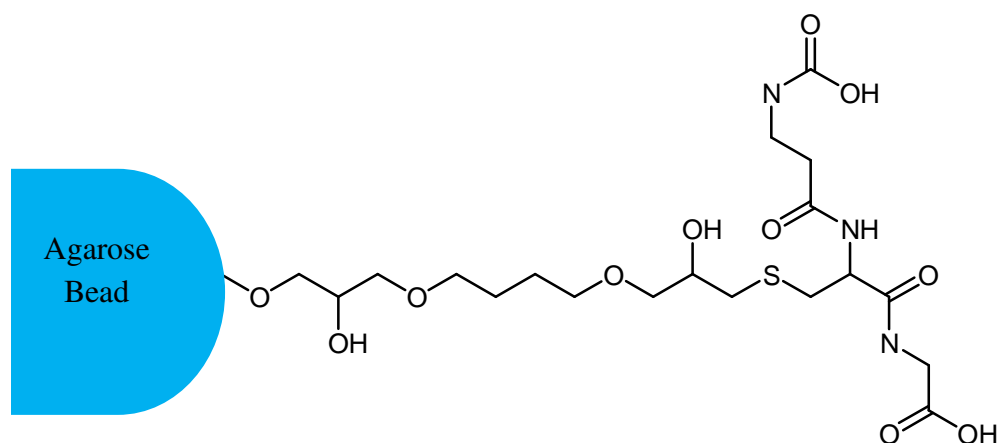


Figure 47: Glutathione S-transferase (GST) bead. Glutathione is a tripeptide (Glu-Cys-Gly) that is the specific substrate for GST. When reduced, glutathione is immobilized through its sulfhydryl group to a solid support, such as a cross-linked agarose bead. Glutathione can be used to capture GST-tagged proteins via the enzyme-substrate binding reaction. The purified GST-fusion protein can be dissociated and eluted from glutathione by addition of excess reduced glutathione (10 mM).

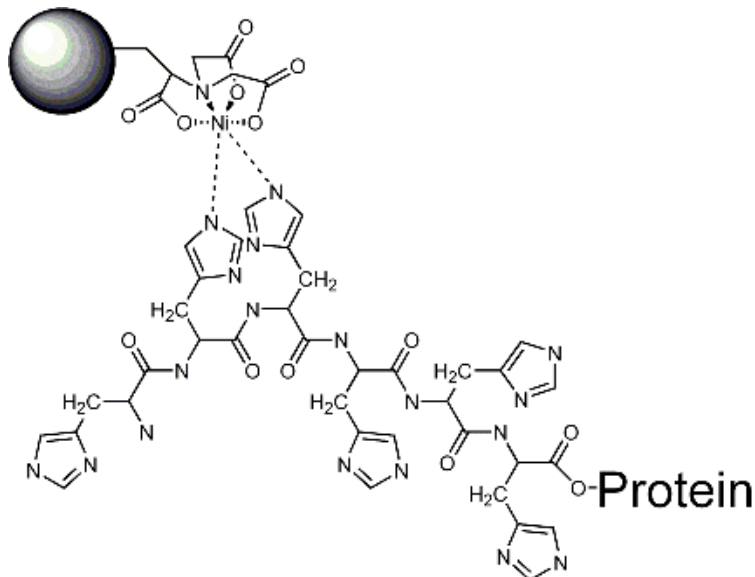


Figure 48: Histidine (His) nickel-nitrilotriacetic acid (NTA) resin. A string of 6 to 9 histidine residues form an easily identifiable tag, which is fused to either the amino or carboxyl terminal. His-tagged proteins are easily purified and detected because the His-tag binds to nickel, which is an immobilized metal ion. A chelating group, such as NTA, which is attached to a solid support, in this case, agarose, helps to immobilize the nickel ion, which then attaches to the His-tag. Elution of the His-tagged protein is done with 250 mM imidazole solution. The imidazole replaces the nickel in the resin, which releases the protein.

After the overnight incubation, the beads were separated from the supernatant by centrifugation at 4,000 rpm at 4°C for 20 minutes. The supernatant was decanted into a new 50 mL conical tube, and a 50 µL aliquot was pipetted into a microfuge tube, in order to resolve a sample on an SDS-PAGE gel. The beads were combined into one conical tube and 1X column buffer (20 mM Tris-HCl (pH 7.4), 200 mM NaCl, 1 mM EDTA, 1 mM sodium azide, and 9 mM β-mercaptol) was added to the conical tube, to a final volume of 30 mL. The conical tube was centrifuged at 4,000 rpm at 4°C for 5 minutes. The supernatant was again decanted into another conical tube, and a 50 µL aliquot was

pipetted into another microfuge tube. The beads were washed with column buffer and centrifuged again. These steps were repeated for a total of 5 washes.

At this point, all of the SRC-2, SRC-2-3, and VDR proteins were left attached to their respective, solid support beads for later use in a co-IP and pull-down assay described in a later chapter. The fraction of the VDR protein attached to the maltose beads was eluted to yield VDR-LBD protein in solution.

In order to elute the VDR protein from the maltose beads, the beads were transferred to a 15 mL conical tube, and 5 mL of the maltose solution, which was 10 mM maltose in column buffer, was added to the beads, followed by inversion of the conical tube. The conical tube was centrifuged at 4,000 rpm at 4°C for 5 minutes. The supernatant was decanted into another 15 mL conical tube, and a 50 μ L aliquot was pipetted into a microfuge tube and set aside to be resolved on an SDS-PAGE gel. Another 5 mL of the maltose elutant was added to the 15 mL conical tube containing the beads and inverted. The conical tube was centrifuged again at 4,000 rpm at 4°C for 5 minutes, the supernatant was again decanted into a separate 15 mL conical tube, and a 50 μ L aliquot was removed into a separate microtube. This process was repeated for a total of 9 elutions.

Once all the elutions were complete, a Bradford assay was conducted on the supernatant, on washes 1 through 5, and on elutions 1 through 9. After the Bradford assay was complete, elutions 3 through 9 were combined, in order to concentrate the VDR protein further in a 10,000 kilodalton spin column by centrifugation at 4,000 rpm and 4°C. After the protein was concentrated, the concentration was determined by a Bradford assay. The Bradford assay was followed by the resolution of the SDS-PAGE gel

containing all of the fractions, including the supernatant, washes, and elutions, in order to verify the presence and purity of the VDR protein.

While the SDS-PAGE gel was resolving, the combined concentrated protein was added to a 10,000 kilodalton dialysis cassette, placed in 4 L of dialysis buffer (20 mM Tris-base (pH 7.4), 100 mM NaCl, 1 mM EDTA, 1 mM sodium azide, 1 mM DTT, 10 percent glycerol, and 0.01 percent NP-40 detergent), and stirred overnight at 4°C .

After an overnight dialysis, the protein was removed from the cassette, and 1 mL aliquots were pipetted into 1.5 mL microtubes. The microtubes containing the purified VDR protein were stored in the -80°C freezer and used as needed for subsequent assays.

Chapter 5: Co-Immunoprecipitation and Pull-Down Assay

Chapter 5.1: Pull-Down Assay using a Solid-Supported VDR and an *in situ*-Generated SRC-2-Biotin with the TNT Transcription and Translation System for the Identification of VDR-CBIs (Promega)

The VDR-coactivator inhibition assay, outlined in Figure 49, was based on the ability of CBIs to disrupt the interaction between VDR and SRC-2 coactivator; thus, removing biotinylated SRC-2 from the solid-supported VDR-LBD protein. Probing for biotin using a chimera protein of streptavidin and alkaline phosphatase (AP) allowed the conversion of substrate, 5-bromo-4-chloro-3-indolyl-phosphate (BCIP), by AP into Indigo-Blue and allowed for the quantification of SRC-2 bound to VDR, in case of the absence or very low concentration of CBI.

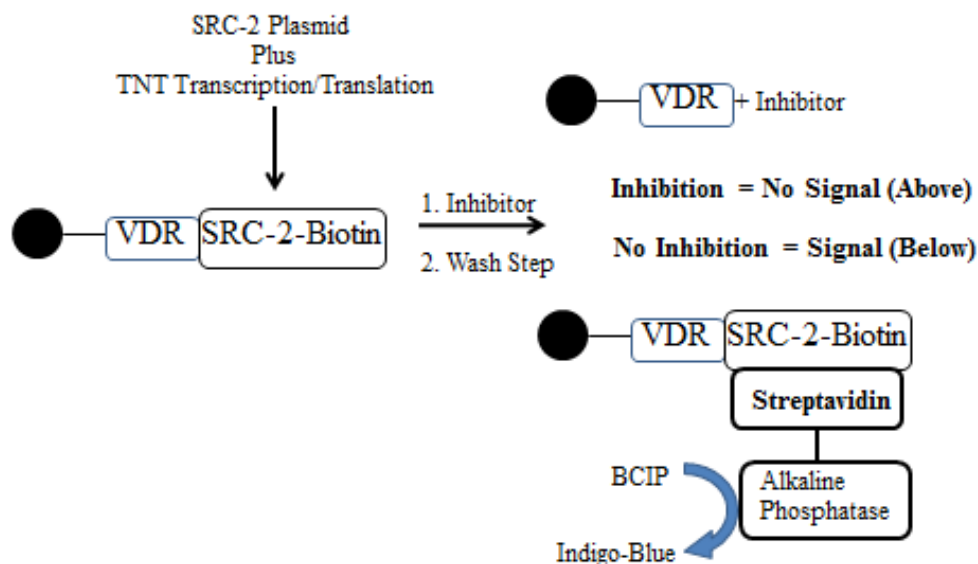


Figure 49: Scheme of the first pull-down assay.

Chapter 5.1.1: Experimental Procedure for the First Pull-Down Assay

Chapter 5.1.1.1: Solid-Supported VDR

The expression and purification of the VDR-LBD-MBP protein was described in chapter 4. The difference between this protocol and the protocol previously described was that the current protocol was stopped before the elution step; thus, generating a solid-supported VDR-LBD protein held to the solid support through the interaction of MBP and covalently bound amylose.

Chapter 5.1.1.2: *In situ*-Generated SRC-2

The Transcription and Translation (TNT from Promega) system is a single tube system, which couples transcription and translation reactions for eukaryotic *in vitro* translation. The system also combines T7 RNA polymerase, RNA polymerase nucleotides, salts, recombinant ribonuclease inhibitor, amino acids, and transcend biotinylated-lysyl-tRNA, which allowed for the generation of SRC-2 protein using an SRC-2 plasmid in a one hour.

Chapter 5.1.1.3: Quantification of SRC-2-Biotin for the First Pull-Down Assay

Into a 1.5 mL microfuge tube, 20 μ L of the TNT quick master mix was pipetted, followed by 1 μ L of methionine, 1 μ L of biotinylated-lysyl-tRNA, and 1 μ L of SRC-2 mutant plasmid containing 3 nuclear interaction domains (NIDs). The reaction tube was incubated at 30°C for time periods ranging from 60 to 90 minutes.

After the incubation, 23 μL of the TNT mixture was diluted in a 1 to 5 serial dilution using 1X SDS-PAGE MOPS running buffer (Invitrogen). Then, 5 μL of each of the 10 TNT mixture concentrations were added to 20 μL of 1X running buffer and 3 μL of loading buffer and dye (Invitrogen) in a microfuge tube. These microfuge tubes were incubated in a 70°C water bath for 10 minutes. After the incubation, 10 μL of each of the dilutions was pipetted into a lane on an SDS-PAGE gel (Invitrogen), and the gel was resolved at 200 V and 120 mA for 45 minutes in 4-morpholine-propane-sulfonic acid (MOPS) running buffer. The proteins resolved in the SDS-PAGE gel were transferred to a polyvinylidene fluoride (PVDF) membrane using the Bio-Rad Western blot instrument at 100 V and 350 mA for 1 hour in 1X tris-buffered saline (TBS) buffer.

Before running the Western blot, the PVDF membrane was first incubated in 20 mL of methanol for 15 seconds, then in 20 mL of Milli-Q water for 2 minutes, and finally, in 20 mL of TBS buffer for 5 minutes. In the meantime, 2 filter paper sheets were incubated in transfer buffer for 30 seconds. The Western transfer apparatus was assembled with the SDS-PAGE gel closest to the cathode terminal and blotted at 100 V and 350 mA for 1 hour in transfer buffer, in order to transfer the SRC-2-biotin protein from the SDS-PAGE gel to the PVDF membrane (Figure 50).

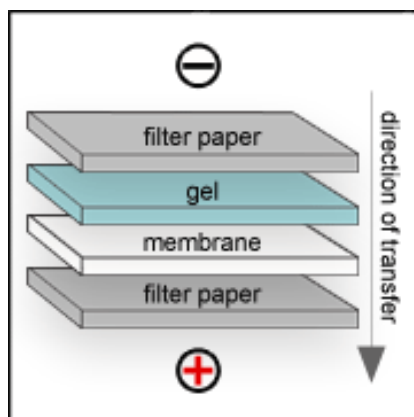


Figure 50: Western blot assembly.

The SRC-2-biotin protein was visualized using the Western Blue Colorimetric System (Promega); therefore, the PVDF membrane was washed for 60 minutes in 15 mL of tris-buffered saline with 20 percent Tween surfactant (TBST), followed by a 45 to 60 minute incubation of TBST buffer containing Streptavidin-AP (6 μ L of Streptavidin-AP in 15 mL of TBST buffer). The membrane was washed twice with 15 mL of TBST buffer for 1 minute each, followed by 2 washes with 15 mL of Milli-Q water for 1 minute each. Western Blue Stabilized Substrate (Promega) was used as colorimetric substrate for AP, while the membrane was allowed to rock back in forth in the solution of 7 mL until the protein bands began to appear, which was usually within 1 to 15 minutes. To stop the color reaction, the membrane was washed 3 times in 15 mL of Milli-Q water for 5 minutes.

The Western Blue solution contains BCIP and nitro blue tetrazolium (NBT). Upon dephosphorylation of the BCIP, a 5-bromo-4-chloro-3-indole, is formed and is further oxidized with NBT to 5, 5'-dibromo-4, 4'-dichloro-indigo, or Indigo-Blue, and diformazan, which is a dark blue and insoluble compound (Figure 51).

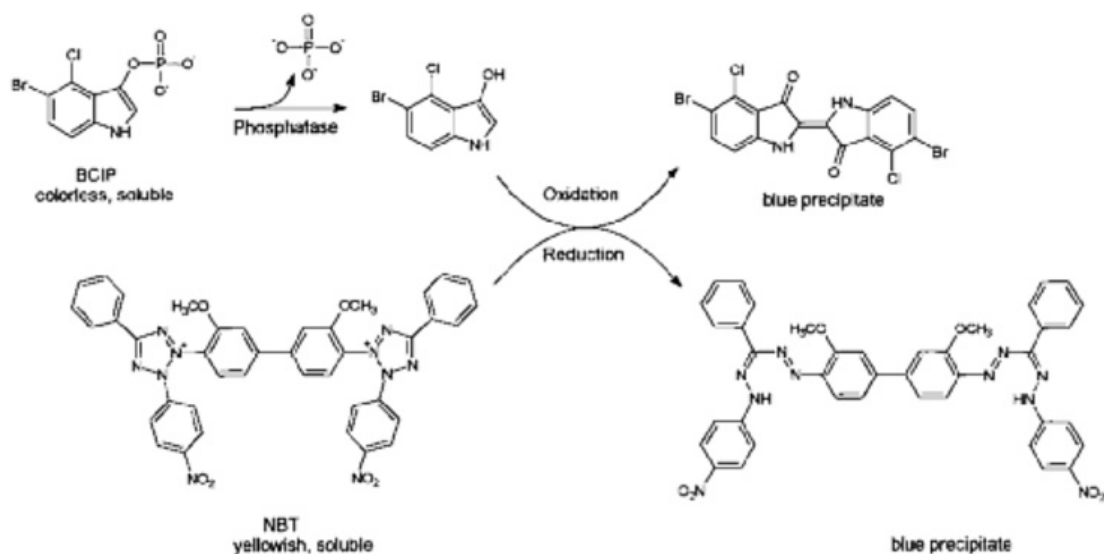


Figure 51: Colorimetric alkaline phosphatase assay.

Figure 52 shows the intensities of different concentrations of SRC-2 generated by the TNT system. The ideal concentration of SRC-2-biotin protein was found to be the 1 to 5 dilution of TNT mixture, as shown in lane 1b of Figure 52. In lane 1c of Figure 52, SRC-2 was still visible, but very faint.

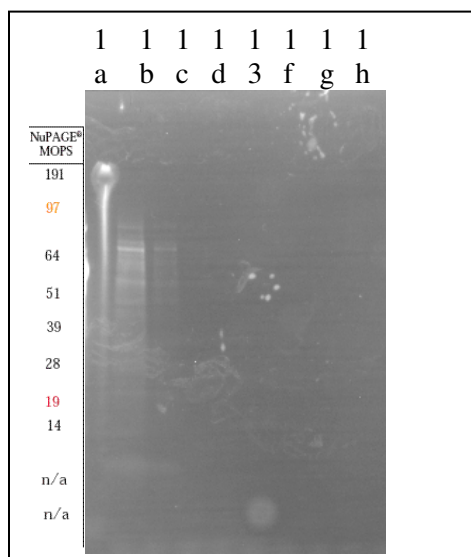


Figure 52: Stained PVDF membrane.

Chapter 5.2: Second Pull-Down Assay: Evaluating VDR-CBI, WL042210D (32a),

Inhibition

After the optimal SRC-2 protein concentration was determined, this protocol was performed in the presence of compound WL042210D (32a), which was identified as a potential CBI of the VDR-SRC-2 interaction; therefore, SRC-2-biotin was generated, as mentioned in the previous protocol, and used in 5 different experimental conditions, as summarized in Tables 2A through 2E.

Table 2A: Condition 1: High Concentration of CBI (200 μ M)

Add	Reagent	Initial Concentration	Initial Volume		Final Concentration	Final Volume
X	VDR Beads		5 μ L			100 μ L
X	VDR Ligand	10 mM	0.5 μ L		50 μ M	100 μ L
X	WL042210D (32a)	10 mM	2 μ L		200 μ M	100 μ L
	DMSO		0 μ L		2%	100 μ L
X	FP Buffer		89 μ L			100 μ L

Table 2B: Condition 2: Medium Concentration of CBI (50 μ M)

Add	Reagent	Initial Concentration	Initial Volume		Final Concentration	Final Volume
X	VDR Beads		5 μ L			100 μ L
X	VDR Ligand	10 mM	0.5 μ L		50 μ M	100 μ L
X	WL042210D (32a)	10 mM	0.5 μ L		50 μ M	100 μ L
X	DMSO		1.5 μ L		2%	100 μ L
X	FP Buffer		89 μ L			100 μ L

Table 2C: Condition 3: Low Concentration of CBI (1 μ M)

Add	Reagent	Initial Concentration	Initial Volume		Final Concentration	Final Volume
X	VDR Beads		5 μ L			100 μ L
X	VDR Ligand	10 mM	0.5 μ L		50 μ M	100 μ L
X	WL042210D (32a)	100 μ M	1 μ L		1 μ M	100 μ L
X	DMSO		1 μ L		2%	100 μ L
X	FP Buffer		89 μ L			100 μ L

Table 2D: Condition 4: VDR-SRC-2 Interaction (Negative Control; No CBI)

Add	Reagent	Initial Concentration	Initial Volume		Final Concentration	Final Volume
X	VDR Beads		5 μ L			100 μ L
X	VDR Ligand	10 mM	0.5 μ L		50 μ M	100 μ L
	WL042210D (32a)	10 mM	0 μ L		0 μ M	100 μ L
X	DMSO		2 μ L		2%	100 μ L
X	FP Buffer		89 μ L			100 μ L

Table 2E: Condition 5: No VDR Ligand (Positive Control; No CBI or VDR Ligand)

Add	Reagent	Initial Concentration	Initial Volume		Final Concentration	Final Volume
X	VDR Beads		5 μ L			100 μ L
	VDR Ligand	10 mM	0.5 μ L		50 μ M	100 μ L
	WL042210D (32a)	10 mM	0 μ L		0 μ M	100 μ L
X	DMSO		2 μ L		2%	100 μ L
X	FP Buffer		89 μ L			100 μ L

In summary, the first microfuge reaction tube contained the CBI at a concentration of 200 μM . The second microfuge reaction tube contained the CBI at a concentration of 50 μM . The third microfuge reaction tube contained the CBI at a concentration of 1 μM . The fourth microfuge reaction tube was the negative control, which had no CBI. The fifth microfuge reaction tube was the positive control, which had no CBI or VDR ligand.

The 5 reactions in the microfuge tubes were incubated on the shaker at room temperature for 30 minutes, followed by the addition of 8 μL of the TNT reaction mixture. After an additional incubation on the shaker for 30 minutes at room temperature, the microfuge tubes were centrifuged for 10 seconds at 3,000 rpm, in order to force the liquid to the bottom of the microfuge tube. Then, 100 μL of each solution was pipetted into separately labeled micro spin columns. The spin columns were centrifuged at 3,000 rpm for 30 seconds. After centrifugation, 100 μL of FP buffer was added to each of the 5 filters of the spin columns, and centrifuged again at 3,000 rpm for 30 seconds. The trap for the bottom of the spin column was exchanged for a clean trap, and 10 μL of a 10 mM maltose solution (36 mg of maltose in 10 mL of FP buffer) was pipetted into the filters of each of the 5 spin columns. The maltose solution eluted VDR from the amylose beads, because VDR had an MBP affinity tag. The spin columns were incubated at room temperature for 5 minutes with the maltose solution before being centrifuged again at 5,000 rpm for 2 minutes. Approximately 5 μL of the liquid was recovered for each reaction. The liquid was pipetted into lanes of an SDS-PAGE gel, which were visualized by a Western blot, as described in the previous protocol.

Unfortunately, no bands were detected in the first pull-down assay conducted with compound WL042210D (32a), as seen in Figure 53. The assay was repeated, doubling the volumes in the TNT reaction mixture and adding 12 μ L of TNT reaction mix to each microfuge tube reaction; however, also in that case, no band were detected (gel not shown).

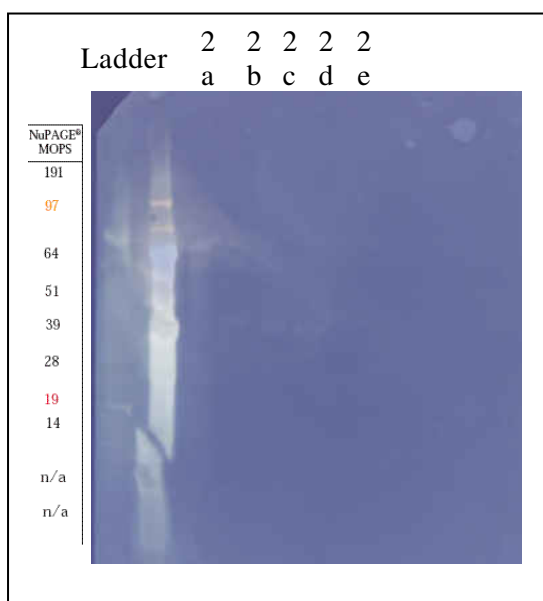


Figure 53: Stained PVDF membrane of the 5 pull-down reactions using VDR-CBI, WL042210D (32a).

Chapter 5.3: Third Pull-Down Assay using a Solid-Supported SRC-2 and VDR-LBD for the Identification of VDR-CBIs

The previously described pull-down assay protocol was modified using SRC-2 coactivator protein attached to a solid support, instead of the VDR protein (Figure 54). Two different SRC-2 proteins were evaluated.

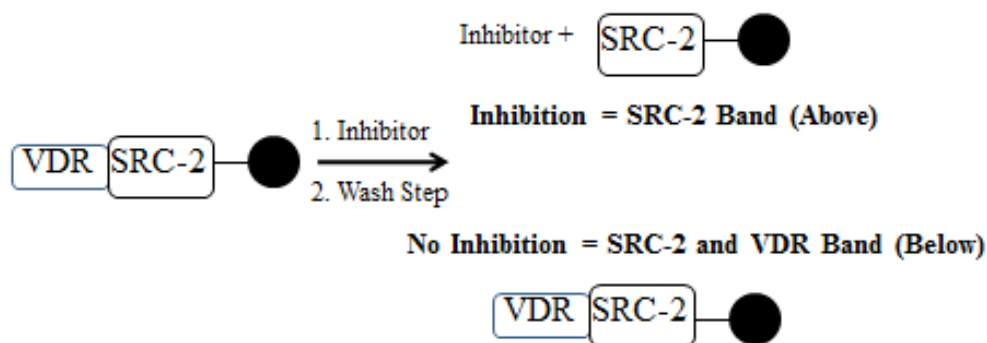


Figure 54: Scheme of the third pull-down assay.

1. An SRC-2 protein containing only 1 NID, called SRC-2-3, was expressed as a His-tagged protein, as previously described in chapter 4. The solid support for this protein was made of nickel-charged NTA chelate, which was immobilized on cross-linked agarose (HisPur Ni-NTA Resin, ThermoScientific). The protein was eluted with a high concentration of imidazole (250 mM).
2. An SRC-2 protein containing 3 NIDs was a larger protein than SRC-2-3 and was expressed as a GST fusion protein. The solid support for this protein was made of glutathione-linked agarose (HisPur Ni-NTA Resin, ThermoScientific) and was eluted with a reduced glutathione buffer (10 mM).

Microfuge tubes were prepared with the following reaction conditions listed in Tables 3A through 3E, in order to quantify VDR-SRC-2 inhibition by compound WL042210D (32a).

Table 3A: Condition 1: High Concentration of CBI (200 μ M)

Add	Reagent	Initial Concentration	Initial Volume		Final Concentration	Final Volume
X	VDR	113 μ M	9 μ L		10.17 μ M	100 μ L
X	Calcitriol	10 μ M	1 μ L		0.1 μ M	100 μ L
X	WL042210D (32a)	10 mM	2 μ L		200 μ M	100 μ L
	DMSO		0 μ L		2%	100 μ L
X	FP Buffer		73 μ L			100 μ L

Table 3B: Condition 2: Medium Concentration of CBI (50 μ M)

Add	Reagent	Initial Concentration	Initial Volume		Final Concentration	Final Volume
X	VDR	113 μ M	9 μ L		10.17 μ M	100 μ L
X	Calcitriol	10 μ M	1 μ L		0.1 μ M	100 μ L
X	WL042210D (32a)	10 mM	0.5 μ L		50 μ M	100 μ L
X	DMSO		1.5 μ L		2%	100 μ L
X	FP Buffer		73 μ L			100 μ L

Table 3C: Condition 3: Low Concentration of CBI (1 μ M)

Add	Reagent	Initial Concentration	Initial Volume		Final Concentration	Final Volume
X	VDR	113 μ M	9 μ L		10.17 μ M	100 μ L
X	Calcitriol	10 μ M	1 μ L		0.1 μ M	100 μ L
X	WL042210D (32a)	100 μ M	1 μ L		1 μ M	100 μ L
X	DMSO		1 μ L		2%	100 μ L
X	FP Buffer		73 μ L			100 μ L

Table 3D: Condition 4: VDR-SRC-2 Interaction (Negative Control; No CBI)

Add	Reagent	Initial Concentration	Initial Volume		Final Concentration	Final Volume
X	VDR	113 μ M	9 μ L		10.17 μ M	100 μ L
X	Calcitriol	10 μ M	1 μ L		0.1 μ M	100 μ L
	WL042210D (32a)	10 mM	0 μ L		0 μ M	100 μ L
X	DMSO		2 μ L		2%	100 μ L
X	FP Buffer		73 μ L			100 μ L

Table 3E: Condition 5: No VDR Ligand (Positive Control; No CBI or VDR Ligand)

Add	Reagent	Initial Concentration	Initial Volume		Final Concentration	Final Volume
X	VDR	113 μ M	9 μ L		10.17 μ M	100 μ L
	Calcitriol	10 μ M	1 μ L		0.1 μ M	100 μ L
	WL042210D (32a)	10 mM	0 μ L		0 μ M	100 μ L
X	DMSO		2 μ L		2%	100 μ L
X	FP Buffer		73 μ L			100 μ L

In summary, two sets of five microfuge reaction tubes were prepared. One set was assayed with SRC-2 with the 3 NIDs, and the second set was assayed with the SRC-2-3 with 1 NID. For each set, the first microfuge reaction tube contained the CBI, WL042210D (32a), at a concentration of 200 μ M. The second microfuge reaction tube contained the CBI at a concentration of 50 μ M. The third microfuge reaction tube contained the CBI at a concentration of 1 μ M. The fourth microfuge reaction tube was the negative control, which had no CBI. The fifth microfuge reaction tube was the positive control, which had no CBI or VDR ligand.

Chapter 5.3.1: Experimental Procedure for the Third Pull-Down Assay

All reactions were incubated on the shaker at room temperature for 2 hours, followed by the addition of 15 μ L of beads and another incubation period of 30 minutes at room temperature on the shaker. Upon completion of the second incubation, the 10 microfuge reaction tubes were centrifuged for 10 seconds at 3,000 rpm, in order to force the liquid to the bottom of the microfuge tube. Then, 100 μ L of VDR-TNT mixture from each microfuge tube was pipetted into separately labeled micro spin columns. The spin columns were centrifuged at 3,000 rpm for 30 seconds. After centrifugation, 100 μ L of FP buffer was added to each of the 10 filters of the spin columns, and centrifuged again at 3,000 rpm for 30 seconds. The trap for the bottom of the spin column was exchanged for a clean trap, and 20 μ L of a 10 mM glutathione solution (30.7 mg of maltose in 10 mL of FP buffer) was pipetted into the filters of each of the 5 GST bead spin columns, and 20 μ L of a 250 mM imidazole solution (85 mg of imidazole in 10 mL of FP buffer) was pipetted into the filters of each of the 5 nickel bead spin columns. The spin columns were

incubated at room temperature for 10 minutes with their respective solution before being centrifuged at 5,000 rpm for 2 minutes.

Approximately 10 μ L of the VDR mixture was recovered after centrifugation, and 3 μ L of the loading buffer and dye was added to each of the 10 microfuge reaction tubes. The solutions were mixed by pipette and incubated in a water bath at 70°C for 10 minutes to denature the protein. The microfuge reaction tubes were centrifuged again at 3,000 rpm for 30 seconds, and 13 μ L from each microfuge reaction tube was pipetted into separate lanes of an SDS-PAGE gel in a gel box containing 1X MOPS running buffer. The gel was resolved for 45 minutes at 200 V and 120 mA, removed from the plastic casing, and rinsed in Milli-Q water 3 times for 5 minutes each time. The gel was incubated for 2 hours using Simply Blue Stain (Invitrogen) and rinsed overnight in Milli-Q water. The image in Figure 55 was obtained from the gel.

Chapter 5.3.2: Results of the Third Pull-Down Assay

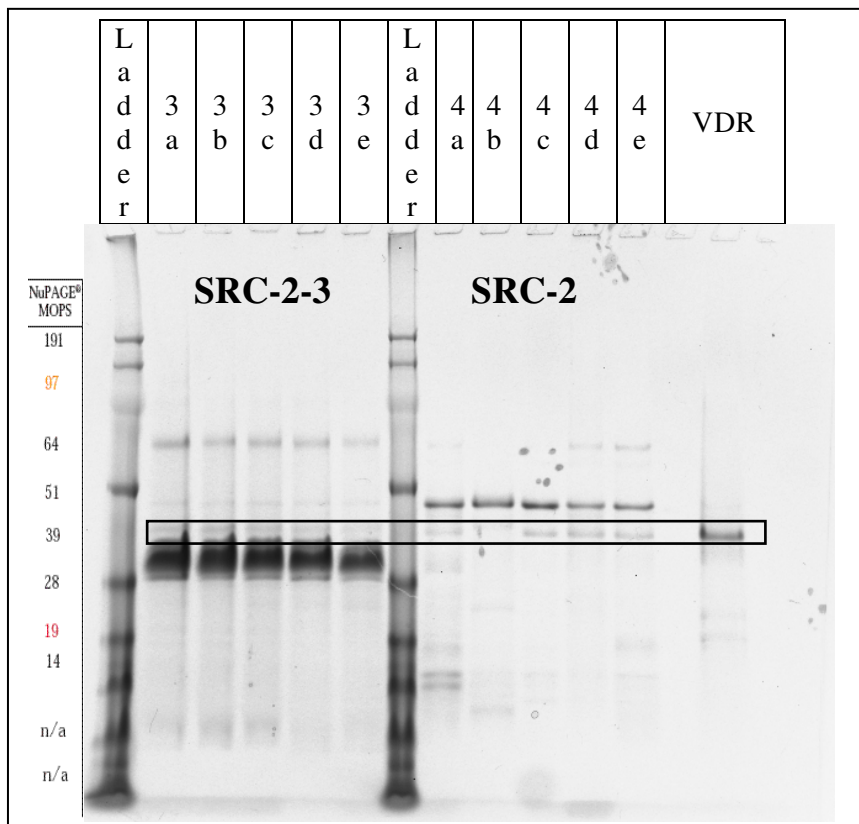


Figure 55: SDS-PAGE gel of the VDR-coactivator pull-down assay using compound WL042210D (32a).

The first column on the left-hand side was the See Blue 2 ladder (Invitrogen). Columns 3a through 3e contained the samples of the SRC-2-3 with 1 NID, and columns 4a through 4e contained the SRC-2 with the 3 NIDs. VDR was used as control. The intensity of the VDR bands changed significantly for the SRC-2 experiment. With increasing concentrations of compound WL042210D (32a), there was a change among the SRC-2 lanes, 4a, 4b, and 4c, with 4c being the most visible band. A similar change

was not observed for the SRC-2-3 lanes, indicating that SRC-2-3 did not bind to VDR, but SRC-2 did.

Chapter 5.3.3: The Fourth Pull-Down Assay with CBIs WL052410G (31b) and CBT-1

Based on the results from the third pull-down assay, 5 experiments each were repeated with 2 other VDR-CBIs, compounds WL052410G (31b) and CBT-1, with the conditions described in Tables 4A through 4E.

Table 4A: Condition 1: High Concentration of CBI (200 μ M)

Add	Reagent	Initial Concentration	Initial Volume		Final Concentration	Final Volume
X	VDR	88 μ M	11.5 μ L		10.12 μ M	100 μ L
X	Calcitriol	10 μ M	1 μ L		0.1 μ M	100 μ L
X	WL052410G (31b)/CBT-1	10 mM	2 μ L		200 μ M	100 μ L
	DMSO		0 μ L		2%	100 μ L
X	FP Buffer		65.5 μ L			100 μ L

Table 4B: Condition 2: Medium High Concentration of CBI (100 μ M)

Add	Reagent	Initial Concentration	Initial Volume		Final Concentration	Final Volume
X	VDR	88 μ M	11.5 μ L		10.12 μ M	100 μ L
X	Calcitriol	10 μ M	1 μ L		0.1 μ M	100 μ L
X	WL052410G (31b)/CBT-1	10 mM	1 μ L		100 μ M	100 μ L
X	DMSO		1 μ L		2%	100 μ L
X	FP Buffer		65.5 μ L			100 μ L

Table 4C: Condition 3: Medium Low Concentration of CBI (50 μ M)

Add	Reagent	Initial Concentration	Initial Volume		Final Concentration	Final Volume
X	VDR	88 μ M	11.5 μ L		10.12 μ M	100 μ L
X	Calcitriol	10 μ M	1 μ L		0.1 μ M	100 μ L
X	WL052410G (31b)/CBT-1	10 mM	0.5 μ L		50 μ M	100 μ L
X	DMSO		1.5 μ L		2%	100 μ L
X	FP Buffer		65.5 μ L			100 μ L

Table 4D: Condition 4: Low Concentration of CBI (1 μ M)

Add	Reagent	Initial Concentration	Initial Volume		Final Concentration	Final Volume
X	VDR	88 μ M	11.5 μ L		10.12 μ M	100 μ L
X	Calcitriol	10 μ M	1 μ L		0.1 μ M	100 μ L
X	WL052410G (31b)/CBT-1	100 μ M	1 μ L		1 μ M	100 μ L
X	DMSO		1 μ L		2%	100 μ L
X	FP Buffer		65.5 μ L			100 μ L

Table 4E: Condition 5: VDR-SRC-2 Interaction (Negative Control; No CBI)

Add	Reagent	Initial Concentration	Initial Volume		Final Concentration	Final Volume
X	VDR	88 μ M	11.5 μ L		10.17 μ M	100 μ L
X	Calcitriol	10 μ M	1 μ L		0.1 μ M	100 μ L
	WL052410G (31b)/CBT-1	10 mM	0 μ L		0 μ M	100 μ L
X	DMSO		2 μ L		2%	100 μ L
X	FP Buffer		65.5 μ L			100 μ L

The microfuge reaction tubes were incubated on the shaker at room temperature for 2 hours. After the 2 hour incubation, 15 μ L of GST beads with SRC-2 coactivator were added to all of the 10 microfuge reaction tubes. These 10 microfuge reaction tubes were incubated for another 30 minutes at room temperature on the shaker. The previous procedure for the spin columns used for the GST beads was repeated for these 10 microfuge reaction tubes. Upon elution of the GST beads with 20 μ L of 10 mM glutathione solution, 10 μ L of the solution from each microfuge reaction tube was recovered. The recovered solution was then mixed with 3 μ L of loading dye and resolved on an SDS-PAGE gel, as seen in Figure 56.

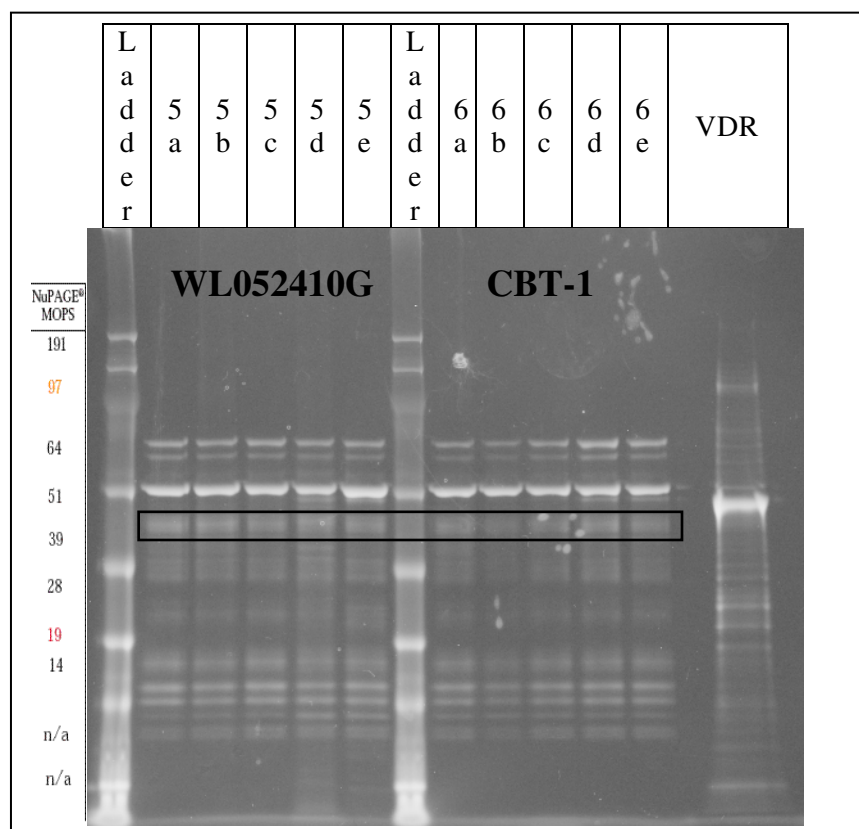


Figure 56: SDS-PAGE gel of the VDR-coactivator pull-down assay using compounds WL052410G (31b) and CBT-1.

The experiment showed that compound CBT-1 was a more active CBI than compound WL052410G (31b), exhibiting a fainter band at higher concentrations; nevertheless, the intensity difference is small, which might be due to unspecific binding or the presence of an overlapping band from the SRC-2 expression. In order to specifically identify the VDR band, VDR-specific antibodies were applied in a co-immunoprecipitation pull-down assay.

Chapter 5.4: Co-Immunoprecipitation Pull-Down Assay using a Solid-Supported SRC-2 and VDR-LBD for the Identification of VDR-CBIs

To verify the inhibition of the VDR-SRC-2 interaction by compound WL052410G (31b), 8 reactions were carried out with the conditions listed in Tables 5A through 5H, which is according to the scheme depicted in Figure 57.

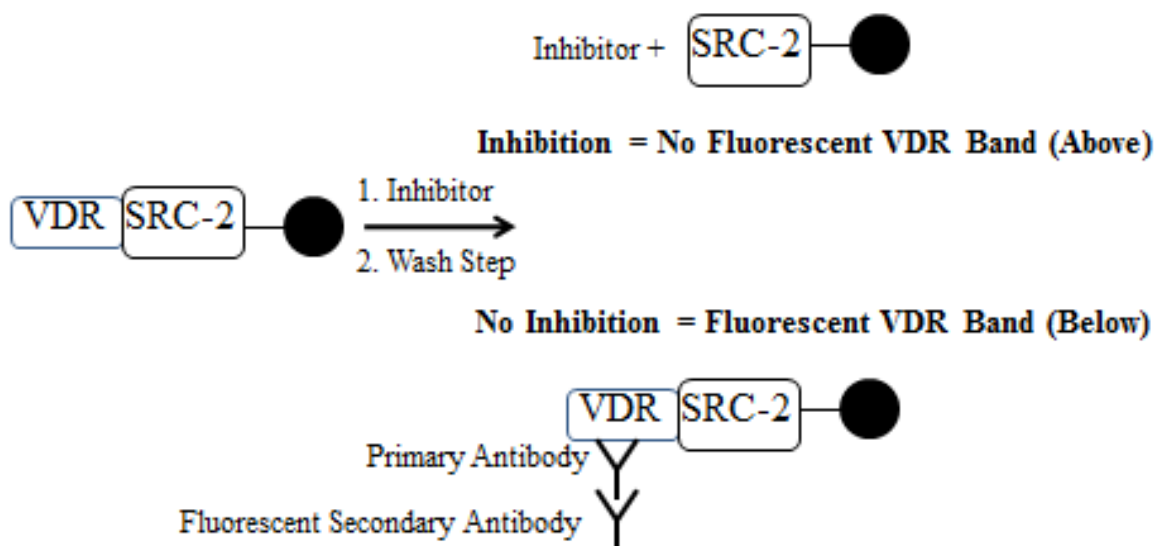


Figure 57: Co-IP pull-down assay scheme.

Table 5A: Condition 1: High Concentration of CBI (200 μ M)

Add	Reagent	Initial Concentration	Initial Volume		Final Concentration	Final Volume
X	VDR	106 μ M	9.5 μ L		10.07 μ M	100 μ L
X	Calcitriol	10 μ M	1 μ L		0.1 μ M	100 μ L
X	WL052410G (31b)	10 mM	2 μ L		200 μ M	100 μ L
	DMSO		0 μ L		2%	100 μ L
X	FP Buffer		68 μ L			100 μ L

Table 5B: Condition 2: Medium High Concentration of CBI (100 μ M)

Add	Reagent	Initial Concentration	Initial Volume		Final Concentration	Final Volume
X	VDR	106 μ M	9.5 μ L		10.07 μ M	100 μ L
X	Calcitriol	10 μ M	1 μ L		0.1 μ M	100 μ L
X	WL052410G (31b)	10 mM	1 μ L		100 μ M	100 μ L
X	DMSO		1 μ L		2%	100 μ L
X	FP Buffer		68 μ L			100 μ L

Table 5C: Condition 3: Medium Low Concentration of CBI (50 μ M)

Add	Reagent	Initial Concentration	Initial Volume		Final Concentration	Final Volume
X	VDR	106 μ M	9.5 μ L		10.07 μ M	100 μ L
X	Calcitriol	10 μ M	1 μ L		0.1 μ M	100 μ L
X	WL052410G (31b)	10 mM	0.5 μ L		50 μ M	100 μ L
X	DMSO		1.5 μ L		2%	100 μ L
X	FP Buffer		68 μ L			100 μ L

Table 5D: Condition 4: Low Concentration of CBI (1 μ M)

Add	Reagent	Initial Concentration	Initial Volume		Final Concentration	Final Volume
X	VDR	106 μ M	9.5 μ L		10.07 μ M	100 μ L
X	Calcitriol	10 μ M	1 μ L		0.1 μ M	100 μ L
X	WL052410G (31b)	100 μ M	1 μ L		1 μ M	100 μ L
X	DMSO		1 μ L		2%	100 μ L
X	FP Buffer		68 μ L			100 μ L

Table 5E: Condition 5: VDR-SRC-2 Interaction (Negative Control; No CBI)

Add	Reagent	Initial Concentration	Initial Volume		Final Concentration	Final Volume
X	VDR	106 μ M	9.5 μ L		10.07 μ M	100 μ L
X	Calcitriol	10 μ M	1 μ L		0.1 μ M	100 μ L
	WL052410G (31b)	10 mM	0 μ L		0 μ M	100 μ L
X	DMSO		2 μ L		2%	100 μ L
X	FP Buffer		68 μ L			100 μ L

Table 5F: Condition 6: No VDR Ligand (Positive Control; No CBI or VDR Ligand)

Add	Reagent	Initial Concentration	Initial Volume		Final Concentration	Final Volume
X	VDR	106 μ M	9.5 μ L		10.07 μ M	100 μ L
	Calcitriol	10 μ M	0 μ L		0.1 μ M	100 μ L
	WL052410G (31b)	10 mM	0 μ L		0 μ M	100 μ L
X	DMSO		2 μ L		2%	100 μ L
X	FP Buffer		69 μ L			100 μ L

Table 5G: Condition 7: SRC-2 Beads Only (SRC-2 Protein Only)

Add	Reagent	Initial Concentration	Initial Volume		Final Concentration	Final Volume
	VDR	106 μ M	0 μ L		10.07 μ M	100 μ L
	Calcitriol	10 μ M	0 μ L		0.1 μ M	100 μ L
	WL052410G (31b)	10 mM	0 μ L		0 μ M	100 μ L
	DMSO		0 μ L		2%	100 μ L
X	FP Buffer		80 μ L			100 μ L

Table 5H: Condition 8: VDR Protein Only

Add	Reagent	Initial Concentration	Initial Volume		Final Concentration	Final Volume
X	VDR	106 μ M	0.2 μ L		2.12 μ M	10 μ L
	Calcitriol	10 μ M	0 μ L		0.1 μ M	10 μ L
	WL052410G (31b)	10 mM	0 μ L		0 μ M	10 μ L
	DMSO		0 μ L		2%	10 μ L
X	FP Buffer		0 μ L			10 μ L
X	Milli-Q Water		10 μ L			10 μ L

Chapter 5.4.1: Experimental Procedure for the First Co-Immunoprecipitation Pull-Down Assay

The reaction conditions represented in Tables 5A through 5F were incubated at room temperature on the shaker for 2 hours. After the 2 hour incubation, 15 μ L of GST beads were added, as well as SRC-2 protein only. After incubating the microfuge tubes for 30 minutes at room temperature and a wash step, the protein was eluted from the solid support and resolved on an SDS-PAGE gel, as described previously. A Western blot was developed from the SDS-PAGE gel, according to the previously described protocol; however, the Western membrane was dried overnight after the protein transfer. The next day, the Western membrane was incubated in methanol for 15 seconds, followed by incubation in a 3 percent bovine serum albumin (BSA) blocking buffer solution (0.6 grams of BSA in 19.40 mL of TBST buffer) on a rocking apparatus for 60 minutes.

Then, a 1 to 10,000 dilution of primary antibody solution of anti-MBP monoclonal antibody (2 μ L of primary VDR antibody in 20 mL of TBST buffer; New England Biolabs) was prepared. The Western membrane was incubated for 60 minutes in the primary antibody solution, washed 3 times in TBST buffer for 5 minutes each wash, and incubated with a 1 to 300 dilution of fluorescent secondary antibody solution of goat anti-mouse IgG-TR (66.7 μ L of secondary antibody in 20 mL of TBST buffer; Santa Cruz Biotechnology) on a rocking apparatus for 60 minutes. After 3 more washes with TBST buffer for 5 minutes each wash, the Western membrane was imaged on the Bio-Rad laser imager.

Chapter 5.4.1.1: Antibodies used for the Co-IP Pull-Down Assay

The basic structural unit of most mammalian antibodies is a glycoprotein of four polypeptide chains; two of which are light chains, and two of which are heavy chains, that are connected by disulfide bonds (Figure 59). The hinge region permits flexibility between the two arms of the Y-shaped antibody molecule, allowing them to open and close to accommodate binding.

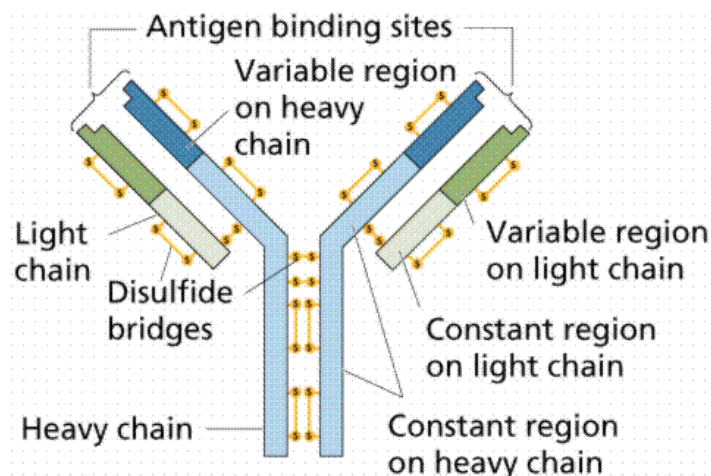


Figure 58: Basic structure of an antibody.

The primary antibody, anti-MBP monoclonal antibody, is a murine, anti-maltose binding protein antibody with an isotype of IgG2a. Immunoglobulin G (IgG) antibodies are distinguished by their two heavy γ chains. The heavy chains also determine the functional activity of the antibody. This particular antibody was used to detect MBP in Western blots.

The secondary antibody, goat anti-mouse IgG-TR, reacts with the heavy chains of the primary antibody and is conjugated with Texas Red fluorophore, which allows for fluorescent detection on a laser imager.

Chapter 5.4.2: Results of the First Co-Immunoprecipitation Pull-Down Assay

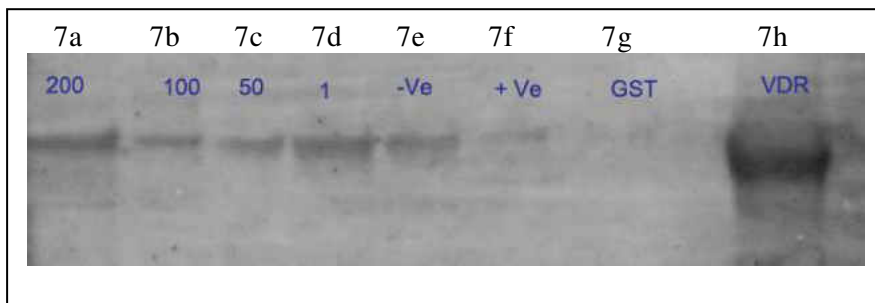


Figure 59: First co-IP VDR-coactivator pull-down assay using compound WL052410G (31b).

Control experiments indicated that SRC-2 bound to VDR in the presence of the calcitriol, as seen in Figure 59, lane 7e, but not in the absence of calcitriol, as seen in Figure 59, lane 7f. The VDR-SRC-2 interaction was blocked in a dose-dependent manner by compound WL052410G (31b), which can be seen in Figure 59, lanes 7b through 7d. Although significant inhibition of the VDR-SRC-2 interaction was observed at a concentrations of 50 μ M and 100 μ M of compound WL052410G (31b), a residual interaction between VDR and SRC-2 could still be detected at these concentrations, due to unspecific binding or insufficient washing.

Interestingly, at a very high concentration of compound WL052410G (31b), the VDR-SRC-2 interaction was still observed, which was most likely caused by the cross-linking of this irreversible inhibitor.

Chapter 5.4.3: The Second Co-Immunoprecipitation Pull-Down Assay

To optimize the conditions of the first co-IP pull-down assay, the following changes were made to the protocol. First, 15 μ L of glutathione solution was used to elute the GST beads, instead of the previous amount of 2 μ L. Additionally in this step, the spin columns were centrifuged at 14,000 rpm for 5 minutes, which eluted 13 to 15 μ L of protein complex, instead of the 10 μ L previously eluted. Furthermore, 5 percent dried milk solution (1 gram of dried milk in 19 mL of TBST buffer) was used to block the membrane, instead of the 3 percent BSA solution. Finally, a 1 to 400 dilution of the secondary antibody solution (50.0 μ L of secondary antibody in 20 mL of TBST buffer) was used instead of a 1 to 300 dilution.

Overall, an improvement was observed with the modified procedure. Unspecific binding was not observed for the negative and positive control reactions, as seen in Figure 60 in lanes 8f and 8g, respectively. Also, full inhibition of VDR-coactivator binding was observed at a concentration of 100 μ M of compound WL052410G (31b), as seen in lane 8b.

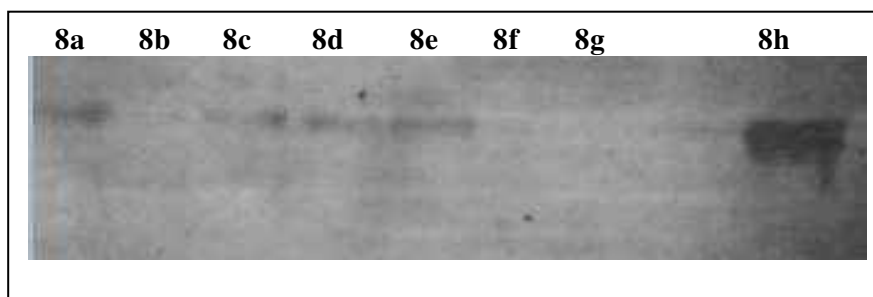


Figure 60: Second co-IP VDR-coactivator pull-down assay using compound WL052410G (31b).

Chapter 5.5: Co-Immunoprecipitation Pull-Down Assay using a Solid-Supported SRC-2 and VDR-LBD for the Identification of a Reversible VDR-CBI, Compound GW 0742

Compound GW 0742 was identified during an HTS as a potential CBI of the VDR-SRC-2 coactivator interaction. Compound GW 0742 was introduced by GlaxoSmithKline in 2003 as a highly selective agonist for PPAR δ .⁴⁴ Since then, compound GW 0742 has been investigated in cell-based assays and *in vivo* assays, in order to understand the role of PPAR δ in hypertension,^{45, 46} diabetes,^{47, 48} inflammation,^{49, 50} obesity,⁵¹ and cancer.⁵²⁻⁵⁴ Interestingly, PPAR agonists have been shown to inhibit the transcription of the VDR target gene, *CYP24A1*, in the presence of 1,25-(OH) $_2$ D $_3$;⁵⁵ therefore, the ability of compound GW 0742 to inhibit the interaction VDR-SRC-2 coactivator was analyzed with the developed co-IP pull-down assay, and determined to inhibit the interaction in a dose-dependent manner.

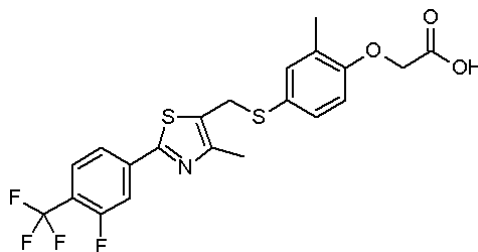


Figure 61: Chemical structure of compound GW 0742.

The following reactions with compound GW 0742 were performed at concentrations of 120 μ M, 80 μ M, 50 μ M, 20 μ M, 10 μ M, 1 μ M, and 0.1 μ M, as summarized in Tables 6A through 6I. The concentration used previously for the band of the VDR protein only was halved from 2.12 μ M in the previous protocols to 1.06 μ M in

this protocol. Additionally, a synthetic VDR agonist ligand, LG 190178⁶⁰, was used instead of calcitriol ligand.

Table 6A: Condition 1: Concentration One of CBI (120 μ M)

Add	Reagent	Initial Concentration	Initial Volume		Final Concentration	Final Volume
X	VDR	106 μ M	9.5 μ L		10.07 μ M	100 μ L
X	LG 190178	100 μ M	1 μ L		1 μ M	100 μ L
X	GW 0742	6 mM	2 μ L		120 μ M	100 μ L
	DMSO		0 μ L		2%	100 μ L
X	FP Buffer		68 μ L			100 μ L

Table 6B: Condition 2: Concentration Two of CBI (80 μ M)

Add	Reagent	Initial Concentration	Initial Volume		Final Concentration	Final Volume
X	VDR	106 μ M	9.5 μ L		10.07 μ M	100 μ L
X	LG 190178	100 μ M	1 μ L		1 μ M	100 μ L
X	GW 0742	2 mM	2 μ L		80 μ M	100 μ L
	DMSO		0 μ L		2%	100 μ L
X	FP Buffer		68 μ L			100 μ L

Table 6C: Condition 3: Concentration Three of CBI (50 μ M)

Add	Reagent	Initial Concentration	Initial Volume		Final Concentration	Final Volume
X	VDR	106 μ M	9.5 μ L		10.07 μ M	100 μ L
X	LG 190178	100 μ M	1 μ L		1 μ M	100 μ L
X	GW 0742	0.67 mM	2 μ L		50 μ M	100 μ L
	DMSO		0 μ L		2%	100 μ L
X	FP Buffer		68 μ L			100 μ L

Table 6D: Condition 4: Concentration Four of CBI (20 μ M)

Add	Reagent	Initial Concentration	Initial Volume		Final Concentration	Final Volume
X	VDR	106 μ M	9.5 μ L		10.07 μ M	100 μ L
X	LG 190178	100 μ M	1 μ L		1 μ M	100 μ L
X	GW 0742	0.22 mM	2 μ L		20 μ M	100 μ L
	DMSO		0 μ L		2%	100 μ L
X	FP Buffer		68 μ L			100 μ L

Table 6E: Condition 5: Concentration Five of CBI (10 μ M)

Add	Reagent	Initial Concentration	Initial Volume		Final Concentration	Final Volume
X	VDR	106 μ M	9.5 μ L		10.07 μ M	100 μ L
X	LG 190178	100 μ M	1 μ L		1 μ M	100 μ L
X	GW 0742	74 μ M	2 μ L		10 μ M	100 μ L
	DMSO		0 μ L		2%	100 μ L
X	FP Buffer		68 μ L			100 μ L

Table 6F: Condition 6: Concentration Six of CBI (1 μ M)

Add	Reagent	Initial Concentration	Initial Volume		Final Concentration	Final Volume
X	VDR	106 μ M	9.5 μ L		10.07 μ M	100 μ L
X	LG 190178	100 μ M	1 μ L		1 μ M	100 μ L
X	GW 0742	25 μ M	2 μ L		1 μ M	100 μ L
	DMSO		0 μ L		2%	100 μ L
X	FP Buffer		68 μ L			100 μ L

Table 6G: Condition 7: Concentration Seven of CBI (0.1 μ M)

Add	Reagent	Initial Concentration	Initial Volume		Final Concentration	Final Volume
X	VDR	106 μ M	9.5 μ L		10.07 μ M	100 μ L
X	LG 190178	100 μ M	1 μ L		1 μ M	100 μ L
X	GW 0742	8 μ M	2 μ L		0.1 μ M	100 μ L
	DMSO		0 μ L		2%	100 μ L
X	FP Buffer		68 μ L			100 μ L

Table 6H: Condition 8: VDR-SRC-2 Interaction (Negative Control; No CBI)

Add	Reagent	Initial Concentration	Initial Volume		Final Concentration	Final Volume
X	VDR	106 μ M	9.5 μ L		10.07 μ M	100 μ L
X	LG 190178	100 μ M	1 μ L		1 μ M	100 μ L
	GW 0742	0 mM	0 μ L		0 μ M	100 μ L
X	DMSO		2 μ L		2%	100 μ L
X	FP Buffer		68 μ L			100 μ L

Table 6I: Condition 9: No VDR Ligand (Positive Control; No CBI or Ligand)

Add	Reagent	Initial Concentration	Initial Volume		Final Concentration	Final Volume
X	VDR	106 μ M	9.5 μ L		10.07 μ M	100 μ L
	LG 190178	0 μ M	0 μ L		0 μ M	100 μ L
	GW 0742	0 mM	0 μ L		0 μ M	100 μ L
X	DMSO		3 μ L		2%	100 μ L
X	FP Buffer		69 μ L			100 μ L

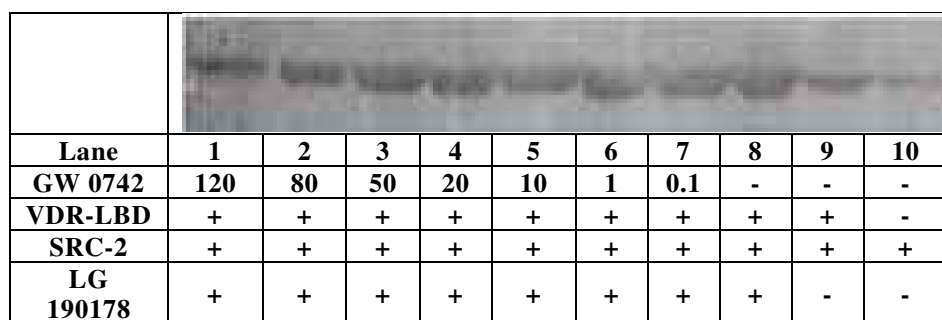
Table 6J: Condition 10: SRC-2 Beads Only (SRC-2 Protein Only)

Add	Reagent	Initial Concentration	Initial Volume		Final Concentration	Final Volume
	VDR	0 μ M	0 μ L		0 μ M	100 μ L
	LG 190178	0 μ M	0 μ L		0 μ M	100 μ L
	GW 0742	0 mM	0 μ L		0 μ M	100 μ L
	DMSO		0 μ L		2%	100 μ L
X	FP Buffer		80 μ L			100 μ L

Table 6K: Condition 11: VDR Protein Only

Add	Reagent	Initial Concentration	Initial Volume		Final Concentration	Final Volume
X	VDR	106 μ M	0.1 μ L		1.06 μ M	10 μ L
	LG 190178	0 μ M	0 μ L		0 μ M	10 μ L
	GW 0742	0 mM	0 μ L		0 μ M	10 μ L
	DMSO		0 μ L		2%	10 μ L
	FP Buffer		0 μ L			10 μ L
X	Milli-Q Water		10 μ L			10 μ L

From this point, the same protocol used in the previous co-IP assay was applied for CBI incubation, spin column purification, resolution on the SDS-PAGE gel, the Western blot transfer, and antibody incubation of the Western blot membrane. The following results in Figure 62 were obtained.

**Figure 62:** Inhibition of the VDR–SRC-2 interaction by compound GW 0742, analyzed by a co-IP pull-down assay.

Control experiments indicated that SRC-2 bound to VDR in the presence of LG 190178 ligand, as seen in Figure 62, lane 8, but not in the absence of the LG 190178 ligand, as seen in Figure 62, lane 9. The faint bands for SRC-2 in the absence of VDR ligand and in the absence of VDR were caused by the unspecific binding between the VDR antibody and the SRC-2 beads. The VDR–SRC-2 interaction was blocked in a dose-dependent manner by compound GW 0742, as seen in Figure 62, lanes 1 through 7. Although significant inhibition of the VDR–SRC-2 interaction was observed at the concentrations of 120 μ M and 80 μ M of compound GW 0742, residual bands could still be detected, partially due to unspecific binding of the VDR antibody to SRC-2 beads, as observed for the controls.

Chapter 5.6: Discussion of the Results of the Co-Immunoprecipitation Pull-Down Assays

When considering small molecule CBIs for the co-IP pull-down assays, the compounds that were most active in transcriptional inhibition and had partial toxicity were selected. This was compound WL052410G (31b), bearing a chlorobenzene group, and compound WL042210D (32a), bearing an aniline group and a methyl group attached to the nitrogen of the indolyl group. The results are published in Nandhikonda et al.²⁹

The first pull-down assay determined that a 1 to 5 serial dilution of the TNT mixture was the most useful concentration in this assay. This assay was then performed in the presence of compound WL042210D (32a), which was identified as an inactive CBI of the VDR-coactivator interaction. Since no bands were detected in this experiment or the experiment using double the volume of TNT reaction mixture, the protocol was

modified to use one of the two SRC coactivator proteins as the protein attached to a solid support, instead of the VDR protein. It was determined that the SRC-2 protein with all 3 NIDs, instead of the SRC-2 protein with only 1 NID, or SRC-2-3, was effective in immunoprecipitating the VDR-small molecule CBI interaction.

After it was determined that the SRC-2 with 3 NIDs was the most effective protein for immunoprecipitation, 2 other VDR-CBIs, compounds WL052410G (31b) and CBT-1, were tested. The results showed that compound CBT-1 was slightly more active at inhibition than compound WL052410G (31b), which might be due to unspecific binding or the presence of an overlapping band from the SRC-2 expression. The results were verified for compound WL052410G (31b) by performing an additional experiment using 2 VDR-specific antibodies in the first co-immunoprecipitation pull-down assay.

The control experiments indicated that SRC-2 bound to VDR in the presence of calcitriol, but not in the absence of calcitriol. The VDR-SRC-2 interaction was blocked in a dose-dependent manner by compound WL052410G (31b). Although significant inhibition of the VDR-SRC-2 interaction was observed at a concentrations of 50 μ M and 100 μ M of compound WL052410G (31b), a residual interaction between VDR and SRC-2 could still be detected at these concentrations, due to unspecific binding, insufficient washing, or the cross-linking of this irreversible inhibitor.

A few changes were made in the protocol to eliminate the residual interaction between VDR and SRC-2 at higher concentrations. These included adding 15 μ L of glutathione solution to elude the GST beads, instead of the previous amount of 2 μ L, centrifuging the spin columns at 14,000 rpm for 5 minutes, which eluted 13 to 15 μ L of protein complex, instead of the 10 μ L previously eluted, adding 5 percent dried milk

solution (1 gram of dried milk in 19 mL of TBST buffer) to block the Western membrane, instead of the 3 percent BSA solution, and performing a 1 to 400 dilution of the secondary antibody solution (50.0 μ L of secondary antibody in 20 mL of TBST buffer), instead of a 1 to 300 dilution. By making these changes, unspecific binding was eliminated for the reactions. Also, full inhibition of VDR-coactivator binding was observed at a concentration of 100 μ M of compound WL052410G (31b).

Compound GW 0742 was identified during an HTS as a potential CBI of the VDR-SRC-2 coactivator interaction. This compound was used in the developed co-IP pull-down assay at concentrations that varied from 120 μ M to 0.1 μ M. Two additional changes to the protocol included changing the concentration of the VDR protein only from 2.12 μ M to 1.06 μ M and using a synthetic LG 190178⁶⁰ ligand, instead of calcitriol.

SRC-2 was shown to bind to VDR in the presence of LG 190178 ligand, but not in the absence of the ligand. The faint bands for SRC-2 in the absence of ligand and in the absence of VDR were caused by the unspecific binding between the VDR antibody and the SRC-2 beads. The VDR-SRC-2 interaction was shown to be blocked in a dose-dependent manner by compound GW 0742. Although significant inhibition of the VDR-SRC-2 interaction was observed at the concentrations of 120 μ M and 80 μ M of compound GW 0742, residual bands could still be detected, partially due to unspecific binding of the VDR antibody to SRC-2 beads. The results have been recently published in *Biochemistry*.⁵⁶

Chapter 6: References

1. Jurutka, P. W., Whitfield, G. K., Hsieh, J. C., Thompson, P. D., Haussler, C. A., and Haussler, M. R. (2001) Molecular nature of the vitamin D receptor and its role in regulation of gene expression, *Rev Endocr Metab Disord* 2, 203-216.
2. Yamada, S., Shimizu, M., and Yamamoto, K. (2003) Vitamin D receptor, *Endocr Dev* 6, 50-63.
3. Toell, A., Polly, P., and Carlberg, C. (2000) All natural DR3-type vitamin D response elements show a similar functionality in vitro, *Biochem J* 352 Pt 2, 301-309.
4. Brumbaugh, P. F., and Haussler, M. R. (1974) 1 Alpha,25-dihydroxycholecalciferol receptors in intestine. I. Association of 1 alpha,25-dihydroxycholecalciferol with intestinal mucosa chromatin, *J Biol Chem* 249, 1251-1257.
5. Reddy, G. S., and Tserng, K. Y. (1989) Calcitroic acid, end product of renal metabolism of 1,25-dihydroxyvitamin D3 through C-24 oxidation pathway, *Biochemistry* 28, 1763-1769.
6. Esvelt, R. P., Schnoes, H. K., and DeLuca, H. F. (1979) Isolation and characterization of 1 alpha-hydroxy-23-carboxytetranorvitamin D: a major metabolite of 1,25-dihydroxyvitamin D3, *Biochemistry* 18, 3977-3983.
7. Horst, R. L., Reinhardt, T. A., Ramberg, C. F., Koszewski, N. J., and Napoli, J. L. (1986) 24-Hydroxylation of 1,25-dihydroxyergocalciferol. An unambiguous deactivation process, *J Biol Chem* 261, 9250-9256.
8. Vanhooke, J. L., Benning, M. M., Bauer, C. B., Pike, J. W., and DeLuca, H. F. (2004) Molecular structure of the rat vitamin D receptor ligand binding domain complexed with 2-carbon-substituted vitamin D3 hormone analogues and a LXXLL-containing coactivator peptide, *Biochemistry* 43, 4101-4110.
9. Kim, J. Y., Son, Y. L., and Lee, Y. C. (2009) Involvement of SMRT corepressor in transcriptional repression by the vitamin D receptor, *Mol Endocrinol* 23, 251-264.
10. Hu, X., and Lazar, M. (1999) The CoRNR motif controls the recruitment of corepressors by nuclear hormone receptors., *Nature* 402, 93-96.
11. Nagy, L., Kao, H., Love, J., Li, C., Banayo, E., Gooch, J., Krishna, V., Chatterjee, K., Evans, R., and Schwabe, J. (1999) Mechanism of corepressor binding and release from nuclear hormone receptors., *Genes Dev* 13, 3209-3216.
12. Heinzl, T., Lavinsky, R. M., Mullen, T. M., Soderstrom, M., Laherty, C. D., Torchia, J., Yang, W. M., Brard, G., Ngo, S. D., Davie, J. R., Seto, E., Eisenman, R. N., Rose, D. W., Glass, C. K., and Rosenfeld, M. G. (1997) A complex containing N-CoR, mSin3 and histone deacetylase mediates transcriptional repression, *Nature* 387, 43-48.
13. Nagy, L., Kao, H. Y., Chakravarti, D., Lin, R. J., Hassig, C. A., Ayer, D. E., Schreiber, S. L., and Evans, R. M. (1997) Nuclear receptor repression mediated by a complex containing SMRT, mSin3A, and histone deacetylase, *Cell* 89, 373-380.

14. Masuyama, H., Brownfield, C. M., St-Arnaud, R., and MacDonald, P. N. (1997) Evidence for ligand-dependent intramolecular folding of the AF-2 domain in vitamin D receptor-activated transcription and coactivator interaction, *Mol Endocrinol* 11, 1507-1517.
15. Hong, H., Kohli, K., Garabedian, M. J., and Stallcup, M. R. (1997) GRIP1, a transcriptional coactivator for the AF-2 transactivation domain of steroid, thyroid, retinoid, and vitamin D receptors, *Mol Cell Biol* 17, 2735-2744.
16. Li, H., Gomes, P. J., and Chen, J. D. (1997) RAC3, a steroid/nuclear receptor-associated coactivator that is related to SRC-1 and TIF2, *Proc Natl Acad Sci U S A* 94, 8479-8484.
17. Yuan, C., Ito, M., Fondell, J., Fu, Z., and Roeder, R. (1998) The TRAP220 component of a thyroid hormone receptor-associated protein (TRAP) coactivator complex interacts directly with nuclear receptors in a ligand-dependent fashion., *PNAS* 95, 7939-7944.
18. Rachez, C., Lemon, B., Suldan, Z., Bromleigh, V., Gamble, M., Naar, A., Erdjument-Bromage, H., Tempst, P., and Freedman, L. (1999) Ligand-dependent transcription activation by nuclear receptors requires the DRIP complex., *Nature* 398, 824-828.
19. Lamblin, M., Spingarn, R., Wang, T. T., Burger, M. C., Dabbas, B., Moitessier, N., White, J. H., and Gleason, J. L. (2010) An o-aminoanilide analogue of 1alpha,25-dihydroxyvitamin D(3) functions as a strong vitamin D receptor antagonist, *J Med Chem* 53, 7461-7465.
20. Kato, Y., Nakano, Y., Sano, H., Tanatani, A., Kobayashi, H., Shimazawa, R., Koshino, H., Hashimoto, Y., and Nagasawa, K. (2004) Synthesis of 1alpha,25-dihydroxyvitamin D3-26,23-lactams (DLAMs), a novel series of 1 alpha,25-dihydroxyvitamin D3 antagonist, *Bioorg Med Chem Lett* 14, 2579-2583.
21. Inaba, Y., Yoshimoto, N., Sakamaki, Y., Nakabayashi, M., Ikura, T., Tamamura, H., Ito, N., Shimizu, M., and Yamamoto, K. (2009) A new class of vitamin D analogues that induce structural rearrangement of the ligand-binding pocket of the receptor, *J Med Chem* 52, 1438-1449.
22. Nakabayashi, M., Yamada, S., Yoshimoto, N., Tanaka, T., Igarashi, M., Ikura, T., Ito, N., Makishima, M., Tokiwa, H., DeLuca, H. F., and Shimizu, M. (2008) Crystal structures of rat vitamin D receptor bound to adamantyl vitamin D analogs: structural basis for vitamin D receptor antagonism and partial agonism, *J Med Chem* 51, 5320-5329.
23. Saito, N., and Kittaka, A. (2006) Highly potent vitamin D receptor antagonists: design, synthesis, and biological evaluation, *Chembiochem* 7, 1479-1490.
24. Cho, K., Uneuchi, F., Kato-Nakamura, Y., Namekawa, J., Ishizuka, S., Takenouchi, K., and Nagasawa, K. (2008) Structure-activity relationship studies on vitamin D lactam derivatives as vitamin D receptor antagonist, *Bioorg Med Chem Lett* 18, 4287-4290.
25. Herdick, M., Steinmeyer, A., and Carlberg, C. (2000) Antagonistic action of a 25-carboxylic ester analogue of 1alpha, 25-dihydroxyvitamin D3 is mediated by a lack of ligand-induced vitamin D receptor interaction with coactivators, *J Biol Chem* 275, 16506-16512.

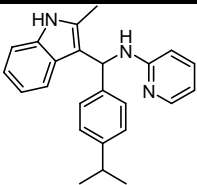
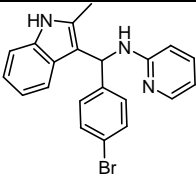
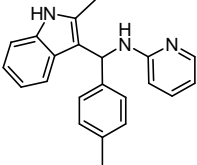
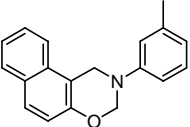
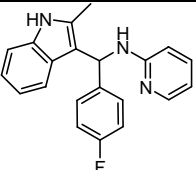
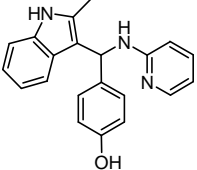
26. Ishizuka, S., Kurihara, N., Miura, D., Takenouchi, K., Cornish, J., Cundy, T., Reddy, S. V., and Roodman, G. D. (2004) Vitamin D antagonist, TEI-9647, inhibits osteoclast formation induced by 1 α ,25-dihydroxyvitamin D₃ from pagetic bone marrow cells, *J Steroid Biochem Mol Biol* 89-90, 331-334.
27. Mita, Y., Dodo, K., Noguchi-Yachide, T., Miyachi, H., Makishima, M., Hashimoto, Y., and Ishikawa, M. (2010) LXXLL peptide mimetics as inhibitors of the interaction of vitamin D receptor with coactivators, *Bioorganic & Medicinal Chemistry Letters* 20, 1712-1717.
28. Moore, T. W., and Katzenellenbogen, J. A. (2009) Inhibitors of Nuclear Hormone Receptor/Coactivator Interactions, *Annu Rep Med Chem* 44, 443-457.
29. Nandhikonda, P., Lynt, W. Z., McCallum, M. M., Ara, T., Baranowski, A. M., Yuan, N. Y., Pearson, D., Bikle, D. D., Guy, R. K., and Arnold, L. A. (2012) Discovery of the first irreversible small molecule inhibitors of the interaction between the vitamin D receptor and coactivators, *J Med Chem* 55, 4640-4651.
30. Zlokarnik, G., Negulescu, P. A., Knapp, T. E., Mere, L., Burres, N., Feng, L., Whitney, M., Roemer, K., and Tsien, R. Y. (1998) Quantitation of transcription and clonal selection of single living cells with beta-lactamase as reporter, *Science* 279, 84-88.
31. Bourguet, W., Germain, P., and Gronemeyer, H. (2000) Nuclear receptor ligand-binding domains: three-dimensional structures, molecular interactions and pharmacological implications, *Trends Pharmacol Sci* 21, 381-388.
32. Ihrke, G., Neufeld, E. B., Meads, T., Shanks, M. R., Cassio, D., Laurent, M., Schroer, T. A., Pagano, R. E., and Hubbard, A. L. (1993) Wif-B Cells - an in-Vitro Model for Studies of Hepatocyte Polarity, *Journal of Cell Biology* 123, 1761-1775.
33. Rawlings, N. D., and Barrett, A. J. (1994) Families of Serine Peptidases, *Method Enzymol* 244, 19-61.
34. Graham, F. L., Smiley, J., Russell, W. C., and Nairn, R. (1977) Characteristics of a human cell line transformed by DNA from human adenovirus type 5, *J Gen Virol* 36, 59-74.
35. Fiers, W., Contreras, R., Haegemann, G., Rogiers, R., Van de Voorde, A., Van Heuverswyn, H., Van Herreweghe, J., Volckaert, G., and Ysebaert, M. (1978) Complete nucleotide sequence of SV40 DNA, *Nature* 273, 113-120.
36. Brand, A. H., and Perrimon, N. (1993) Targeted gene expression as a means of altering cell fates and generating dominant phenotypes, *Development* 118, 401-415.
37. Ehrenfeld, G. M., Shipley, J. B., Heimbrook, D. C., Sugiyama, H., Long, E. C., van Boom, J. H., van der Marel, G. A., Oppenheimer, N. J., and Hecht, S. M. (1987) Copper-dependent cleavage of DNA by bleomycin, *Biochemistry* 26, 931-942.
38. Abraham, E. P., and Chain, E. (1988) An enzyme from bacteria able to destroy penicillin. 1940, *Rev Infect Dis* 10, 677-678.
39. Jablonski, A. (1933) Efficiency of anti-Stokes fluorescence in dyes, *Nature* 131, 839-840.

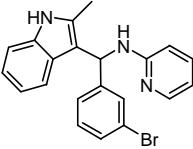
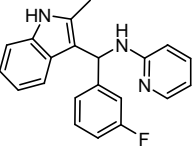
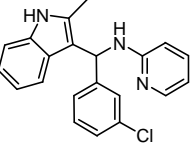
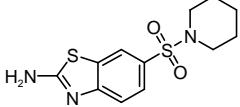
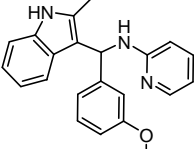
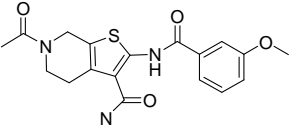
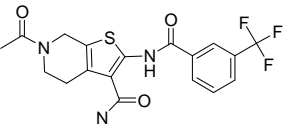
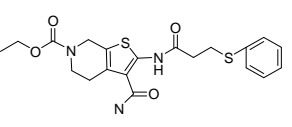
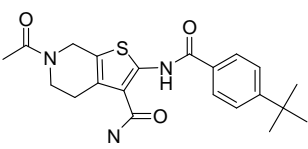
40. Lavis, L. D., and Raines, R. T. (2008) Bright Ideas for Chemical Biology, *ACS Chemical Biology* 3, 142-155.
41. Stokes, G. G. (1852) On the change of refrangibility of light, *Philosophical Transactions of the Royal Society of London* 142, 463-562.
42. Lakowicz, J. R. (2006) *Principles of Fluorescence*, 3rd ed., Springer, New York.
43. Periasamy, A., Vogel, S. S., and Clegg, R. M. (2012) FRET at 65: A Celebration of Forster, *J Biomed Opt* 17.
44. Sznajdman, M. L., Haffner, C. D., Maloney, P. R., Fivush, A., Chao, E., Goreham, D., Sierra, M. L., LeGrumelec, C., Xu, H. E., Montana, V. G., Lambert, M. H., Willson, T. M., Oliver, W. R., Jr., and Sternbach, D. D. (2003) Novel selective small molecule agonists for peroxisome proliferator-activated receptor delta (PPARdelta)--synthesis and biological activity, *Bioorg Med Chem Lett* 13, 1517-1521.
45. Harrington, L. S., Moreno, L., Reed, A., Wort, S. J., Desvergne, B., Garland, C., Zhao, L., and Mitchell, J. A. (2010) The PPARbeta/delta agonist GW0742 relaxes pulmonary vessels and limits right heart hypertrophy in rats with hypoxia-induced pulmonary hypertension, *PLoS One* 5, e9526.
46. Zarzuelo, M. J., Jimenez, R., Galindo, P., Sanchez, M., Nieto, A., Romero, M., Quintela, A. M., Lopez-Sepulveda, R., Gomez-Guzman, M., Bailon, E., Rodriguez-Gomez, I., Zarzuelo, A., Galvez, J., Tamargo, J., Perez-Vizcaino, F., and Duarte, J. (2011) Antihypertensive effects of peroxisome proliferator-activated receptor-beta activation in spontaneously hypertensive rats, *Hypertension* 58, 733-743.
47. Maria Quintela, A., Jimenez, R., Gomez-Guzman, M., Jose Zarzuelo, M., Galindo, P., Sanchez, M., Vargas, F., Cogolludo, A., Tamargo, J., Perez-Vizcaino, F., and Duarte, J. (2012) Activation of peroxisome proliferator-activated receptor-beta/-delta (PPARbeta/delta) prevents endothelial dysfunction in type 1 diabetic rats, *Free Radic Biol Med*.
48. Matsushita, Y., Ogawa, D., Wada, J., Yamamoto, N., Shikata, K., Sato, C., Tachibana, H., Toyota, N., and Makino, H. (2011) Activation of peroxisome proliferator-activated receptor delta inhibits streptozotocin-induced diabetic nephropathy through anti-inflammatory mechanisms in mice, *Diabetes* 60, 960-968.
49. Galuppo, M., Di Paola, R., Mazzon, E., Esposito, E., Paterniti, I., Kapoor, A., Thiemermann, C., and Cuzzocrea, S. (2010) GW0742, a high affinity PPAR-beta/delta agonist reduces lung inflammation induced by bleomycin instillation in mice, *Int J Immunopathol Pharmacol* 23, 1033-1046.
50. Zingarelli, B., Piraino, G., Hake, P. W., O'Connor, M., Denenberg, A., Fan, H., and Cook, J. A. (2010) Peroxisome proliferator-activated receptor {delta} regulates inflammation via NF-{kappa}B signaling in polymicrobial sepsis, *Am J Pathol* 177, 1834-1847.
51. Harrington, W. W., C, S. B., J, G. W., N, O. M., J, G. B., D, C. L., W, R. O., M, C. L., and D, M. I. (2007) The Effect of PPARalpha, PPARdelta, PPARgamma, and PPARpan Agonists on Body Weight, Body Mass, and Serum Lipid Profiles in Diet-Induced Obese AKR/J Mice, *PPAR Res* 2007, 97125.

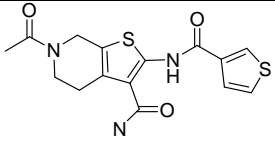
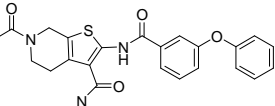
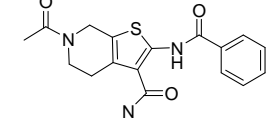
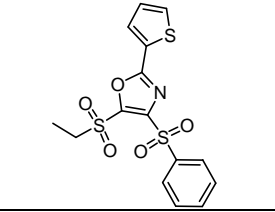
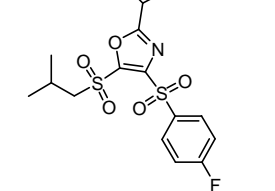
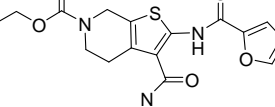
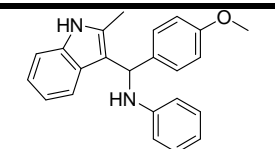
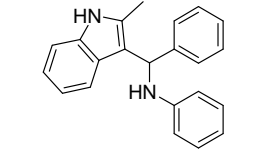
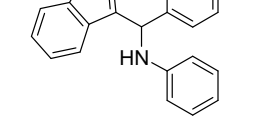
52. Bility, M. T., Devlin-Durante, M. K., Blazanin, N., Glick, A. B., Ward, J. M., Kang, B. H., Kennett, M. J., Gonzalez, F. J., and Peters, J. M. (2008) Ligand activation of peroxisome proliferator-activated receptor beta/delta (PPAR beta/delta) inhibits chemically induced skin tumorigenesis, *Carcinogenesis* 29, 2406-2414.
53. Hollingshead, H. E., Killins, R. L., Borland, M. G., Girroir, E. E., Billin, A. N., Willson, T. M., Sharma, A. K., Amin, S., Gonzalez, F. J., and Peters, J. M. (2007) Peroxisome proliferator-activated receptor-beta/delta (PPARbeta/delta) ligands do not potentiate growth of human cancer cell lines, *Carcinogenesis* 28, 2641-2649.
54. Marin, H. E., Peraza, M. A., Billin, A. N., Willson, T. M., Ward, J. M., Kennett, M. J., Gonzalez, F. J., and Peters, J. M. (2006) Ligand activation of peroxisome proliferator-activated receptor beta inhibits colon carcinogenesis, *Cancer Res* 66, 4394-4401.
55. Sertznig, P., Dunlop, T., Seifert, M., Tilgen, W., and Reichrath, J. (2009) Cross-talk between vitamin D receptor (VDR)- and peroxisome proliferator-activated receptor (PPAR)-signaling in melanoma cells, *Anticancer Res* 29, 3647-3658.
56. Nandhikonda, P., Yasgar, A., Baranowski, A. M., Sidhu, P. S., McCallum, M. M., Pawlak, A. J., Teske, K., Feleke, B., Yuan, N. Y., Kevin, C., Bikle, D. D., Ayers, S. D., Webb, P., Rai, G., Simeonov, A., Jadhav, A., Maloney, D., and Arnold, L. A. (2013) Peroxisome Proliferation-Activated Receptor delta Agonist GW0742 Interacts Weakly with Multiple Nuclear Receptors, Including the Vitamin D Receptor, *Biochemistry* 52, 4193-4203.
57. Gould, S. J., and Subramani, S. (1988) Firefly Luciferase as a Tool in Molecular and Cell Biology, *Anal Biochem* 175, 5-13.
58. Fraga, H., Fernandes, D., Novotny, J., Fontes, R., and da Silva, J. C. G. (2006) Firefly luciferase produces hydrogen peroxide as a coproduct in dehydroluciferyl adenylate formation, *Chembiochem* 7, 929-935.
59. Arnold, L. A., Estebanez-Perpina, E., Togashi, M., Shelat, A., Ocasio, C. A., McReynolds, A. C., Nguyen, P., Baxter, J. D., Fletterick, R. J., Webb, P., and Guy, R. K. (2006) A high-throughput screening method to identify small molecule inhibitors of thyroid hormone receptor coactivator binding, *Sci STKE* 2006, pl3.
60. Boehm, M. F., Fitzgerald, P., Zou, A., Elgort, M. G., Bischoff, E. D., Mere, L., Mais, D. E., Bissonnette, R. P., Heyman, R. A., Nadzan, A. M., Reichman, M., and Allegretto, E. A. (1999) Novel nonsecosteroidal vitamin D mimics exert VDR-modulating activities with less calcium mobilization than 1,25-dihydroxyvitamin D3, *Chem Biol* 6, 265-275.

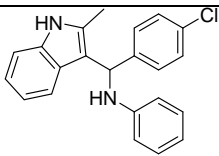
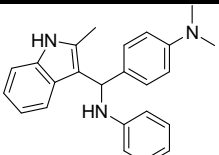
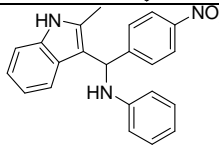
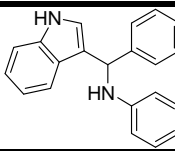
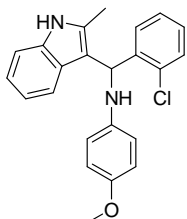
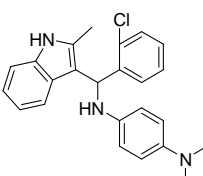
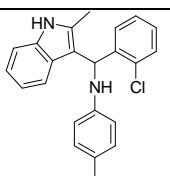
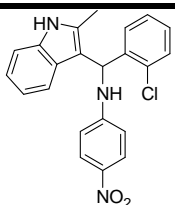
Appendix

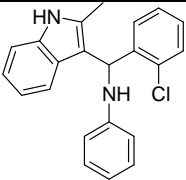
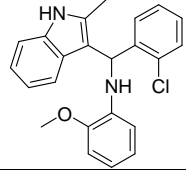
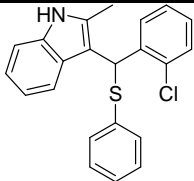
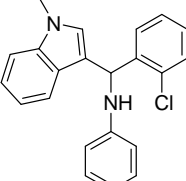
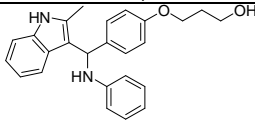
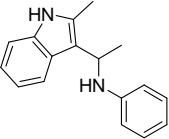
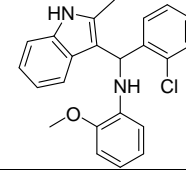
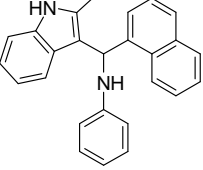
Table 7: Summary of the compounds tested, with respect to their ability to inhibit VDR-mediated transcription using the Gene BLAzer assay, as well as their cytotoxicity, which was determined by the Cell Titer-Glo luminescence assay. All results are given in micromolar concentrations.

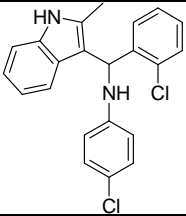
Number ¹	Structure	Inhibition of VDR-Mediated Transcription IC ₅₀ Values (μM)	Percent Toxicity at the Given Concentration Or LD ₅₀ Toxicity Values (μM)
F1387-0020		12.3	11.7
F1387-0036		12.4	21.5
F1217-0092		Low Activity	90% (62.5 μM)
F0910-7407		Low Activity	20% (62.5 μM)
F0743-0032		Low Activity	90% (62.5 μM)
F0842-0039		8.6	90% (62.5 μM)

F1387-0021		Low Activity	90% (62.5 μ M)
F1387-0022		Low Activity	70% (62.5 μ M)
F1387-0034		Low Activity	90% (62.5 μ M)
F1420-1568		No Activity	30% (62.5 μ M)
F1387-0028		Low Activity	70% (62.5 μ M)
F1298-0533		No Activity	Non-Toxic
F1298-0551		No Activity	Non-Toxic
F1298-0074		Low Activity	90% (62.5 μ M)
F1298-0581		Low Activity	90% (62.5 μ M)

F1298-0621		No Activity	14.1
F1298-0587		17.6	Non-Toxic
F1298-0522		No Activity	Non-Toxic
D093-0045		5.8	10.1
D093-0086		6.6	8.4
F1298-0025		No Activity	Non-Toxic
WL052410D (30c)		12.4	90% (22.5 μ M)
WL052510D (30a)		10.8	90% (22.5 μ M)
WL052510F (30d)		12.2	90% (22.5 μ M)

WL052510H (30b)		9.1	90% (22.5 μ M)
WL052510K (30e)		No Activity	Non-Toxic
WL052510M (30f)		11.4	90% (22.5 μ M)
WL052510O (32b)		Low Activity	90% (22.5 μ M)
WL052410K (31c)		7.2	12.8
WL052410N (31e)		Low Activity	9.6
WL060110G (31d)		8.8	16.9
WL060110H (31f)		Low Activity	60% (22.5 μ M)

WL040710D (31a)		11.2	90% (22.5 μ M)
WL042210G (31h)		12.0	90% (22.5 μ M)
WL061410C (32c)		Low Activity	90% (22.5 μ M)
WL042210D (32a)		No Activity	30% (22.5 μ M)
WL060310C (30i)		No Activity	10% (22.5 μ M)
WL061410K (30g)		Low Activity	70% (22.5 μ M)
WL042210G (31h)		8.1	9.8
WL042210K (30h)		10.5	11.4

WL052410G (31b)		4.9	14.2
--------------------	---	-----	------

[†]Numbers are given in Nandhikonda et al. *J. Med. Chem.* **2012**, 50,4640-51.